TÉCNICO LISBOA

Auto-ignition of spontaneous hydrogen leaks

Tomás Horta e Costa Gomes da Costa

Thesis to obtain the Master of Science Degree in

Mechanical Engineering

Supervisors: Prof. Edgar Caetano Fernandes
Prof. Aires José Pinto dos Santos

Examination Committee

Chairperson: Prof. Carlos Frederico Neves Bettencourt da Silva
Supervisor: Prof. Aires José Pinto dos Santos
Member of the Committee: Prof. Miguel Abreu de Almeida Mendes

November 2020

Acknowledgments

I wish to start by thanking Prof. Edgar Fernandes and Prof. Aires dos Santos for the orientation and support demonstrated along this journey.

I would also like to sincerely thank Sandra Dias from IN+ for the constant availability which contributed a lot for the development of this thesis.

I also wish my sincere thanks to the whole "Di Baldi", Guilherme, Afonso, Sebastião, Castro, Amaral, Bernardo e Tio Dufra, for their companionship and being there for whenever needed in these last few years.

I would also like to thank my close family, Mother, Father and sisters for the constant support and help that played a vital part in this journey. Finally a very special thanks to Matilde for her constant support no matter what and for helping me in the times of biggest frustration. Your support was the absolute cornerstone for the completion of this thesis. A sincere thank you for all the conversations and the constant push that you gave me to pursue and persist.

This work was developed at the Thermofluids, Combustion and Energy Systems laboratory of the IN+ - Center for Innovation, Technology and Policy Research.

Resumo

Com o aumento da procura por combustíveis mais limpos para substituir os de origem fóssil, o interesse pelo hidrogénio tem vindo a aumentar radicalmente no decorrer do último século em todo o tipo de indústrias. Com isto, vários problemas e preocupações têm vindo a aparecer devido ao facto de que ainda se sabe pouco acerca deste gás incolor, inodoro e facilmente inflamável.

Esta tese tem como principal objetivo o estudo de ignição espontânea de uma fuga de hidrogénio.

Para melhor analisar este caso particular e para melhor perceber o fenómeno da ignição espontânea de fugas inesperadas de hidrogénio a alta pressão, um estudo numérico aliado a simulação CFD foi levada a cabo para melhor perceber o que acontece quando o hidrogénio e o ar reagem no local de fuga. A modelação CFD involve um tubo de choque em que o hidrogénio, a alta pressão, está separado do ar atmosférico por um diafragma.

Analisando os resultados conclui-se que, devido às diferenças de pressões do hidrogénio e do ar, no caso do diafragma rebentar, o fluxo de combustível pode criar uma onda de choque transiente dentro do tubo, originando um aquecimento que permite a ignição do hidrogénio. Para além disto, foi possivel concluir que quanto mais comprida for a geometria que leva o hidrogénio a entrar em contacto com o ar atmosférico mais fraca se torna a mistura não permitindo a sua ignição mesmo que a temperatura seja alta o suficiente.

Um dos casos estudados foi modelado com um tubo com o comprimento de 1 metro (com 50cm de secção após o diafragma) e 40 bar de pressão inicial. A temperatura da mistura chegou a valores superiores a 1200K, muito superior a 737K, temperatura esta a necessária para ocorrer ignição espontânea do hidrogénio em condições estequiométricas. No início do tubo as condições eram propícias para ocorrer auto-ignição do hidrogénio, contudo com o desenvolvimento do escoamento dentro do tubo, a mistura começou a alastrar-se levando a que as condições já não se mantivessem propícias à ignição da mistura. Contudo, outro caso foi avaliado com a mesma pressão inicial, desta vez com apenas 360mm de tubo em que os resultados apresentados mostram uma mistura estequiométrica para temperaturas perto de 1000K dentro do tubo. Neste caso já estão reunidas as condições para haver ignição espontânea do hidrogénio e para que ocorra a produção de chama para a atmosfera.

Palavras-chave: Hidrogénio, Auto-ignição, Alta pressão, Onda de choque, CFD

Abstract

With the increasing search for cleaner fuels to replace fossil, interest in hydrogen has spiked during the last century in all sorts of industries. With that several issues and concerns started to appear given that so little is known about the handling of this odorless, colorless and easily flammable gas.

This thesis is devoted to the study of the self-ignition of hydrogen leaks. In order to analyse this particular case and to understand the physical phenomena behind spontaneous ignition of sudden high-pressure hydrogen releases, analytical calculations and a CFD simulation was carried out in order to understand what happens inside the hole where hydrogen is mixed with air. The modeling involved a shock tube where high-pressure hydrogen was separated from the atmospheric air by a rupture disk.

It was concluded that due to the high-pressure difference of the fuel to the atmosphere, a sudden release of the fuel could lead to a transient shock wave inside the tube that could, through mixing of shock-heated air and cold expanding hydrogen, ignite and form a flame still on the inside of the tube as the temperatures reached would be higher than the spontaneous ignition temperatures. It was also found that if the downstream geometry of the hole is too long, even if the temperatures are high enough that the spontaneous ignition temperature is reached, the mixture will become lean leading to no ignition of the mixture.

This was the case for a 0.5 meter long tube downstream of the hole, with 40 bar of initial pressure where temperatures reached as high as 1200K, well above the 773K necessary for the spontaneous ignition of hydrogen. Although in the beginning of the tube conditions were gathered to allow spontaneous ignition of the mixture, with the flow developing along the length of the tube, the mixture started to become lean leading to the extinction of possible flame originated in the beginning of the tube. On the other hand, a tube with 180mm downstream of the hole, was tested for the same pressure where the results showed a stoichiometric mixture in the driven section with temperatures up to 1000K reached inside the tube. For this case the conditions are gathered for spontaneous ignition and for flame spouting into the atmosphere.

Keywords: Hydrogen, Auto-ignition, High-pressure, Shock wave, CFD

Contents

List of Tables

List of Figures

Nomenclature

Greek symbols

Γ	Effective diffusity
γ	Heat Capacity Ratio
κ	Thermal conductivity coefficient $[W/(m * K)]$
μ	Molecular viscosity coefficient $[N * s/m^2]$
∇	Vector differential operator
ω	Specific dissipation rate
$\overline{\overline{\tau}}$	Stress tensor
$\overline{\overline{\tau}}_{eff}$	Effective stress tensor
Φ	Fuel-Air equivalence ratio
ρ	Density $[Kg/m^3]$

Roman symbols

$\vec{F}$	External body forces
$\vec{g}$	Gravitational body forces
$\vec{J_j}$	Diffusion flux of species j
a	Speed of sound $[m/s]$
C_p	Heat capacity at constant pressure
C_v	Heat capacity at constant volume
cs	shock speed $[m/s]$
E	Energy $[J]$
FAR	Fuel-air ratio
$G_{k,\omega}$	Generation of k and ω

h Sensible enthaply $[J]$

h_j Enthalpy at the local temperature $[J]$

k Turbulence kinetic energy $[m/s]$

k_{eff} Thermal effective conductivity

M_s Shock Mach number

R_i Rate of production of species i by the chemical reaction

S_h Heat of chemical reaction

S_i Rate of creation of species i, by addition of the dispersed phase

S_m Mass added to the continuous phase

$S_{k,w}$ User defined source terms

t time $[s]$

$Y_{i,j}$ Mass fraction of the species j

P Pressure $[bar]$

p Local pressure $[bar]$

T Temperature $[K]$

$\vec{v}$ Velocity vector

u, v, w Velocity Cartesian components

Subscripts

$1, 2, 3, 4$ Computational indexes.

∞ Free-stream condition.

x, y, z Cartesian components.

ref Reference condition.

Chapter 1

Introduction

1.1 Motivation

Since the beginning of time, human kind has been very curious to whatever surrounds them, making multiple experiences and discovering all sorts of knowledge that is now used in the modern world. One of the first things that mankind discovered was fire which would be categorised as one of the first chemistry reactions made by humans.

Hydrogen was observed for the first time in the 16th century by Paracelsus while dissolving metals in sulfuric acid. Over 250 years of experiments with this gas were made while calling it "inflammable air", name given by Henry Cavendish in the 18th century who was the first to recognize it as a discrete gas and that when burned with oxygen, produces water. Later in 1783, Antoine Lavoisier named the gas hydrogen which means "water-former", in Greek [1].

While experimenting with hydrogen, Henry Cavendish also discovered that it was 7 to 11 times lighter than air which enabled Jacques Charles to invent the first hydrogen-filled balloon in the same year that hydrogen was named. These balloons were later named after the German count Ferdinand von Zeppelin who implemented the idea of rigid airships lifted by hydrogen where the first flight took part in 1900 [2]. At first it was used for transportation of passengers. However by 1914, with the outbreak of the First World War it started being used as observation platforms and as bombers. Later, in 1937 a very well known accident occurred where a zeppelin called Hindenburg was destroyed in a midair fire over New Jersey taking a total of 36 lives. The incident was broadcast live on radio and filmed, causing a lot of damage on hydrogen's reputation as the ignition of the leaking gas was widely believed to be the cause of the fire. It was later refuted, as it was discovered that it was not the hydrogen that had ignited but the aluminized fabric coating by static electricity. This lead to the cease of commercial hydrogen lifted airship travel and to its usage in much less volatile environments.

Because of its very simple atomic structure composed only of an electron and a proton, the hydrogen atom, has been central to the development of the theory of atomic structure and quantum theory.

Throughout the 20th century, as hydrogen was being highly studied and many properties were starting to be discovered, it started to become recognized as a very promising gas and fuel. For this reason, hydro-

gen started gaining a lot of interest in multiple branches of modern society such as: fertilizer production, mainly the synthesis of ammonia; industrial applications which include the electronics industry (used as a protective and carrier gas, in deposition processes, for cleaning, in etching, in reduction processes, etc.), and applications in electricity generation, for example generator cooling or for corrosion prevention in power plant pipelines; and fuel production as it is used to process crude oils into refined fuels like gasoline and diesel but it can also be used to remove contaminants from these fuels such as sulphur [3].

With the advance in these industries, hydrogen started attracting new uses, energy based ones. In the energy field, it is mostly used through Fuel Cells [3] where a combination of hydrogen and oxygen with water and heat as by-products produce electricity through an electrochemical device. These currently have two applications, transportation and electricity generation. Although it is something that is not yet mature enough for production in series, several branches of the transportation industry are looking into the transfer to cleaner fuels and hydrogen is a good candidate to contribute to its decarbonisation. Buses alongside with some prototype passenger cars are already being moved by hydrogen fuel cells, predominantly in North America, Europe and increasingly also in Asia. Although it is a clean fuel with excellent physicochemical properties, hydrogen has not been able to gain acceptance as a fuel for motorized transport as it requires very high safety regulations. However, it is portrayed as the fuel of the future for scientists and engineers all over the world for not only for being a fuel with great properties, but also for being one of the most abundant chemical substance in the universe [3].

With the increasing usage of hydrogen in several industries throughout the last 100 years, several issues concerning safety have made it very difficult to progress and expand its usage as a clean fuel. These safety issues include its transportation, storage and usage. As it is a very volatile gas and can be very explosive as it combusts with just one-tenth of the energy required for gasoline, the safety concerns turn to avoid combustion at all costs. On top of explosive issues, hydrogen burns with a pale blue flame, that is almost invisible during daylight hours,as seen in figure 1.1, so fires are almost impossible to see with the naked eye which can be very dangerous in case of leakage for passers-by.

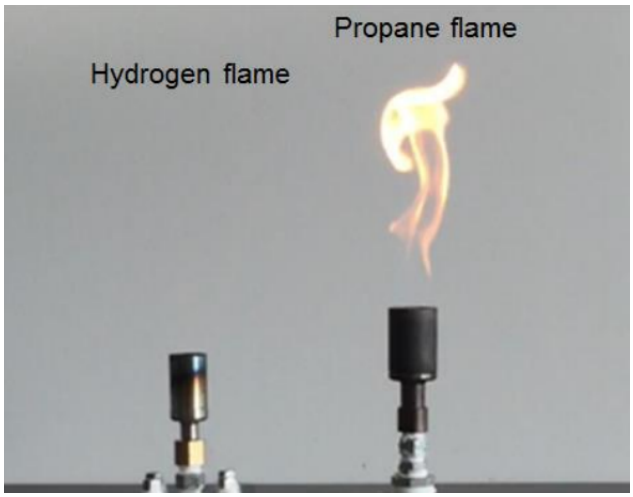

Figure 1.1: Hydrogen flame (left) and propane flame (right) showing entirely invisible characteristics of the hydrogen flame from Okino et al.[4]

When handling high-pressure hydrogen, improper use of valves, damage to the ducts/reservoirs or

embrittlement can lead to high velocity leaks that can ignite with minimum effort, whether it is a spark, static electricity or even just a hot surface as hydrogen ignites with very minimal energy. Many have been the reported accidents involving high-pressure flammable gas with spontaneous ignition, however, in total, the majority of the incidents have no known cause leading to the absence of knowledge on how to avoid such accidents.

In order to consider hydrogen as a fuel for any sort of use, safety must be one of the main issues to cover. For that reason, many studies have been made around the subject of hydrogen auto-ignition, how it happens and why it happens.

This study serves the purpose of increasing the knowledge around this subject and this thesis has, as main goal, the objective of evaluating the results presented in the literature and presenting additional information in order to contribute, in a small scale, to the implementation of hydrogen as a fuel in today's society.

1.2 Literature Review

The state of art has as objective the comprehension and understanding of the concepts and phenomena that is inherent to spontaneous ignition of hydrogen leaks, more specifically the diffusion ignition case. The understanding of the physical and chemical process behind diffusion ignition is the first step to being able to contribute to the already knowing facts around this topic.

The present chapter starts by approaching the physicochemical characteristics of hydrogen followed by a revision of postulated mechanisms. After this, there is a characterization of diffusion ignition and an evaluation of the known studies made around this subject.

1.2.1 Compressed gas properties for different fuels

Considering the volatility of hydrogen, its potential for fires and explosions has always been one of the major safety concerns. Due to historical events and numeral experiments, hydrogen reputation among the common society has been denigrated, perhaps unfairly, in relation to certain accidents like the Hindenburg disaster, in 1937. Due to its ignition and combustion properties, which are very different from other flammable hydrocarbons, hydrogen is much more prone to ignite. In 2001, Alcock et al. [5], gathered information on compressed gas properties that can explain why hydrogen is a much more dangerous fuel to handle and why, indirectly, it has not been adopted in the modern society. When looking at table 1.1 and 1.2 we can see some properties for hydrogen, methane, propane and gasoline that concern fire safety. From all the points presented, those that should get most of the attention for hydrogen are: the minimum ignition energy which is extremely low and approximately 10 times less than what it is needed for gasoline; flammability range which is much wider than normal; and how easy it is leaked. In figure 1.2 it is possible to see the difference between the ignition energy required for hydrogen/air and methane/air mixtures along with the flammability limits.

The hydrogen gas molecule is the smallest there is and it has a greater propensity to escape through small openings than other gaseous or liquid fuels. Considering high-pressure systems used for storage of

hydrogen, in case of a leak the flow is most likely supersonic due to the high-pressure release, which means that, according to table 1.1, hydrogen would leak 2.9 times faster than methane (natural gas) and about 5 times faster than propane, volumetrically speaking. On the other hand, it is argued that in the presence of high-pressure hydrogen leaks, being a very diffusive gas and, in most conditions, more buoyant than other gaseous fuels, in the presence of a leak it tends to disperse and not reach its flammability range.

The spontaneous ignition of confined flammable gas leak is normally due to an explosion accompanied by a fireball. If the burning velocity is slow, there will only be deflagration which is also called a flash fire. However, the burning velocity can increase due to turbulence or obstacles and if it increases to a certain point with a certain concentration it can transition from deflagration to detonation which is self-sustained as long as the combustion mixture stays within the detonation range. Comparing hydrogen to the other fuels in table 1.2 we can see that the ability for hydrogen to detonate or transition from deflagration to detonation is more likely than the other gases for not only having a wider range of detonability volumetric concentration but also for having a higher burning velocity at stoichiometric concentration.

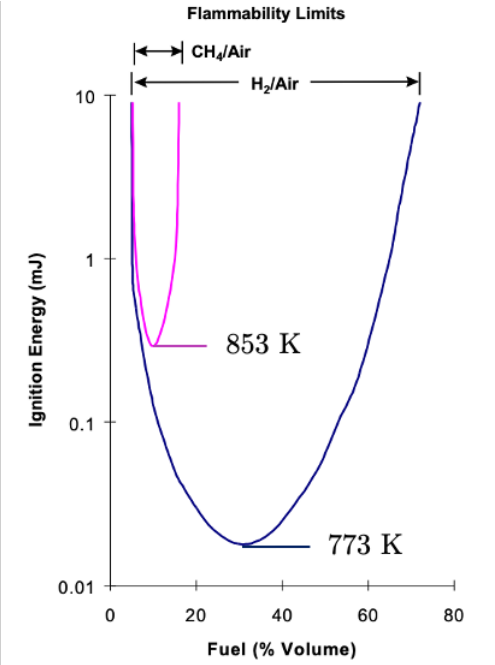

Figure 1.2: Ignition energy of hydrogen/air and methane/air as a function of volumetric concentration of fuel (Alcock et al. [5])

There is also a very big disparity of minimum ignition energy from hydrogen to other flammable hydrocarbons and gaseous fuels which might lead to more accidents than with other fuels. The minimum ignition energy for hydrogen/air mixture is very close to stoichiometric conditions, i.e. 29.5% hydrogen in air which might not be harmful as, due to high diffusity of hydrogen it is very unlikely to reach these values. On the other hand, the minimum ignition energy is so low that something so simple as static electricity produced by the human body, is sufficient to ignite a hydrogen leak.

Table 1.1: Compressed gas properties and relative leak rates for hydrogen, methane and propane at 20°C and 1 atm (Alcock et al.[5]

)

Property*	Hydrogen	Methane	Propane
Molecular weight (g/mol)	2.02	16.04	44.1
Diffusion coefficient in air (cm2 /s)	0.61	0.16	0.12
Viscosity at NTP (g/cm-s x 10-5)	89	11.7	80
Density at NTP (kg/m3)	0.0838	0.6512	1.870
Ratio of specific heats, Cp/Cv at NTP	1.308	1.383	1.14
Relative leak rates (volumetric):			
Subsonic flow			
Diffusion	1	0.26	0.20
Laminar Flow	1	0.77	1.11
Turbulent Flow	1	0.35	0.21
Sonic flow	1	0.34	0.20

Table 1.2: Compressed gas properties for flammability purposes for hydrogen, methane and propane at 20°C and 1 atm (Alcock et al.[5])

Property*	Hydrogen	Methane	Propane	Gasoline
Flammability limits (vol. % in air)				
Lower limit (LFL)	4	5.3	2.1	1
Upper limit (UFL)	75	15	9.5	7.8
Detonability limits (vol. % in air)				
Lower limit (LDL)	11-18	6.3	3.1	1.1
Upper limit (UDL)	59	13.5	7	3.3
Maximum burning velocity (m/s)	3.46	0.43	0.47	
Concentration at maximum (vol. %)	42.5	10.2	4.3	
Burning velocity at stoichiometric (m/s)	2.37	0.42	0.46	0.42
Concentration at stoichiometric (vol. %)	29.5	9.5	4.1	1.8
Minimum ignition energy (mJ)	0.02	0.29	0.26	0.24
Adiabatic Flame Temperature in Air (K)	2318	2158	2198	2470

1.2.2 Review of postulated mechanisms

When handling a high-pressure gas, it is expected that unwanted discharges can occur specially in consumer handling situations. However, accidents of more abrupt nature can also occur like sudden rupture of pipelines/reservoirs causing unexpected high-speed expanding flow into the surrounding atmosphere. Moreover, when this is applied to flammable gas, the danger factor increases exponentially as it can transition into jet fire or even explosion upon mixture with an oxidizing atmosphere like air. As previously mentioned different fuels react differently to certain conditions and some are more prone to combustion and as observed, hydrogen is more susceptible to combust than other hydrocarbons or fuels.

Over the last century, several combustion incidents have been reported due to high-pressure hydrogen leaks without a determined cause. In 2007, Astbury and Hawksworth [6] published a paper where they found that 86.3% of all incidents regarding hydrogen ignition, until then, had no determined cause, out of

81 reported accidents. However, when looking into non-hydrogen releases it was found that in 65.5% of the incidents, the ignition source was not identified suggesting that hydrogen could more easily self-ignite than other spontaneous gas releases. Out of the incidents that had an identified cause, they enumerated several postulated mechanisms for hydrogen spontaneous ignition.

Reverse Joule-Thompson effect

It specifies that when a gas rapidly expands, it naturally cools if it is under the Joule–Thomson inversion temperature initially, however if it is over that temperature, which for hydrogen is 193K(-80°C), when compressed and it leaks into the atmosphere, it heats up. However, for very high initial pressures, the temperature rise is very small, in range of 9/10 degrees which is far from the rise needed to reach the temperature of hydrogen auto-ignition.

Electrostatic ignition

The name speaks for itself but as previously mentioned, hydrogen has a very low minimum ignition energy which makes it very easy to ignite where even the spark from static electricity produced by the human body can be enough to lead to deflagration of a high-pressure leak.

Diffusion ignition

Phenomena first postulated by Wolański and Wójcicki [7], who demonstrated that it is possible to achieve ignition when high-pressure hydrogen is admitted into a shock-tube filled with air. Spontaneous ignition was possible due to the presence of a shock-wave which lead to a substantial increase of temperature of the hydrogen-air mixture.

Sudden adiabatic compression

It occurs when a gas, obeying ideal gas law, is compressed adiabatically with constant entropy. For a compression ration of 10 to 1, at atmospheric pressure and 273k, it was predicted that through the pressure ratio and the following equations,

$$\frac{P_2}{P_1} = \left(\frac{V_1}{V_2}\right)^{\gamma} = (10)^{1.4} = 25.7 \tag{1.1}$$

$$T_2 = \frac{P_2 V_2 T_1}{P_1 V_1} = \frac{25.7 \times 1 \times 273}{10} = 701.6K \tag{1.2}$$

hydrogen would have an increment of temperature of almost 500k.

Hot surface ignition

Often used to determine the auto-ignition temperatures of flammable gases and liquids, it consists of having the surroundings at a high enough temperature that the rate of oxidation generates more heat

than is being lost to the surroundings, so allowing the oxidation chain-reaction to progress and facilitating spontaneous ignition.

The review of these postulated mechanics was made back in 2007 through a platform called MHIDAS, Major Hazard Incident Database Service, which at the time reported a total of 81 hydrogen accidents. Today, there is a new platform called HIAD[8], Hydrogen Incident and Accident Database, which is a free access database that keeps track of all the accidents related with hydrogen worldwide. As of the 22nd of August, 2020, there is a total of 364 accidents involving hydrogen that transitioned into jet fire or explosions. While most of them have an associated cause (about 86%), in about 14% of the accidents the cause is still unknown.

Taking into account all the postulated mechanisms mentioned above, there is not one that is more likely to happen than the others. However, considering that the percentage of unknown causes is still substantial, it is something that has to be looked into.

1.2.3 Context of the problem

As hydrogen is progressing to become the fuel of the future, many have been the countries which are drawing a plan to implement hydrogen in today's society. Of these countries is Portugal, which by 2030 expects to have hydrogen injected into the natural gas transportation network.

This network is composed by 3 different transportation nets. The first is called the high-pressured transportation net which complements all of the piping that leaves the main natural gas stations and transports it all over the country and it operates at 80 bar. The primary net takes over as the natural gas starts approaching major cities and therefore has an operating pressure of 16-20 bar. Lastly, the secondary net is responsible for the transportation of natural gas into the houses of the people with an low operating pressure in the range from 200mbar to 4 bar. This being said, since these operating pressures are higher than the atmospheric pressure, if by any reason, some damage is done to the pipes, these will originate in high-pressured leaks. Due to big pressure difference, these leaks will most likely cause a shock wave that, if strong enough will cause such compression that the flow of gas will reach very high-temperatures. Considering that methane has an auto-ignition temperature of 853K while hydrogen only needs 773K to ignite, these operating pressures might be safe for the use of natural gas. However, considering a lower auto-ignition temperature for hydrogen, tests must be made in order to ensure that hydrogen is safe to be used in these operating pressures. This being said, the method to study in this thesis was diffusion ignition due to the assumption of a shock wave in the hole that spouts the flammable gas into the atmosphere.

1.2.4 Diffusion ignition Theory

As previously mentioned, diffusion ignition was first studied in 1972 by Wolański and Wójcicki [7]. What they meant by "diffusion ignition" was the ignition produced by the discharging jet, when the fuel expanding through a shock tube came into contact with an oxidizing atmosphere heated by the shock wave. The reason why it was named, diffusion ignition, is because they identified diffusive mixing.

Throughout their investigation two scenarios were studied.

In the first scenario, an analytical approach was made in order to predict under what conditions the mixture would auto-ignite. For this, ammonia synthesis gas was used, composed of a 3:1 mixture of hydrogen and nitrogen and it was predicted that ignition would be achieved once an upstream pressure of 39 bar, which is the typical pressure used in ammonia synthesizer plants, was obtained causing a shock-wave mach number of 2.8 or higher with a temperature of 575K. They also calculated that in the presence of a reflected shock by an obstacle, ignition could occur for a much lower mach number of only 1.7 which corresponded to an upstream pressure of just 13 bar. They then demonstrated diffusive ignition by using a shock tube like structure and discharging high-pressured hydrogen through the rupture of a membrane into a cylindrical chamber containing oxygen. A diffusion theory was then developed to correlate the ignition delays with the formed shock wave. Although it was tested in a confined atmosphere Wolański and Wójcicki never demonstrated what would happen in the case of a rapid discharge into an open atmosphere.

1.2.5 Spontaneous Ignition studies

In 1990 Chaineaux et al. [9], coined the term "spontaneous ignition" which they used after achieving it by discharging high pressurized hydrogen at approximately 100 bar through a 12mm hole extended by a tube with 120mm of length and 15mm inside diameter producing a sort of CD nozzle. However, this was not their only experiment as several other tube lengths, smaller ones, where also tested but with no visible ignition. They also said that the spontaneous ignition was "nearly instantaneous" which leads to the understanding that there is a delay between the discharge and the visible fire.

In 2007 several studies concerning spontaneous ignition were made experimentally proving it was indeed possible to achieve spontaneous ignition for lower pressures contrary to what was thought before.

Mogi et al.[10] studied the effect of tube length, by varying it from 3 to 300mm, using 5 and 10mm nozzle diameters on spontaneous ignition. They were able to get jet fire ignition at an approximately 60 bar with a 185mm tube and a 5 mm diameter nozzle. They also stated that "the pressure at which these ignitions occur appear to be decreasing with the increasing length" of the tube and also confirmed that "the blast from the fireball formed on self-ignition of the hydrogen jet caused an extremely rapid pressure rise".

Still in the same year Golub et al.[11] made a very similar experimental study where it was accompanied with CFD work. From the experimental part, ignition was achieved using a very similar configuration as Mogi et al. [10] with the same pipe length and nozzle diameter but this time ignition was achieved with just 40 bar of high-pressurized hydrogen. They concluded that the reason for the possible spontaneous ignition was "the heating by the primary shock wave of the surrounding oxidizer, resulting in gas ignition on the contact surface". However, through the numerical experiment, the conclusion was very different where the results showed that self-ignition was only possible when the initial hydrogen pressure was in the range of 150-400 bar, and both hydrogen and air were at 300k and the hole diameter exceeded 3mm.

Finally, still in 2007 Dryer et al.[12] released a paper where more than 200 experiments were done using several downstream geometries (downstream of the burst disk) and several burst pressures concluding

that for a downstream geometry of 127mm of length and 4mm diameter ignition would be certain from hydrogen pressures of 22.4 bar up, with a possible ignition at a minimum pressure of 20.6 bar. With the work presented it was possible to conclude that "within the storage and pipeline pressures used today and/or contemplated in the future for hydrogen, transient shock processes associated with rapid pressure boundary failure have the capacity to produce spontaneous ignition of the compressed flammable released into air, providing sufficient mixing is also present".

In 2010, Bragin et al.[13] presented a paper with the objective of studying the "physical phenomena underlying the spontaneous ignition of hydrogen following a sudden release from high-pressure storage and transition to sustained jet fire" through the study of large-eddy simulation (LES). For this they modeled a tube with an open end to a chamber of larger dimensions to simulate the outside atmosphere. They compared the results with the results printed from Mogi et al. [10] validating the LES model in order to be used for engineering design of pressure relief devices.

Xyabo et al [14] in 2012 demonstrated through 2D axisymmetric numerical model that near the "outer-edge of the tube mouth, the vortexes are prone to take shape, which contribute to the mixing of hydrogen and air resulting in intenser and longer time combustion" alongside with a study of density and temperature inside the tube which they stated that following the combustion of the mixture, the local temperatures and density, sharply increase.

Although there is more literature to be discussed, it was concluded that the investigations that were more up to date were the ones mentioned above. Although some experiments such Mogi [10], Golub [11] and Dryer's [12], test the effects that a longer tube has in the spontaneous ignition the only conclusion drawn was that the longer the tube tested, the lower the driver pressure required for the mixture to ignite.

After reviewing the literature, it was understood that there is a big gap of information on the fact that most of the work done is on whether the mixture ignites, or not, under certain conditions and very little work exists on what happens inside the tube that leads the mixture to ignite.

Besides the cited literature, along the dissertation several other articles, papers, books and websites such as [15], [16], [17], [18], [19], [20], [21], [22], [23], [24], were used to better comprehend the thematic of the problem on a more holistic way.

1.3 Objectives

Although there are several other experiments made around spontaneous ignition of flammable gas, little work exists on what happens inside the tube leading the discharged pressurized gas into the atmosphere and how its dimensions influence the temperature, density and velocity profiles inside the tube. Moreover, natural gas is widely used in modern society and considering its physicochemical properties, it can also suffer from spontaneous ignition due to the same process of high-pressure hydrogen expansion. The aim of this study is to complement what already exists and to study the effects of the dimensions of the shock tube for hydrogen in order to facilitate the engineering design of future pressure relief systems or even high-pressure storage devices. As this thesis is supposed to comprise real cases, it is assumed that the

involving environment of the geometry studied is at 298k and 1 bar emulating the atmospheric conditions.

1.4 Thesis Outline

In the following chapters several issues will be addressed in order to fully understand and study the phenomena of spontaneous ignition of high-pressured gaseous fuel leaks.

In chapter 2, an overview of the theory behind the phenomena is addressed as well as analytical calculations using equations from the shock-tube theory.

In chapter 3 the implementation of the theory into the numerical work is approached. In this chapter, we talk about how the numerical work was done, what assumptions were chosen and why.

In chapter 4 the results are presented. These complement two cases. The first case, the results from both CFD and analytical approaches are compared in order to verify and validate the assumptions made. In the second case, only CFD results are presented as the length of the tube is tested as well as what exactly happens inside the tube is shown through time.

Finally in chapter 5 we have the conclusions where the final work is resumed and explained followed by possible future work to be done around this subject.

Chapter 2

Background

In order to better understand the physical and chemical phenomena behind spontaneous ignition through diffusive ignition, an analytical approach is required to complement the numerical study.

This chapter focuses on the overview of the theoretical component that involves shock tube theory and what happens inside it. For this reason 1D fluid dynamics equations of pressure, temperature, density, velocity and time can be studied for various sections of the tube.

As the flow inside a shock tube can describe accurately what happens inside a hole that separates a high-pressure environment from a low pressure environment, from now on, the hole will be addressed as a shock tube like geometry.

2.1 Overview of shock tube theory

2.1.1 The Shock tube

The shock tube is composed of two parts which are denoted as the driver section and the driven section. The driver section contains high-pressure gas at pressure P_4, while the driven section contains low-pressure gas at pressure P_1. These sections are separated by a diaphragm designed to burst at a certain pressure, which is normally fixed in place by the two sections that close on it, as it can be observed in figures 2.1 and 2.2

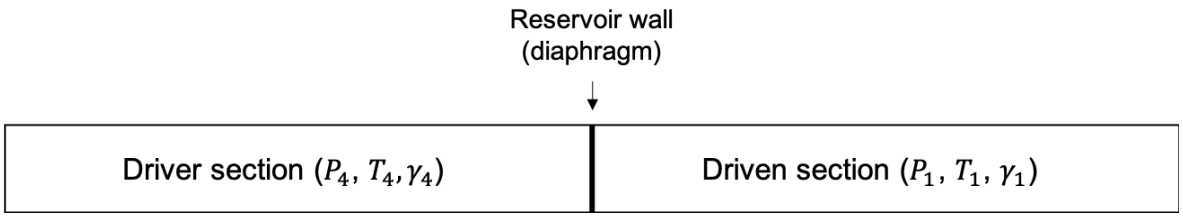

Figure 2.1: Diagram illustrating the driver and driven sections of a shock tube(at t=0), similar to the model used numerically.

Like previously said and can be seen in figure 2.1, the diaphragm is emulating the wall that separates a high-pressure storage system, the driver section, and the atmosphere which is portrayed as the driven

section.

Figure 2.2: Example of how an aluminum diaphragm is clamped in a shock tube, photo taken by Achim Hering.

Once the designed pressure is achieved the diaphragm bursts releasing the high-pressure gas, very rapidly, through the driven section creating a shock wave moving in the same direction. In the driven section, rarefaction waves, as Shapiro [25] mentions, move in the opposite direction of the shock wave due to the expansion of the high-pressure gas. The region nominated as 1 is the region that is located in front of the shock wave that, before it is produced, is at rest with atmospheric properties. Likewise, region 4 properties before the shock wave, are those of the high-pressure contained gas. Once the diaphragm is ruptured, two additional regions appear as regions 2 and 3. Region 2 is located behind the shock wave and region 3 is right behind it separated by the contact surface and portrays the effects of the expansion on the gas properties like temperature, density and pressure. This can all be seen in figure 2.3, which is a diagram that shows the shock tube regions once the diaphragm bursts through time.

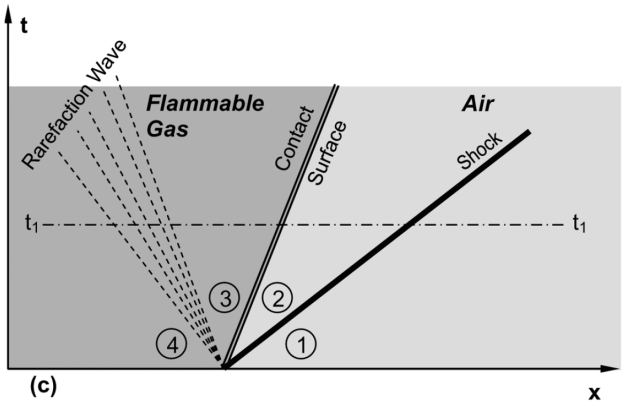

Figure 2.3: Position of contact surface in a shock environment as a function of time. (From Shapiro, 1954.[25])

Since hydrogen and methane are going to be tested in the driver section, a lot of properties that lead to the calculations, are different. However, in the driven section the properties are always the same as the

gas studied is always air at atmospheric conditions (300K and 1 atm). Table 2.1 lists these properties, where γ is the ratio between the specific heats of each species, R is the universal gas constant and auto-ignition temperatures are the lowest recorded ones. All of this information was taken for hydrogen, methane, ethane, propane and butane as well as for air in order to compare values and to further help in the calculations presented in section 2.2. These properties values were taken from the engineering toolbox [26].

Species	Known properties		
	Auto-ignition temperature(K)	Adiabatic exponent(γ)	Universal Gas constant(R)
Hydrogen	773	1.41	4124.2
Methane	853	1.32	518.28
Ethane	788	1.18	276.51
Propane	728	1.13	188.56
Butane	678	1.09	143.05
Air	-----	1.40	287.05

Table 2.1: Know properties for the gases to be studied from the engineering toolbox [26]

Although the initial temperatures, both in the driver and driven sections, is the same (300K), the species in both regions are different with different gas constants which leads to different speed of sound values in both sections of the shock tube. For that, the speed of sound can be calculated as,

$$a = \sqrt{\gamma RT} \tag{2.1}$$

The following equations, were extracted from Liepmann et al. [27], however it is quite simple to deduct these equations through simple deductions from the Navier-Stokes equations.

2.1.2 Pressure

When analysing how a shock tube works, the most influential property is pressure because it only works with a big difference of pressure between the driver and driven sections. Knowing these pressures, P_4 and P_1 respectively, through a simple shock tube equation (2.2), simplified by Liepmann et al.[27], it is possible to calculate $\frac{P_2}{P_1}$. From this pressure ratio, also known as the shock strength, pressure in region 2 is easily calculated.

$$\frac{P_4}{P_1} = \frac{P_2}{P_1}\left[1 - \frac{(\gamma_4 - 1)(a_1/a_4)(P_2/P_1 - 1)}{(\sqrt{2\gamma_1})(\sqrt{2\gamma_1 + (\gamma_1 + 1)(P_2/P_1 - 1)})}\right]^{\frac{-2\gamma_4}{\gamma_4 - 1}} \tag{2.2}$$

Considering that the pressure on either side of the contact surface is the same, we can assume that $P_2 = P_3$. Another property known as expansion strength is the quotient between P_4 and P_3 as the ratio

$\frac{P_4}{P_3}$. Since the driver pressure is always known, this ratio is easily calculated as,

$$\frac{P_3}{P_4} = \frac{P_2/P_1}{P_4/P_1} \tag{2.3}$$

with these two equations (2.2 and 2.3), it is possible to plot the entire pressure profile inside the tube as shown in figure

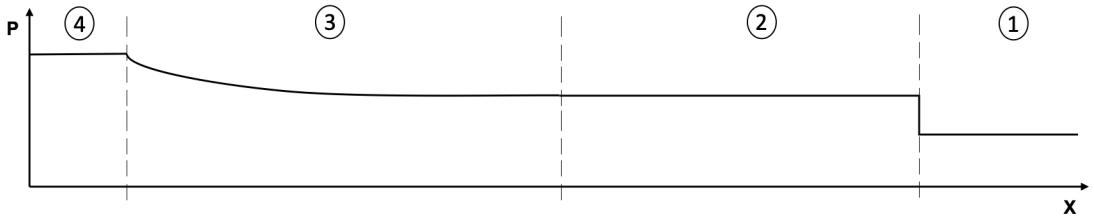

Figure 2.4: Pressure profile along the length of the tube

The curvature between sections 3 and 4 is caused by the rarefaction waves.

2.1.3 Temperature

Although the pressure across the contact surface is the same, temperature and density are different. Due to rapid release of high-pressure flow with great velocity, a shock wave is formed, heating the flow as it travels through the driven section. On the other way around, flow of high-pressure driver gas expands through the driver section on the opposite direction of the shock wave thus cooling it.

By observing figure 2.3 it is clear to say that when the contact surface breaks, section 2 and 3 are formed and the former diaphragm acts as a division from the expanding cooled gas and the shock heated flow. The following equations from Liepmann et al. [27], 2.4 and 2.5, are used to determine the temperature ratios between these two sections and the respective temperatures of each of the sides of the contact surface.

$$\frac{T_3}{T_4} = \left(\frac{P_3}{P_4}\right)^{\frac{(\gamma_4-1)}{\gamma_4}} = \left(\frac{P_2/P_1}{P_4/P_1}\right)^{\frac{(\gamma_4-1)}{\gamma_4}} \tag{2.4}$$

$$\frac{T_2}{T_1} = \frac{1+\frac{\gamma_1-1}{\gamma_1+1}\frac{P_2}{P_1}}{1+\frac{\gamma_1-1}{\gamma_1+1}\frac{P_1}{P_2}} \tag{2.5}$$

Through these two equations it is possible to find the ratio of temperatures across the contact surface as,

$$\frac{T_3}{T_2} = \frac{(T_3/T_4)\,T_4}{(T_2/T_1)\,T_1} \tag{2.6}$$

Using equation 2.5 and 2.6, a temperature profile along the length of the tube is easily drawn as the one presented in figure 2.5.

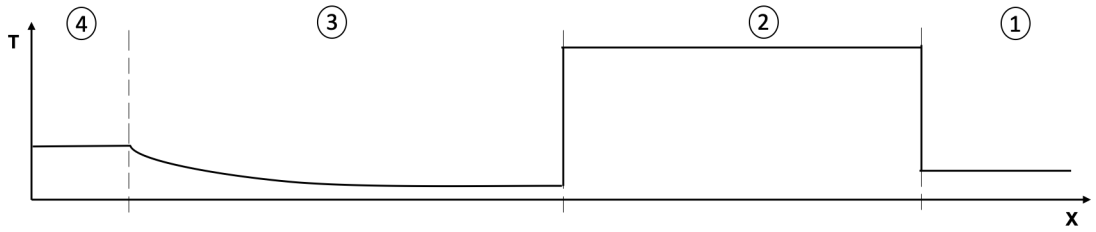

Figure 2.5: Temperature profile along the length of the tube

2.1.4 Density

Assuming ideal gas across the shock tube, $P = \rho RT$ is used for the calculation of density across the contact surface. Remembering that $P_3 = P_2$ it is possible to conclude that the density ratio is inversely proportional to the temperature ratio,

$$\frac{\rho_2}{\rho_3} = \left(\frac{T_2}{T_3}\right)^{-1} \tag{2.7}$$

However this would only be true if the gas was the same in the driver and in the driven section. Since the problem considered is studying the input of two different gases in the two different sections, the correct equation is,

$$\frac{\rho_2}{\rho_3} = \left(\frac{R_2 T_2}{R_3 T_3}\right)^{-1} \tag{2.8}$$

2.1.5 Mach number

Gaydon and Hurle [28], in 1963, developed equations for the the relations between the initial ratio of pressures with the shock Mach number and the ratio of temperatures across the shock wave and the shock Mach number, as it is possible to see in the following equations.

$$\frac{P_4}{P_1} = \frac{2\gamma_1 {M_s}^2 - (\gamma_1 - 1)}{\gamma_1 + 1}\left[1 - \frac{\gamma_4 - 1}{\gamma_1 + 1}\frac{a_1}{a_4}\left(M_s - \frac{1}{M_s}\right)\right]^{\frac{-2\gamma_4}{\gamma_4 - 1}} \tag{2.9}$$

$$\frac{T_2}{T_1} = \frac{\left[2\gamma_1 {M_s}^2 - (\gamma_1 - 1)\right]\left[(\gamma_1 - 1)M_s^2 + 2\right]}{(\gamma_1 + 1)^2 M_s^2} \tag{2.10}$$

These simplified equations led to the possibility of studying the critical pressure to which the flammable driver gas would auto-ignite. By knowing T_2 it was possible to calculate at what Mach number it would reach those temperatures and then calculate the minimum critical pressure to produce such shock wave.

2.1.6 Time

A shock wave is transient phenomena so it is time dependent as it is possible to understand through figure 2.3. As the shock Mach number increases, so does its speed and the lesser time the shock wave needs to travel through the length of the tube. The following equations explain just that, with M_s being

the shock Mach number, c_s the shock speed, a_1 the speed of sound through air, Δt the time the shock takes to travel the length of the tube, and l as the length of the tube.

$$M_s = \frac{c_s}{a_1} \tag{2.11}$$

$$\Delta t = \frac{l}{c_s} \tag{2.12}$$

Another thing to consider when addressing time is that spontaneous ignition inside the tube does not happen solely on the event of a large increase of temperature, sufficient mixing between the fuel and the oxidizing atmosphere is also necessary. This being said, one of the factors that influences mixing quality is time and the more time the reaction has, better mixing might occur. In conclusion, if we have two cases that produce the same Mach number but in one of the cases the tube is longer, the one with the longer tube will have a bigger reaction time, increasing the odds of a better mixture in the end, resulting in a much easier inflammation of the mixture.

2.1.7 Boundary layer influence

Although a lot of the properties' behaviour in the shock tube are explained in the above sections, none of the governing equations take into account the viscosity present in the gas.

Although the gas viscosity is mush less influential than the viscosity of a liquid, when considering flow inside a closed boundary, like a tube, specially when considering high-speed flows it is certain that the viscosity of the fluid will originate a boundary layer.

With the appearance of a boundary layer near the wall, as the flow develops through the tube, the shock wave will reflect off of it leading to the appearance of oblique shocks, resulting in a bigger increase of temperature of the fuel/air mixtures formed in the contact region. From figure 2.6, from Dryer et al. [12], as the normal shock travels through the tube, the boundary layer thickens, leading to a bigger increase of temperature and a straightening of the shock. This increase of temperature is due to the interactions of the normal shock with the boundary layer. Due to growth of the boundary layer, the normal shock cannot extend fully to the walls of the tube causing reflected oblique shocks of of the boundary layer which will interact with the flow causing more compression and thus more temperature growth . With this, the normal shock grows smaller and smaller as the boundary layer thickens slowing the flow down to the sonic point.

From figure 2.6 it is possible to identify four different steps to the flow of a shock wave in a tube. In the first schematic, the configuration prior to the burst of the disk which is separating the high-pressure flammable gas from the atmosphere. In the second one, the burst of the disk which originates the multidimensional shock and the formation of the fuel/air mixture. In the third, the interactions between the reflected and the contact surface enhance the mixing. Finally in the last one it is possible to see the convergence of the reflected shocks at the centerline lead an increase of temperature. The light grey near the tube walls represent the growth of the boundary layer with the flow development.

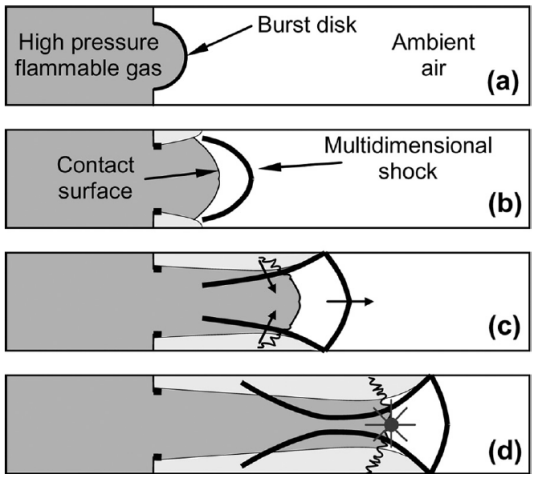

Figure 2.6: Development of a normal shock in a duct after the burst of a disk that was once separating a high-pressure flammable gas from the ambient air, from Dryer et. al[12]

2.2 Analytical calculations

When discussing any engineering topic, verification of the results studied is one of the most important steps to be made. However, in this particular case, the analytical study on the effects of the length of the tube on the various properties exhibited on the previous section is very difficult as there are no functions yet to be able to comprehend the effects that it has. For this reason, this subject is going to be addressed by the numerical experiment.

By better observing the equations mentioned in the previous section, it is possible to conclude that the only equation that complements the length of the tube is equation 2.12, which calculates the time it takes for the shock wave to travel through a certain length (l) at a certain shock speed (c_s). This shock speed derives from the shock Mach number in equation 2.11, which is the quotient between this speed and the speed of sound through air (a_1). This means that the only connection there is between the length of the tube is through the shock Mach number, which is influenced by the initial pressure ratio in equation 2.9, and influences the temperature across the shock ratio through equation 2.10. Therefore, in this section the calculations made will mostly be around the effects of the properties on the shock Mach number and its influence on the properties inside the tube. Also considering that the shock wave is the indirect leading cause for spontaneous ignition, through shock heated mixture, and that the main cause that leads to the shock wave is the initial pressure ratio, this study will focus primarily on equations 2.9 and 2.10.

2.2.1 Influence of pressure on the shock wave

When speaking about shock waves in tubes, the difference of pressure between the high-pressure and low pressure regions is crucial to be addressed. Although this is not the only thing that can lead to a shock wave, it most certainly is one of the main aspects that influence it.

Through Bernoulli principle (2.13), at constant elevation, we have that if P_1 is greater than P_2, $V2$

will be greater than $V1$. This means that, when we have a high-pressure gas confined and separated, by a wall, from a low-pressure gas, if the separating wall is removed, the flow will move in the direction of the low-pressured gas in order to try and find an equilibrium. As Le Chatelier claims "If a dynamic equilibrium is disturbed by changing the conditions, the position of equilibrium moves to counteract the change".

Looking at the previous subsection for pressure (2.1.2) we can observe through the equations that, even if P_4 is increased or decreased, the ratio of P_3/P_4 will not change much from the ratio P_2/P_1 which will increase proportionally with P_4/P_1. However, the only thing that changes in figure 2.4 is that when P_4 is increased, the jump from region 2 to region 1 will be bigger.

$$P_1 + \frac{1}{2}\rho {v_1}^2 = P_2 + \frac{1}{2}\rho {v_2}^2 \tag{2.13}$$

As previously mentioned, when we increase the pressure difference, the flow speed increases as well which leads to a bigger Mach number. Through equation 2.9 this is easily provable. Using the values from table 2.1, we can calculate the values for the speed of sound in the air, in the driven section (a_1) and, using the values for all the other gases we can do the same but for the driver section using equation 2.1 and constant initial temperature of 300K.

Species	Speed of sound (m/s)
Hydrogen	1316,4
Methane	451,5
Ethane	311,8
Propane	251,9
Butane	215,6
Air	346,1

Table 2.2: Speed of sound, a, through various gases

With these values it is possible to calculate through equation 2.9 the values of the shock Mach number, assuming a shock wave is formed. As shown in figure 2.7 we can see that as we raise the initial pressure ratio P_4/P_1, which corresponds to the increase of the pressure in the driver section as P_1 is left as atmospheric, the Mach number goes up, which means the higher the initial pressure ratio, the stronger the shock wave.

Another observation that can be made is that apart from hydrogen, every other gas studied increases its Mach number much slower which means that, since their auto-ignition temperatures are more or less in the same range (between 678K for butane and 853K for methane), in order to achieve spontaneous ignition, it is going to need a much higher input of initial pressure ratio to achieve such temperatures.

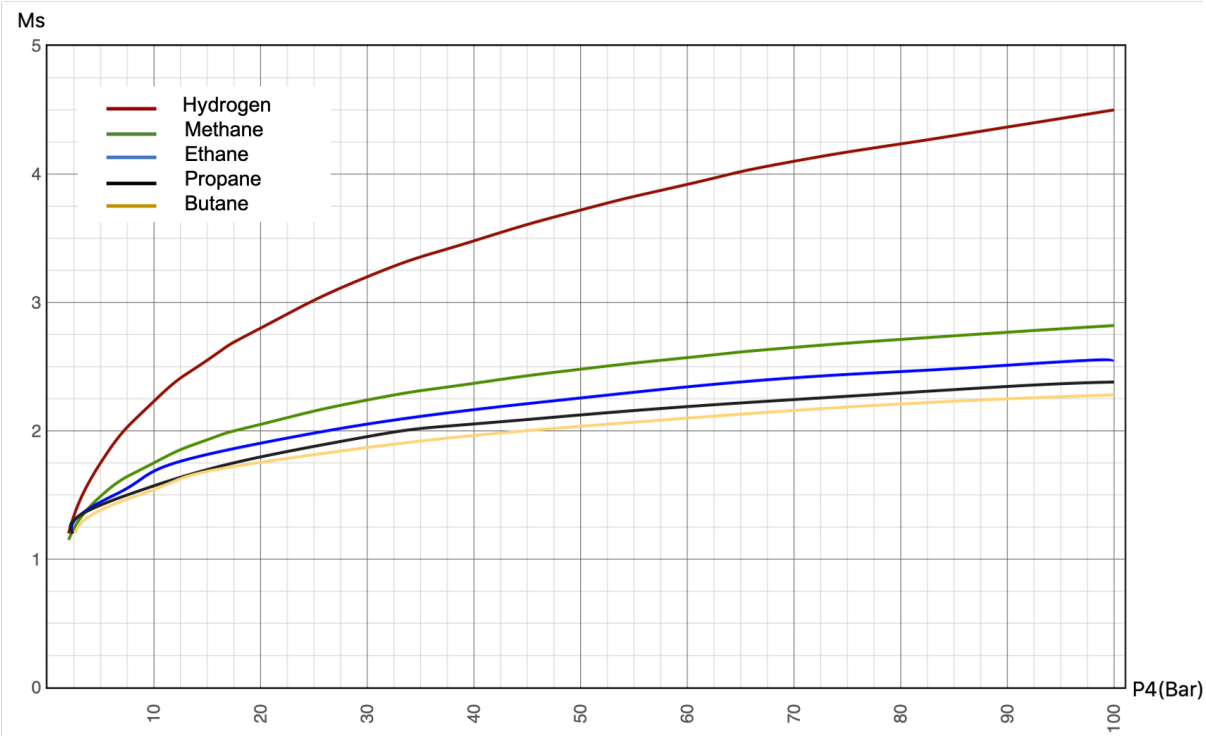

Figure 2.7: Shock wave Mach number(M_s) as a function of the driver pressure(P_4), using equations 2.9

Equation 2.10 gives the ratio of temperatures across the shock, depending on the surrounding environment and the shock Mach number. Knowing the spontaneous ignition temperatures and using this equation, it is possible to calculate the necessary Mach number in order to achieve these temperatures. By calculating these shock Mach numbers it is also possible to know the required pressure in order to produce such shock waves. This pressure is called critical pressure of ignition. As table 2.3 shows for various common gaseous fuels studied, even though the auto-ignition temperatures are not that different, the critical ignition pressure varies a lot, specially comparing hydrogen to the rest of the species.

Gas	Known substance parameters			Calculated Values	
	Auto-ignition temperature (K)	Adiabatic exponent	Universal Gas constant	Mach number	Critical ignition pressure (bar)
Hydrogen	773	1.41	4124.2	2.91	22.5
Methane	853	1.32	518.28	3.15	187.9
Ethane	788	1.18	276.51	2.97	259.8
Propane	728	1.13	188.56	2.79	286.4
Butane	678	1.09	143.05	2.64	276.0

Table 2.3: Theoretical critical pressure of ignition of common gaseous fuels

2.2.2 Influence of pressure on temperature

Like previously mentioned, pressure difference is one of the main properties to consider when talking about shock waves. When discussing spontaneous ignition by diffusive mixing, this property gains even more focus as it affects everything, directly and indirectly. One of the factors that affects directly is

temperature as can be observed from section 2.1.3. However, it also affects it indirectly through the shock Mach number as described in equation 2.9 in section 2.1.5.

As it is possible to calculate the critical ignition pressure through the previous knowledge of the auto-ignition temperatures, it is also possible to do the opposite route by calculating the temperature of the mixture behind the shock wave with the initial pressure ratio.

As it is observed in figure 2.8 temperature, much like the Mach number, increases with the initial pressure ratio as it was expected from the fact that a stronger shock wave, delivers a bigger temperature ratio across the shock.

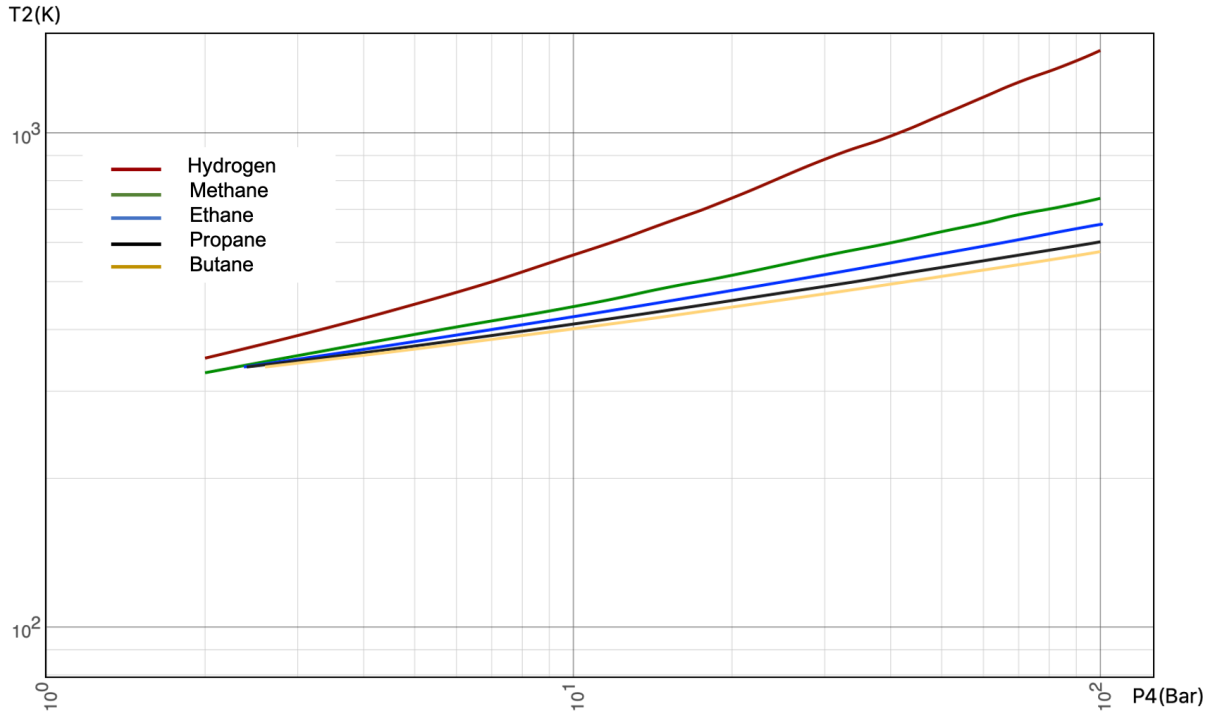

Figure 2.8: Temperature behind the shock wave(T_2) as a function of the driver pressure(P_4), using equations 2.9 and 2.10

When analysing the figure in more detail, hydrogen temperature increases at a much faster rate than other common gaseous fuels which explains how carefully it needs to be handled. As previously mentioned it is much easier to self-ignite than other fuels as the hydrogen-air mixture reaches its critical temperature at much lower pressure difference. As Dryer et al.[12] managed to get hydrogen ignition at only 20.6 bar whereas for methane, with an ignition at 853K, it needs a gas phase driver pressure closer to 200 bar.

Another thing that is easily noticeable is the fact that methane, ethane, propane and butane curves evolve much slower than the hydrogen curve. While methane and hydrogen appear to be capable of reaching compression values of P_4 to cause ignition, ethane, propane and butane being liquefied gaseous fuels, are unable to reach the necessary driver pressures to do so.

Methane can be stored in the physically adsorbed state at around 35 bar and hydrogen production plants usually store and transport hydrogen at about 20 to 25 bar. Since the other studied gaseous fuels behaviour, at this range of pressures, is very similar to methane, future calculations as well as the

numerical experiment, will be on hydrogen and methane for the 5 to 40 bar range in order to preform a study on real life examples.

In the next section, calculations on both hydrogen and methane will be made for initial pressures of 5, 10, 20, 30 and 40 bar in order to, in chapter 4, preform a numerical verification with the results from the CFD experiment.

2.2.3 Analytical calculations for hydrogen and methane

In this subsection, two tables will be presented with all the calculations that will be used to verify the numerical experiment done in chapter 4. For this, governing equations such as 2.2, 2.3, 2.4, 2.6, 2.8, 2.9, 2.10 and 2.11 will be used. One thing to keep in mind is that all the calculations are going to be executed with constant initial temperature on either side of the shock-tube at rest, at 300k, and that the driven section pressure is always constant at 1 atm.

Just like it was expected, from the previous sections, hydrogen evolves in a much more abrupt manner than methane in any of the properties studied. This proves the fact that hydrogen can be much more dangerous than methane or many other gaseous fuels at lower pressures, just by looking at the ratio of Mach numbers produced for increasing initial pressures. This causes the temperature to spike much more in the presence of hydrogen, as we can see from the tables, where it is expected for hydrogen to spontaneously ignite at about 20 bars of pressure.

Although not present in the table, another property to be considered in the calculations is the time the shock wave takes to travel through the tube. Even though it is something that is not considered in the governing equations, it is quite straightforward to see that if the length of the shock tube is the same but the pressure input changes, so will the shock wave change. If the pressure increases a stronger shock wave will be produced, as observed in the table by the ratio of P_2/P_1. With this increase in strength so will the Mach number increase which means that, for a stronger shock wave, faster outward flow will be produced and it will take less time for the shock to travel through the tube.

In conclusion, the most probable way to achieve spontaneous ignition of rapid release of a high-pressure combustible gaseous fuel into an oxidizing atmosphere, is to have the perfect combination between initial pressure and time for mixing. However, even though it is affected by both of these conditions, the crucial one is initial pressure as it is the one that allows the mixture to reach the auto-ignition temperatures, which means that bellow a certain pressure, auto-ignition is impossible to occur through diffusive ignition.

Hydrogen	$P_4/P_1(Bar)$:	5	10	20	30	40
Properties:						
Mach number (M_s)		1.75	2.23	2.80	3.20	3.48
Shock speed (c_s)		605 m/s	772 m/s	969 m/s	1108 m/s	1204 m/s
Shock strength (P_2/P_1)		3.43	5.64	9	11.65	13.86
Expansion strength (P_3/P_4)		0.686	0.564	0.450	0.388	0.347
Expansion Temp. ratio (T_3/T_4)		0.896	0.847	0.793	0.759	0.735
Expansion Temperature (T_3)		267 K	252.4 K	236.3 K	226.2 K	219 K
Contact Surf. Temp. Ratio (T_3/T_2)		0.593	0.446	0.320	0.256	0.223
Shock wave Temp. ratio (T_2/T_1)		1.510	1.899	2.477	2.966	3.302
Shock heated Temperature(T_2)		450 K	566 K	738 K	884 K	984 K
Density ratio (ρ_2/ρ_3)		8.526	6.407	4.601	3.677	3.198

Table 2.4: Hydrogen calculations for the shock tube numerical verification

Methane	$P_4/P_1(Bar)$:	5	10	20	30	40
Properties:						
Mach number (M_s)		1.49	1.75	2.05	2.24	2.37
Shock speed (c_s)		516 m/s	606 m/s	710 m/s	775 m/s	820 m/s
Shock strength (P_2/P_1)		2.43	3.44	4.75	5.67	6.39
Expansion strength (P_3/P_4)		0.486	0.344	0.238	0.189	0.159
Expansion Temp. ratio (T_3/T_4)		0.839	0.772	0.706	0.668	0.640
Expansion Temperature (T_3)		250 K	230.1 K	210.4 K	199.1 K	190.7 K
Contact Surf. Temp Ratio (T_3/T_2)		0.639	0.517	0.409	0.353	0.318
Shock wave Temp. ratio (T_2/T_1)		1.312	1.493	1.728	1.893	2.01
Shock heated Temperature(T_2)		391 K	445 K	515 K	564 K	599 K
Density ratio (ρ_2/ρ_3)		1.154	0.934	0.737	0.637	0.575

Table 2.5: Methane calculations for the shock tube numerical verification

Chapter 3

Numerical Model

In the present chapter the numerical implementation of the experiment will be approached. This chapter serves the purpose of showing and explaining the process behind the CFD work.

3.1 Problem statement

As previously mentioned in chapter 2, the flow inside a tube is affected by viscous effects. Since the study of this problem revolves around what happens inside the shock tube in terms of pressure, temperature, density and velocity with the change of tube length a simple 1D fluid dynamics approach should be sufficient. However, when considering high speed flow inside closed boundary, viscous effects must be considered and so, even though the governing equations do not present a dependency of viscosity, it must be taken into account that flow, specially near the walls of the tube, might be affected by the boundary layer.

3.1.1 Implementation of the numerical model

The computational work was done through Ansys platform. The student version was downloaded in order to pursue the CFD work, which allowed geometries with meshes up to 512k nodes which would be enough to model the case studied. Although the Ansys workbench possesses a lot of CFD programs that allow the user to study a big array of different aspects, considering the problem being studied, the approach needed was one that studied fluid flow and for this a program called Fluent, which has been used to study the flow inside pipes, was used.

Through the use of Fluent, two cases where studied. In the first case, a shock tube was designed with a specific length in order to test the equations from the previous chapter where only the initial pressures were changed. This allows the verification of the values calculated prior and the verification of the boundary conditions applied. The length used in the tube was 1 meter where it was divided equally into two sections creating a driver and a driven section with 0.5m each and a diameter of 0.02m. Although the dimension seems very big considering the proposed problem, it was only used for comparison grounds. The driver was then initialized with 5, 10, 20, 30, and 40 bar in order to verify the calculations made

prior.

In the second case, the effects of the length of the tube are studied. This is done by varying the length of the tube while the pressure applied to the driver section remains the same, allowing the comprehension of the effect that the length of the tube might have on the properties studied, in the event of a rapid release of high-pressure combustible gas. The pressure in the driver section always remained at 20 bar while the length of the tube varied from 0.360m, 0.420m and 0.480m divided by the two sections, driver and driven, equally sized. While the first case was studied for methane/air and hydrogen/air mixtures, the second case was only studied for hydrogen.

3.2 Computational Model

Throughout this section, everything that was done in the program Ansys fluent is going to be thoroughly addressed in order to better understand the process that lead to the CFD analysis.

3.2.1 Geometry

As mentioned in the previous section, two cases were elaborated to study two different approaches to the problem. This lead to the projection of two different geometries. However, the way that they were executed was the same.

In order to design the geometry to be studied through fluent, 2 different modelers can be chosen, DesignModeler and SpaceClaim. As SpaceClaim is widely used to produce 3D geometries and is much more recent than DesingModeler, which incurs in more program errors, DesignModeler was the chosen editing software to create the 2D geometry.

In order to model a shock tube, first a rectangle was designed and transformed into a face with the dimensions presented in the following table,

Case studied	Diameter (m)	Length (m)	Pressures studied (bar)
Effect of pressure on the studied properties	0.02	1	5; 10; 20; 30; 40
Effect of the tube lenght on the studied properties	0.02	0.36; 0.42; 0.48	20

Table 3.1: Dimensions of the designed rectangle to model the shock tube.

After designing the rectangle and turning it into a face from the sketch to face tool, face split was used in order to divide the face into two equally sized sections at the center of the coordinate system, thus creating the driver and driven section. Since the division of the face is in the origin of the coordinate system, the driver section extends its length from $\frac{-length}{2}$ to 0 on the x coordinate and the driven section from 0 to $\frac{length}{2}$ on the x coordinate. The diameter is also divided into 2 where the half of it is in the

positive side of the y axis and the other half of it in the negative side of the y axis making the shape symmetric on both coordinates.

3.2.2 Meshing

When working with CFD, one of the most important and influential parts of the study is the meshing. Meshing or grid generation is the act of subdivision a continuous geometric space into discrete geometric and topological cells. This is done so that, when solving a problem, the solution it is as detailed as possible. Which means that, the more divided the continuous geometry, the more detailed the solution. However, as mentioned in section 3.1.1, the Fluent student version only allows the user a maximum of 512k nodes.

Grid refinement study

When meshing a geometry in order to get a solution, a grid refinement study is always necessary. What this does is, as you refine the mesh and check the solution, there will be a certain threshold above which the solution does not change anymore. When this happens the mesh presented is the one that is best to use. Such process is shown in figure 3.1. Since there are two cases being studied with different dimensions,

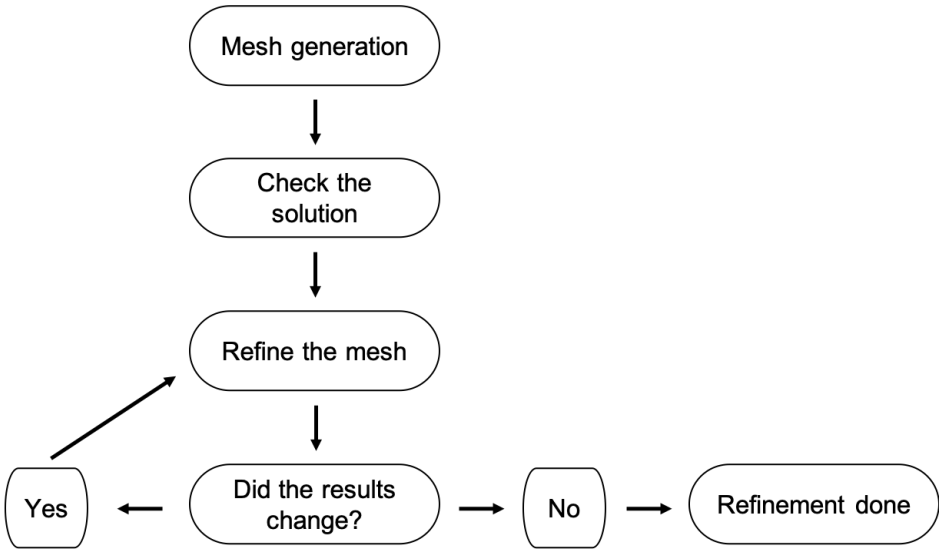

Figure 3.1: How to do a grid refinement study.

there was the need to do a grid refinement study for each case. Luckily enough, while studying the mesh for each case, the solution was converging as the mesh was refined, which means that, even though it might not be completely refined, due to the maximum nodes allowed, it converged.

Mesh tab

After completing the design of the tube, we pass on to the mesh tab where two thing are executed. The mesh/grid refinement study and attributing names to the various sections of the the design.

In order to mesh, there were two steps to be done, the first being face meshing. Since the rectangle was split into two sections, there were 2 sections to face mesh where the shape of elements chosen was

quadrilaterals, in order to not exceed the number of elements allowed and to have an uniform mesh. After face meshing, sizing of each side of the design was applied. This step allows the user to choose the size of the elements or simply choose the number of elements it desires. It also allows the user to choose if they want an uniform spacing of the element or the majority of the elements to converge to a certain place. In this case it was meshed uniformly throughout its length. Since there was a total of four designs to mesh, one for the case where the effect of the initial pressure is tested and the other three where the effect of the length of the tube was tested, it was required that all four undergo a mesh refinement study and the results are presented in the table as follows.

	Diameter (m)	Length (m)	Element Size (m)	N° of elements	N° of Nodes
Case 1	0.02	1	$2e^{-4}$	$5.01e^{5}$	$5.05101e^{5}$
Case 2	0.02	0.36	$1.2e^{-4}$	$5.01e^{5}$	$5.04168e^{5}$
		0.42	$1.29e^{-4}$	$5.07936e^{5}$	$5.11349e^{5}$
		0.48	$1.3856e^{-4}$	$5.0257e^{5}$	$5.06182e^{5}$

Table 3.2: Mesh characteristics, after refinement study, for every case studied.

After completing the mesh, the various sections of the design were labeled and since the design was always the same (only the dimensions changed), the labels were always named the same as it is possible to see in figure 3.2. This process is called named selections and is done in order to better identify the different regions studied in the solution.

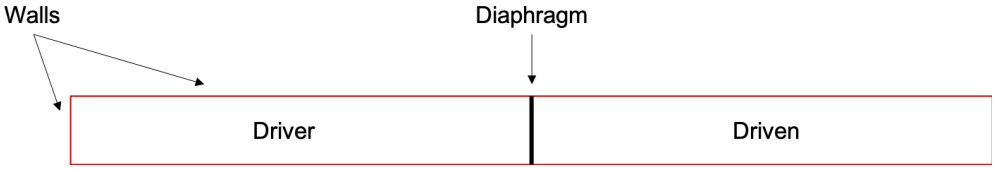

Figure 3.2: Labels attributed to the different parts of the design

3.2.3 Setup

When solving a problem in fluent, the setup tab is one of the most important steps as it is where the user establishes every condition for the problem such as flow type, type of base solver, steady or unsteady, boundary conditions, etc.

In order to get the best solution, when opening the setup tab, a menu appears and for this case, double precision was picked in order to get better results with four solver processes in parallel. This allows the solution to be computed much faster as it divides the mesh by the number of solvers and each solver focuses only on that section of the mesh.

Since this problem studies the formation of a shock wave inside a closed boundary, density-based solver is chosen. This solves the continuity, energy and species equations simultaneously coupled together. This

solver is widely recognized as the best one to solve high-speed compressible flows and shock resolution problems. Figure 3.3 explains how the density-based solver works in steps.

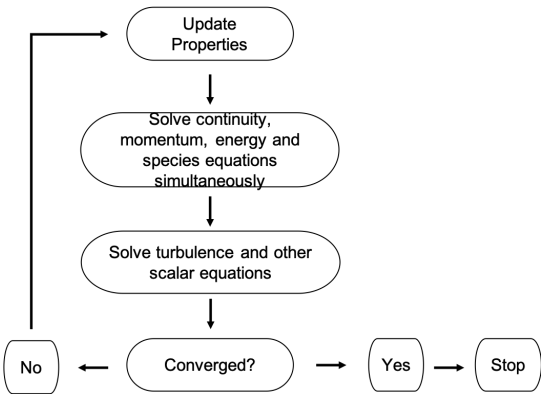

Figure 3.3: Density-based solver steps for calculating a solution from fluent guide [29]

The case studied is presented with a travelling shock wave through time, so in to order study such phenomena, transient flow was selected.

Since the flow over a shock wave is being studied, energy equation must be selected and since we are in the presence of compressible flow, in order to calculate the density properly, ideal gas law must be used in order to use the previously mentioned ideal gas equation $P = \rho RT$. Another assumption to be done is considering the tube adiabatic, so that there is no heat transfer between the tube and the surrounding atmosphere.

As the flow is only being studied for the inside of the tube, it could be possible to assume inviscid flow. However, Shapiro [25] demonstrated that a moving shock wave inside a tube is affected by the boundary layer near the walls, creating oblique shocks (figure 3.4) and adding heat to the mixture through viscous heating.

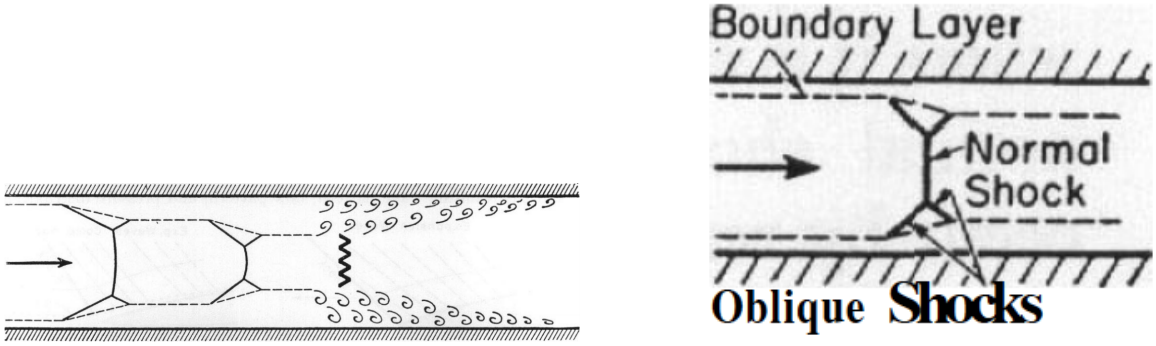

Figure 3.4: Example of the existing boundary layer in the presence of a shock inside a tube. From Shapiro [25]

This being said and considering that the flow is only analysed inside the tube, turbulent flow has to be used. As the flow inside the shock tube will produce velocities of up to 1200m/s with low viscosity($10e^{-5}$ range), it will produce Reynolds numbers on the range of $10e^{4}$ which is well above the values stated for the transition from laminar to turbulent (turbulent flow from Re>4000 [26]). So in order to study turbulent flow RANS was chosen over LES as it would take a lot more time to solve the problem. For

this k- ω standard turbulent model [29] was chosen. This is a two equation model that allows two extra transport equations to represent the turbulent properties of the flow which allow the account of the effects of convection and diffusion turbulent energy. So adding to the continuity, momentum, energy and species equations, Fluent now solves 6 transport equations. Fluent presents all of the constants and they were remained as default with the following values in 3.5 for the turbulent model.

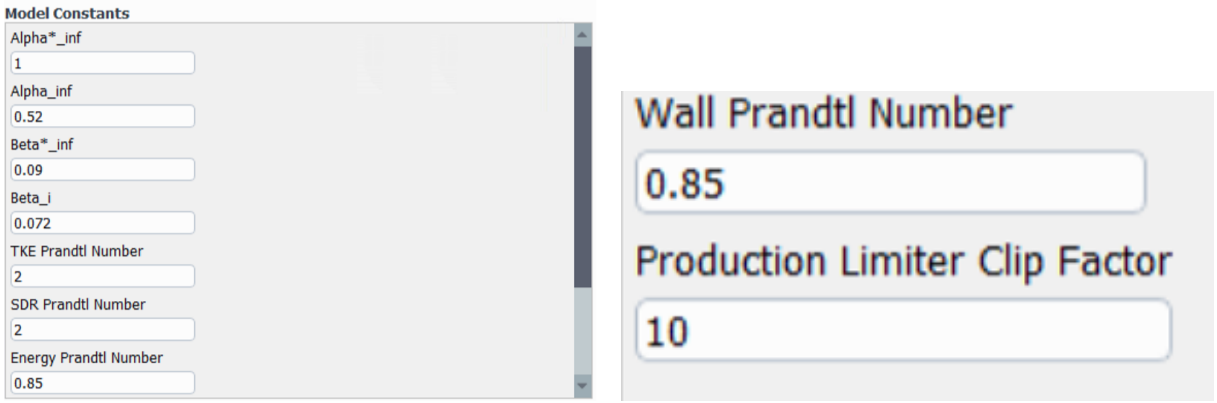

Figure 3.5: K-w standard turbulence model default constants taken from fluent [30]

Since there is viscosity, the one picked was Sutherland's viscosity where each species' viscosity is calculated by using a common equation which computes the dynamic viscosity of the species with the absolute temperature of an ideal gas, as said in the fluent manual [29]. Species transport was enabled where, like previously said, the mixtures hydrogen/air and methane/air were studied as ideal gas.

Considering that ideal gas was the density method chosen, the boundary conditions operating pressure had to be set to 0 so that the solution could be initialized with the absolute pressure.

In the methods tab, the chosen formulation was Roe-FDS scheme. The time formulation picked was implicit as it solves the problem of stability, for this the courant number was left untouched and remained default with the value of 5. Second order upwind for the discretization was selected as it provides optimum accuracy.

After the selection of all the parameters described above, it was required that the solution was initialized. This gives the program the initial values and conditions that it requires to start the solution. Therefore, since the initial conditions are known, initial temperature, initial pressure and initial mass fractions were patched.

In the driver section the initial high-pressure gas (methane and hydrogen) was patched with the corresponding pressure. For the first case studied, the high-pressure input was 5, 10, 20, 30 and 40 bar while the pressure input for the second case remained at 20 bar throughout the study of the different lengths with only hydrogen as the gas studied. In this same section, the mass fractions of hydrogen and methane were patched with the value of 1 in order to initialize the driver with only these 2 gases. In the driven section atmospheric pressure was patched for all cases and the mass fractions were patched as 23% O_2 and 77% N_2. Both sections were patched with the same initial temperature of 300K.

After initializing, the only step left to do was to run the calculations. For this a total of 100 time steps with 20 iterations each was selected, granting a total of 2000 iterations. The time-step was chosen

by trial-error until the scaled residuals presented the best convergence possible.

In order to gather all of the information above, the following table 3.3 presents all of the assumptions made in an organized fashion for better understanding.

Propertie	Assumption
• Double Precison	Yes
• Solver Processes	4
• Type	Density-based solver
• Time	Transient
• Energy equation	On
• Species transport	On (H2/air and CH4/air)
• Viscous flow type	K-w standard turbulence model
• Heat exchange	No
• Density	Ideal gas law
• Viscosity	Sutherland
• Boundary conditions	0 operating pressure
• Formulation	Implicit
• Flux type	Roe-FDS
• Flow discretization	Second-order upwind
• Courant number	5
• Solution initialization:	
○ Pressure	5/10/20/30/40 atm – Driver 1 atm – Driven
○ Temperature	300K across both sections
○ Mass fraction	H2 and CH4 as 1-Driver O2 as 23% and N2 as 77%-Driven
• Time step size	Dependent on the case
• Number of time steps	50
• Iterations per time step	20
• Total number of iterations	1000

Table 3.3: Table presenting all of the assumptions made in order to setup the best solution to study the problem.

3.2.4 Governing transport equations

As Fluent is a CFD analysis software, not only does it allow to run several different analysis, but the governing transport equations are also much more complex than the ones used in the analytical approach, as all of them derive from the Navier-Stokes equations.

With the current implementation of the numerical model, Fluent solves 6 different transport equations in time due to the fact that it is a transient analysis. The equations that Fluent solves are: continuity for mass conservation, the momentum conservation, the energy equation, the species transport equation and since a 2 equation turbulence model is used, an equation for turbulence kinetic energy and another for the specific dissipation rate are used. All of the following equations and information were taken from the Fluent manual [29].

Continuity equation

Fluent solves, for all flows, the conservation equation for mass. This equation, also called continuity equation, can be written as follows:

$$\frac{\partial \rho}{\partial t} + \nabla \cdot (\rho \vec{v}) = S_m \tag{3.1}$$

This equation is the general form of mass conservation equation which is valid for incompressible and compressible flows. Since this is a problem with compressible flow, the equation can be applied. S_m represents the mass added to the continuous phase and any user-defined sources, which is equal to zero since there is no added mass to the system.

Momentum equation

Besides the conservation equation for mass, Fluent solves the momentum equation for all flows as well. This equation can be written as follows:

$$\frac{\partial}{\partial t}(\rho \vec{v}) + \nabla \cdot (\rho \vec{v}\vec{v}) = -\nabla p + \nabla \cdot (\overline{\overline{\tau}}) + \rho \vec{g} + \vec{F} \tag{3.2}$$

where p is the static pressure, $\overline{\overline{\tau}}$ is the stress tensor and $\rho \vec{g}$ and $\vec{F}$ are the gravitational body force and external body forces respectively. Considering the problem in question, $\rho \vec{g}$ and $\vec{F}$ are ignored.

Energy equation

As seen from the implementation, the energy equation is enabled. Fluent solves this equation in the following form:

$$\frac{\partial}{\partial t}(\rho E) + \nabla \cdot (\vec{v}(\rho E + p)) = \nabla \cdot \left(k_{eff} \nabla T - \sum_j h_j \vec{J}_j + (\overline{\overline{\tau}}_{\text{eff}} \cdot \vec{v}) \right) + S_h \tag{3.3}$$

where k_{eff} is the effective conductivity that complements turbulent thermal conductivity, which is defined by the turbulent model used. $\vec{J}_j$ is the diffusion flux of species j and the first 3 terms of the right side of the equation represent energy transfer due to conduction, species diffusion, and viscous dissipation,

respectively. S_h includes the heat of the chemical reaction, which is zero since it is an adiabatic reaction. E is defined as:

$$E = h - \frac{p}{\rho} + \frac{v^2}{2} \tag{3.4}$$

where the sensible enthalpy, considering that ideal gas is used, is defined as:

$$h = \sum_j Y_j h_j \tag{3.5}$$

where Y_j is the mass fraction of the species j and h_j its entalphy at the local temperature defined as:

$$h_j = \int_{T_{\text{ref}}}^{T} c_{p,j}\, dT \tag{3.6}$$

with T_{ref} as 298.15K.

Species transport equation

Since the numerical work is done with the transport of mixture through a closed boundary, species transport must be enable so that two different gas can be run for the same geometry (fuel and air). With species transport enabled, Fluent predicts the local mass fraction of each species, Y_i, through the solution of a convection-diffusion equation. This conservation equation can be written with a general form as:

$$\frac{\partial}{\partial t}(\rho Y_i) + \nabla \cdot (\rho \vec{v} Y_i) = -\nabla \cdot \vec{J_i} + R_i + S_i \tag{3.7}$$

Where R_i and S_i represent the rate of production of species i by chemical reaction and the rate of creation by addition of the dispersed phase, respectively.

Transport equations for standard k-w turbulence model

As mentioned before the standard k-w model used by Fluent is a two equation turbulence model. This is based on the Wilcox k-w model, which incorporates modifications for low-Reynolds-number, compressibility and shear flow spreading. It is based in an empirical model based on the transport equations of turbulence kinetic energy and specific dissipation rate, k and w respectively. Over the years this model as been updated, where production terms have been added to both equations, improving the model to predict free shear flows. For all of the reasons mentioned above, it was the turbulence model used as it complements what is needed to be studied in this problem.

The turbulence kinetic energy, k, is calculated from the following equation:

$$\frac{\partial}{\partial t}(\rho k) + \frac{\partial}{\partial x_i}(\rho k u_i) = \frac{\partial}{\partial x_j}\left(\Gamma_k \frac{\partial k}{\partial x_j}\right) + G_k - Y_k + S_k \tag{3.8}$$

while the specific dissipation rate, w, is calculated from the following equation:

$$\frac{\partial}{\partial t}(\rho w) + \frac{\partial}{\partial x_i}(\rho w u_i) = \frac{\partial}{\partial x_j}\left(\Gamma_w \frac{\partial w}{\partial x_j}\right) + G_w - Y_w + S_w \tag{3.9}$$

In these equations G_k and G_w represent the generation k and w, respectively. G_k is due to mean velocity gradients. Γ_k and Γ_w represent effective diffusity of k and w, respectively. S_k and S_w, as from previous equations, are user defined source terms. Since the model used was run with default values mentioned in figure 3.5, all of the user defined source terms are ignored.

With these equations and assumptions from table 3.3, Fluent was run and the results were displayed in the next chapter.

Chapter 4

Results and discussion

Two cases are going to be highlighted. The first one where only the initial pressure is changed, maintaining the length of the tube, which will be verified with the analytical calculations, and the second one where the length of the tube is tested to see what happens to the properties inside the tube.

4.1 Problem Description

Besides pressure relief systems, when handling high-pressure gas inside vessels, damaging, misusage of valves, human error or even just erosion caused by time can lead to rapid-release of the flammable gas into the atmosphere and this could lead to inflammation or even deflagration like it was addressed in chapter 1.

This thesis serves the purpose of studying not only why this happens as well as if the length of the hole affects in any way possible the properties inside the hole.

In the previous chapters, it was explained why can spontaneous ignition occur from rapid release of high-pressure flammable gas. In this chapter, the results of the CFD experiment are going to be shown in order to better understand and visualize what happens inside the tube that leads the high-pressure gas into the atmosphere. As it is known, when the diaphragm bursts, its possible to define 4 regions inside the shock tube. Region 4 and 1, which are the initial regions, where region 4 represents the high-pressured reservoir and region 1 represents the atmosphere. Region 2 and 3 which are the regions across the contact surface, where region 2 is located behind the shock wave and region 3 is located behind the contact surface. The following figure 4.1 shows the 4 regions clearly.

In order to compare both results, from analytical work and CFD, a verification will be done for each individual case.

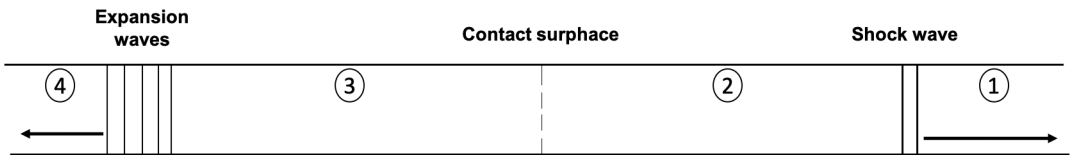

Figure 4.1: Diagram illustrating the different regions across the shock tube once the diaphragm bursts

4.2 CFD Results And Discussion

Since there are two case studies in this chapter, the first case, which is the one where the initial pressure is changed to see its effects on the shock wave properties, is going to be called case 1 from now on in order to facilitate the understanding of the study.

Much like case 1, the second case where the length of the tube is changed in order to study its effects on the shock wave properties, is going to be called case 2 from now on. Although case 1 is being studied for both hydrogen and methane, case 2 is only being studied for hydrogen due to, in section 2.2.3, it was proven that for a pressure of 22.5 bar, hydrogen would reach high enough temperatures to cause its ignition. For that matter 20 bar will be studied in order to see if it will be enough to cause spontaneous ignition now that viscous flow is used.

Since the pool of results is quite big as they were printed for two different gases, there will be a clear distinction between the cases as well as between hydrogen and methane.

Since the flow type considered in the CFD analysis is viscous, there will always be a difference in the values as the boundary layer affects the flow properties inside the tube. Moreover fluent solves the problem as transient with a certain set of equations, where the analytical calculations are done for a Lagrangian approach, implying a pseudo-steady state . This leads to different results. With the equations presented in the previous chapter it is possible to see a clear difference from the equations used in both approaches.

4.2.1 Case 1: Testing the effects of the initial pressure on the properties development inside the tube

As previously shown in table 3.3, the time step used to obtain the solution was dependent on the case.

Using implicit formulation, the courant number was set as 5 which is the default number. After this, the time step was calculated. However, the time step is not always correct at the first try, and by correct it means that it does not always print the best solution, which means that, to get the best solution, the time step must be changed by trial-and-error in order to get to the best one.

For case 1 we have always the same cell size for the entire structure, which means that the time step depends only on the velocity of the flow. It is known that by increasing the pressure on the high-pressure chamber, flow velocity will increase, which means that as the pressure is increased, the time step used for each solution must decrease as well.

In order to start the solution a first time step was calculated using the shock speed calculated by equation 2.11 with the values of the Mach number presented in table 2.4,

However, using these time step values for the calculation of the solution, led to a very fast and early convergence in which the results presented were not good. Since the iterations were converging too fast, the time step was increased for each case, leading sometimes to divergence until the correct one was chosen. After several tries, the time step that printed the best results was found.

Using these time steps led to flow velocities very different from the shock speed velocities as it would be expected. However, the results printed were a lot more refined which allowed for a better understanding of the problem.

Initial pressure ratio (Bar)	Cell size (m)	Shock speed (m/s)	Time step (s)
5	$2e^{-4}$	605	$3.31e^{-7}$
10		772	$2.59e^{-7}$
20		969	$2.06e^{-7}$
30		1108	$1.81e^{-7}$
40		1204	$1.66e^{-7}$

Table 4.1: Time step calculated for case 1 using the shock speed calculated in table 2.4

Initial pressure ratio (Bar)	Cell size (m)	Time step (s)
5	$2e^{-4}$	$3e^{-6}$
10		$3e^{-6}$
20		$2e^{-6}$
30		$1e^{-6}$
40		$9e^{-7}$

Table 4.2: Corrected time step for each solution studied

The following analysis were made by extracting the profiles for pressure, temperature, density and velocity. In these graphs the properties are analysed at the walls and in the interior of each section allowing for a more holistic analysis. For this it is possible to analyse the property values at the walls of the tube in shades of blue, while the inside of the tube is characterized in red for the driven section and in green for the driver section.

Pressure

For case 1, the input pressures vary while the length of the tube stays the same at 1 meter. As mentioned above, the initial pressure ratio input are 5, 10, 20, 30 and 40. In section 2.1 it is possible to see, through the equations presented, every single aspect of the shock tube properties, whether it is pressure, temperature, density or velocity, are all affected by the pressure difference created between the driver and driven section. By observing section 2.2 it is possible to see how the properties change as a function of the initial pressure ratio as it is presented in table 2.4.

With the assumptions shown in table 3.3 and the time step from the table 4.2, Fluent was run for each initial pressure ratio for the hydrogen/air mixture. From this configuration it was possible to extract the following figures showing the pressure profiles for each initial pressure at the last time step calculated.

Analysing figures 4.2 to 4.4 its possible to see the 4 different regions presented in 4.2. It is also possible to see several distinct things from the figures. The first thing is that, although the initial pressure ratio is increasing, the shock strength (P_2/P_1) does not follow with the same ratio, increasing less as the pressure input goes up. Another thing that is noticeable from the curves of the pressure profiles is that as the initial pressure increases, the pressure distribution inside the tube (in red) becomes more and more heterogeneous because of the increasing Reynolds number. Lastly, the assumption that $P_2 = P_3$ is no longer valid as there is some fluctuation of values. However, in order to be able to compare with the

analytical values, we will assume them as equal, using an average of both values.

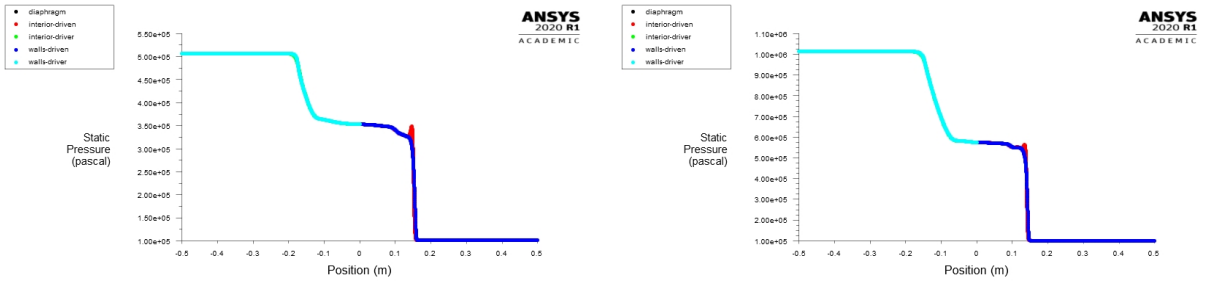

Figure 4.2: Pressure profiles computed using Fluent for initial driver pressures of 5 bar (left) and 10 bar (right) for hydrogen/air mixture for the last time step calculated.

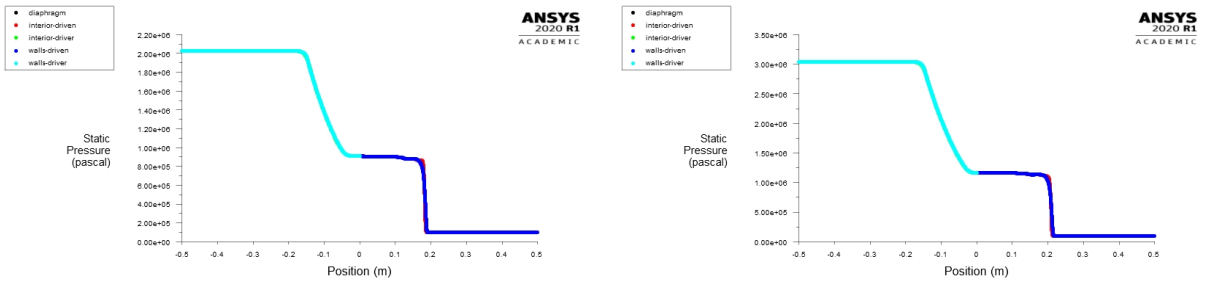

Figure 4.3: Pressure profiles computed using Fluent for initial driver pressures of 20 bar (left) and 30 bar (right) for hydrogen/air mixture for the last time step calculated.

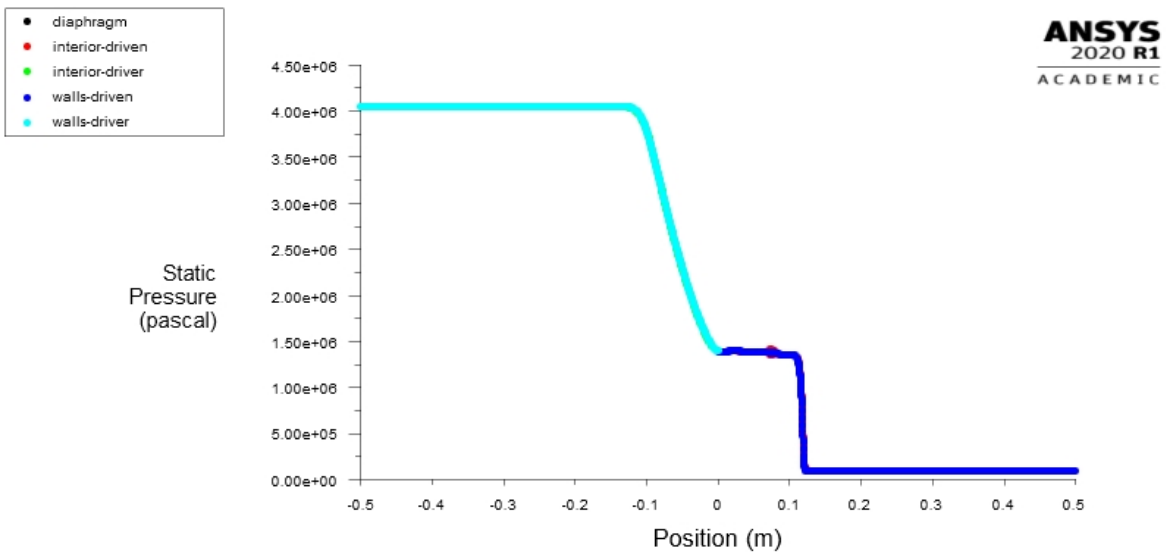

Figure 4.4: Pressure profile computed using Fluent for initial driver pressure of 40 bar for hydrogen/air mixture for the last time step calculated.

Considering viscous flow, pressure values can be different than the values calculated analytically. However, comparing the analytical results with the CFD for the pressure along the length of the tube we get very similar results. As there are four regions to consider but region 4 (Driver) and region 1 (Driven) are known, only region 2 and 3 will be analysed. As previously said, it is assumed that $P_2 = P_3$ so it is possible to compare the analytical calculations for this pressure with the one extracted from Fluent as it is shown in figure 4.5.

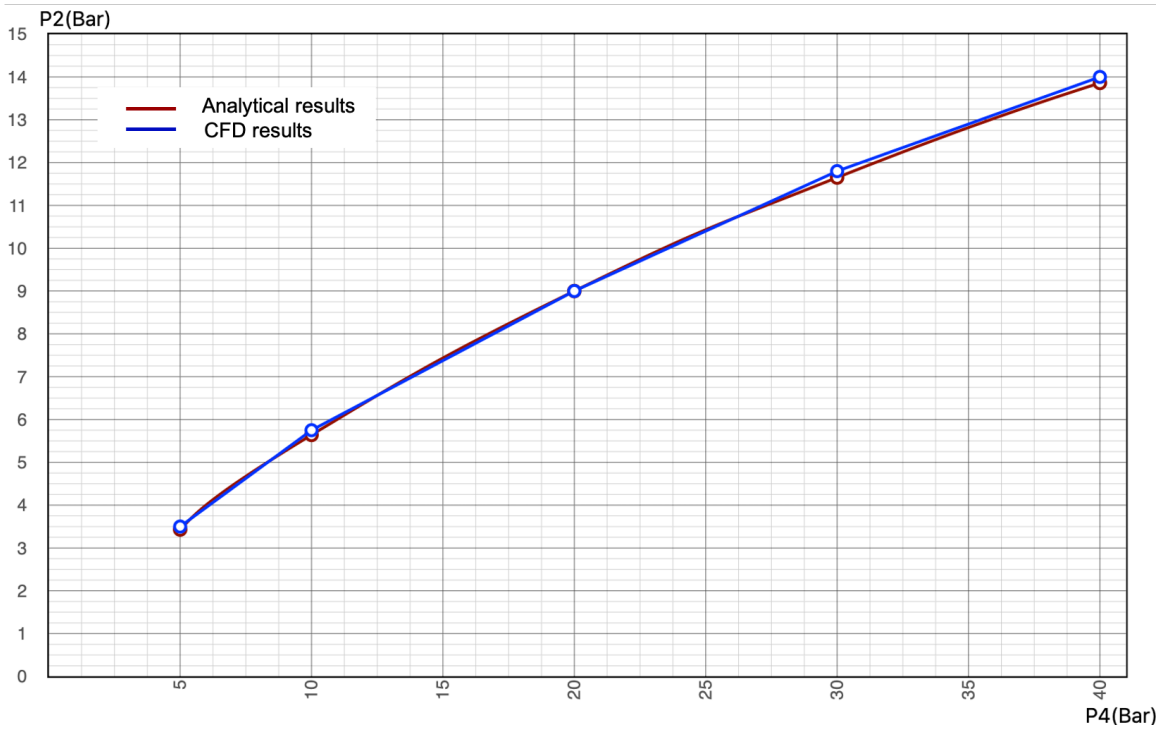

Figure 4.5: P_2 as a function of P_4 calculated analytically and through Fluent for hydrogen/air mixture for the last time step calculated.

Through observation of the graph, we can verify that the analytical model matches the CFD results. Considering the results extracted from Fluent as true, we can calculate the error percentage between the two sets of values through the following equation.

$$Percentage_{error} = \frac{V_{true} - V_{observed}}{V_{true}} \times 100 \tag{4.1}$$

This equation gives max percentile error of 2% as it possible to observe in the following table 4.3, which is a very good value as there is very little difference in both approaches.

Initial pressure ratio (Bar)	P2 analytical (Bar)	P2 Fluent (Bar)	Error %
5	3.43	3.5	+2.00
10	5.64	5.75	+1.91
20	9	9	0
30	11.65	11.8	+1.27
40	13.86	14	+1.0

Table 4.3: Percentage error calculation from the analytical approach vs the CFD approach for the pressure across the contact surface for hydrogen/air mixture for the last time step calculated.

Methane/air mixture in comparison with the hydrogen/air mixture, produce very similar pressure profiles. The four regions are clear and P_2 is very similar to P_3.

From the results obtained for hydrogen/air mixture, P_2, for the initial pressures studied, drops relatively close to half of the initial pressure and so $\frac{P_4}{P_3}$ and $\frac{P_2}{P_1}$ value is close to 2. However, when looking at the results from the methane/air mixture, the pressure at region 2 and 3 is much smaller, for example, when inputting 40 bar at the driver section, the pressure drops to 6.66 times less at the contact surface to an approximated value of 6 bar. This means that the shock strength produced my methane is much smaller than that of hydrogen. These observations can be seen in the following figures 4.6 to 4.8 which represent the pressure profiles for methane/air mixture for the initial pressures studied at the last time step calculated.

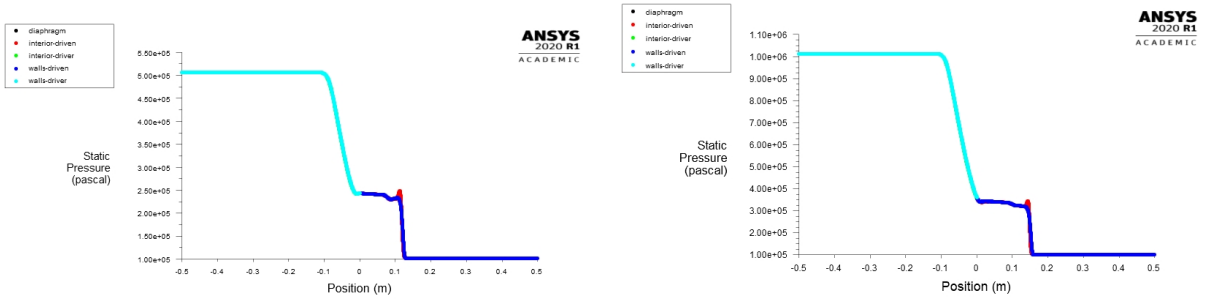

Figure 4.6: Pressure profiles computed using Fluent for initial driver pressures of 5 bar (left) and 10 bar (right) for methane/air mixture for the last time step calculated.

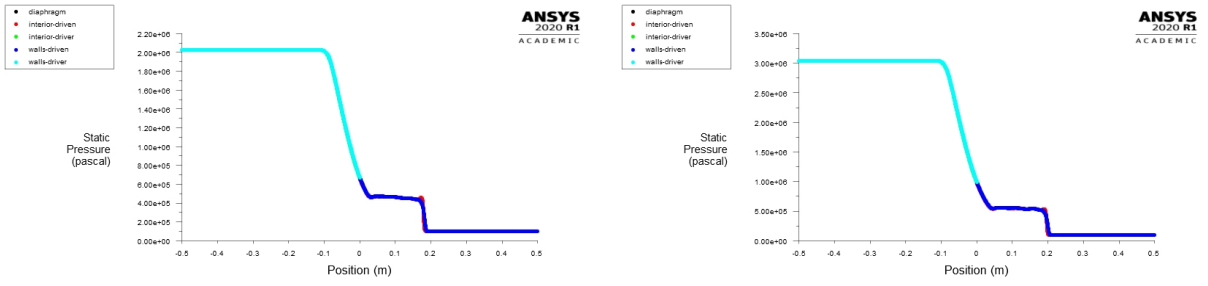

Figure 4.7: Pressure profiles computed using Fluent for initial driver pressures of 20 bar (left) and 30 bar (right) for methane/air mixture for the last time step calculated.

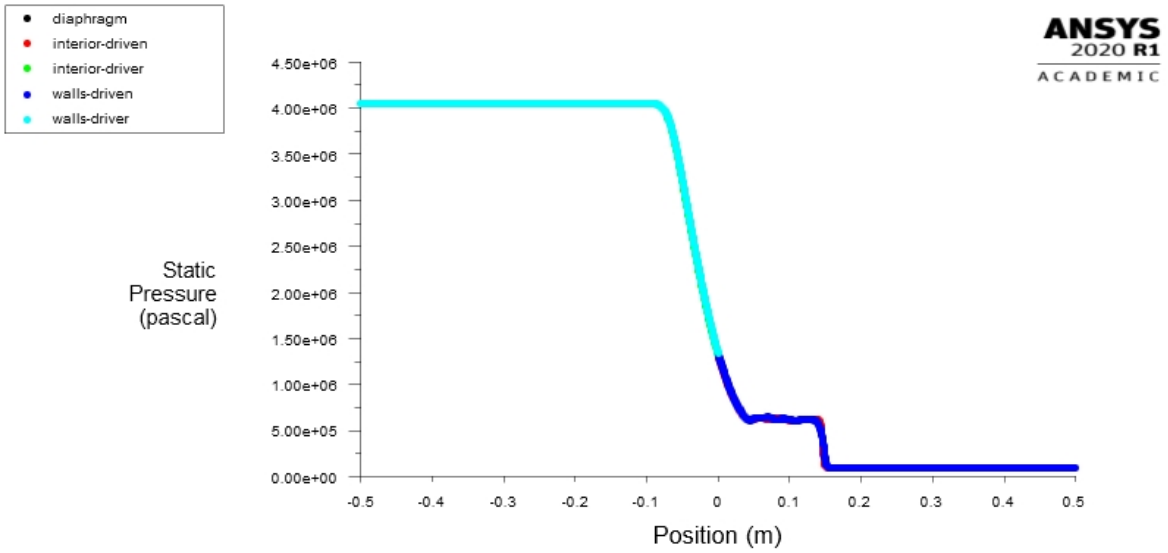

Figure 4.8: Pressure profile computed using Fluent for initial driver pressure of 40 bar for methane/air mixture for the last time step calculated.

Just like for hydrogen/air mixture, comparing the results from the CFD and analytical calculations for methane/air pressure profiles, we get very similar results. Since the only pressure calculated is P_2, which is assumed as equal to P_3, the comparison between the two approaches is applied to these values as seen in the following figure 4.9.

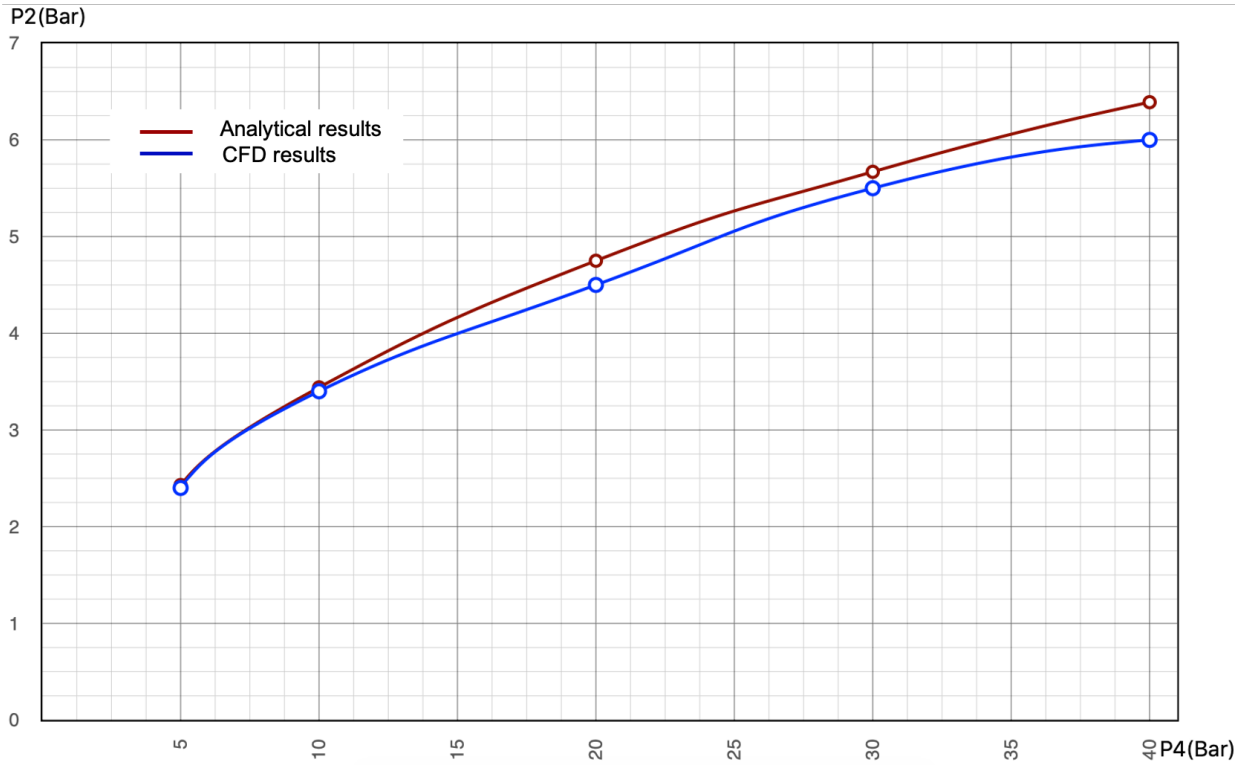

Figure 4.9: P_2 as a function of P_4 calculated analytically and through Fluent for methane/air mixture for the last time step calculated.

For the methane/air mixture, an error calculation is also done using equation 4.2. Producing a maximum error of just 6.5% it is proven, just like for hydrogen/air, the compatibility between the analytical values and the CFD values. However, the error produced by methane/air mixture is bigger than the error produced by the hydrogen/air mixture. This could be explained by the fact that methane produces a weaker shock wave and therefore the results that were expected are lower than the ones from hydrogen/air mixtures. This is possible to see in figure 2.8 as the CFD results come up short of the analytical results, producing a negative error.

Initial pressure ratio (Bar)	P2 analytical (Bar)	P2 Fluent (Bar)	Error %
5	2.43	2.4	-1.25
10	3.44	3.4	-1.17
20	4.75	4.5	-5.56
30	5.67	5.5	-3.1
40	6.39	6.0	-6.5

Table 4.4: Percentage error calculation from the analytical approach vs the CFD approach for the pressure across the contact surface for methane/air mixture for the last time step calculated.

With all the results from figures 4.2 to 4.9 and the tables 4.3 and 4.4 it is possible to conclude that the assumptions made are verified as the error produced from either of the mixtures is very small. It is also verified that in the presence of a shock wave, this will be stronger with increase of initial pressure ratio as expected.

Temperature

Following the pressure results we have the temperature results. From computing the initial pressures mentioned before, instead of extracting just one result, with the temperature profile we are able to extract two results, which the quotient represents the temperature across the contact surface(T_2/T_3).

With figure 4.1, before the contact surface in region 3, the temperature drops due to the expansion of the gas. After the contact surface in region 2 there is a very large temperature spike due to shock relation and shock reflection from the boundary layer.

In analysis of the results taken from Fluent, like predicted, as the initial pressure goes up so does the temperature spike in region 2.

One thing that can be concluded by looking at the graphs from hydrogen/air mixture from figures 4.10 to 4.12, is that at 20 bar if sufficient mixing takes place, it is possible to achieve spontaneous ignition as the temperature reached, 918.2K, is well above the spontaneous ignition temperature of hydrogen registered at 773K and with the results from the experiment from Dryer [12], there is confirmation, both experimentally and numerically.

Another thing that can be concluded by analysis of the graphs from figures 4.10 to 4.12 taken from Fluent, as the driver section is initialized with bigger pressures, the difference between T_2 and T_3 increases as the shock wave gets stronger increasing the maximum temperature reached in the region 2. Moreover, looking at figures 4.10 to 4.12, it can be seen that the gas expands more with the initial pressure increase

and this leads to an even smaller temperature at region 3, behind the contact surface.

On another note, with the shock wave getting stronger, the flow velocity increases. Since the time step size decreases, the number of iterations present less flow time and so the reaction seem to be smaller but in fact the number of iterations should have been higher in order to complement the full flow time.

Lastly, it is observable that the temperature inside the tube is not uniform, and by that it means that the temperature across the tube diameter is not the same. This can be seen in the figures 4.10 to 4.12 by looking at the colours of the profiles as shades of blue represent the temperature at the walls, while the inside of both driver and driven sections are represented as red and green respectively. This is due to the presence of a boundary layer which will change the temperature depending on the distance to the boundary layer where the highest temperature achieved is at the tube walls.

These results were taken for the last time step studied.

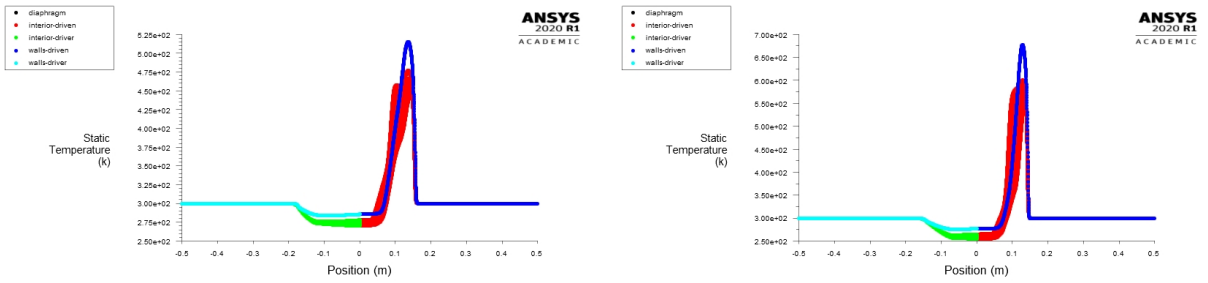

Figure 4.10: Temperature profiles computed using Fluent for initial driver pressures of 5 bar (left) and 10 bar (right) for hydrogen/air mixture for the last time step studied.

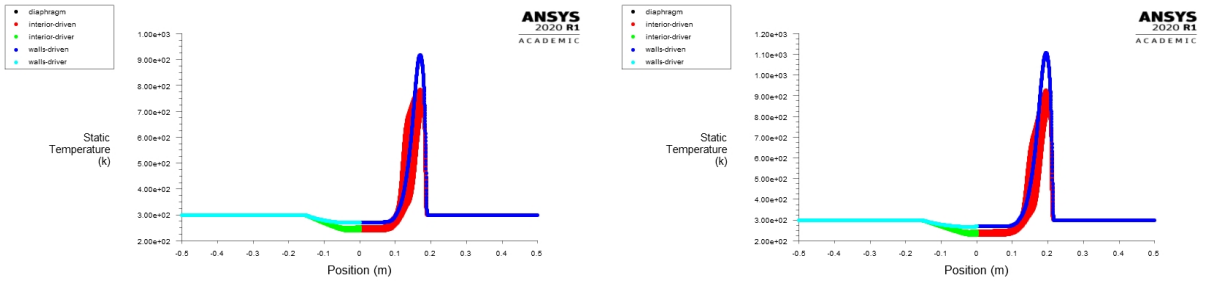

Figure 4.11: Temperature profiles computed using Fluent for initial driver pressures of 20 bar (left) and 30 bar (right) for hydrogen/air mixture for the last time step calculated..

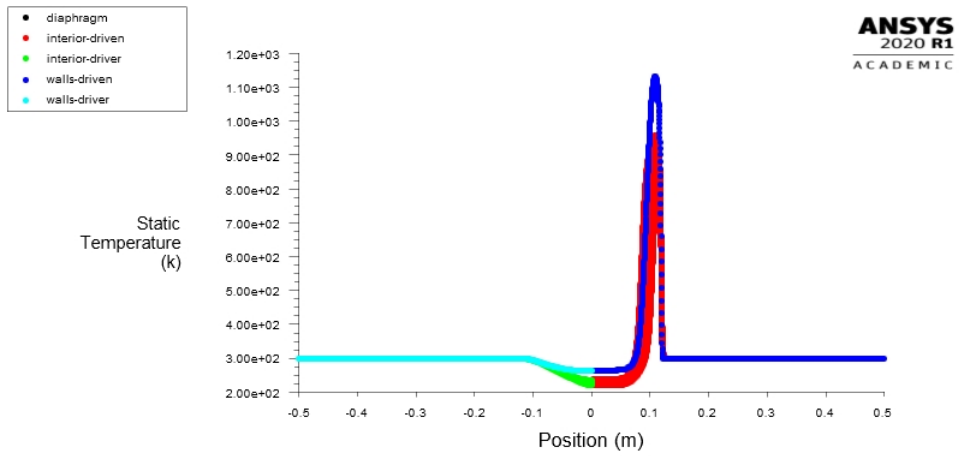

Figure 4.12: Temperature profile computed using Fluent for initial driver pressure of 40 bar for hydrogen/air mixture for the last time step calculated.

Comparing the analytical results with the CFD results for the hydrogen/air temperature profile along the length of the tube we get somewhat similar results. As there are four regions to consider but region 4 (Driver) and region 1 (Driven) are known, only region 2 and 3 will be analysed. It is then possible to compare the analytical calculations for these temperatures with the one extracted from Fluent as it is shown in figure 4.13. Through observation of the graph presented above and extracting the highest temperature recorded as T_2 and the lowest as T_3, we can verify that the analytical model matches the CFD results as the curve presented is very similar. However, the temperatures achieved by the CFD results are higher due to turbulent flow as, through viscous heating, increases the temperature in comparison to the analytical results.

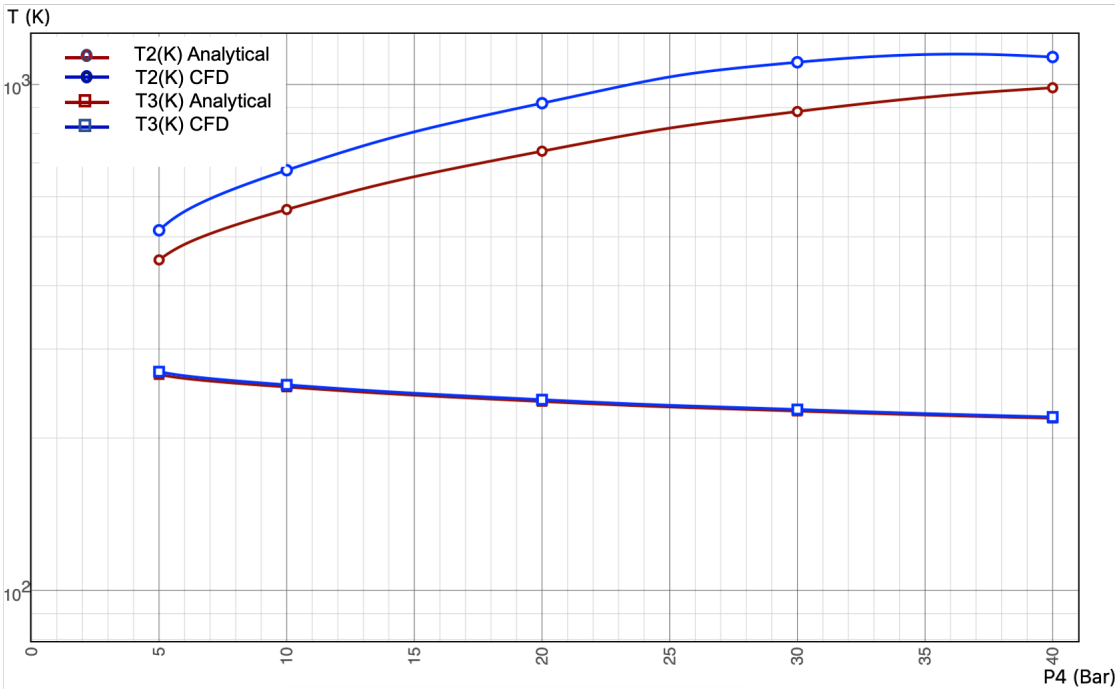

Figure 4.13: T_2 and T_3 as a function of P_4 calculated analytically and through Fluent for hydrogen/air mixture for the last time step calculated.

Using equation 4.2 it is possible to calculate the error generated between the results from Fluent and the results from the analytical equations. Considering the results from Fluent as true, the maximum error achieved is 20.11% for the calculation of T_2 and 1.33% for the calculation of T_3. All of the error calculations are shown in table 4.4

Initial pressure ratio (Bar)	T2 analytical (K)	T2 Fluent (K)	Error %	T3 analytical (K)	T3 Fluent (K)	Error %
5	450	514.9	+12.60	267	270.6	+1.33
10	566	676.9	+16.38	252.4	254.9	+0.98
20	738	918.2	+19.63	236.3	238.2	+0.79
30	884	1106.5	+20.11	226.2	227.8	+0.79
40	984	1131.9	+13.67	219	220.2	+0.54

Table 4.5: Percentage error calculation from the analytical approach vs the CFD approach for temperatures across the contact surface for hydrogen/air mixture for the last time step calculated.

From the results seen in figures 4.10 to 4.12, it is concluded that as the pressure input increases, the maximum temperature achieved behind the shock wave increases as well. However, it is also concluded that as the shock gets stronger, the expansion of the gas becomes greater in region 3 as T_3 decreases with the increase of pressure. Although the error is quite considerable, for the range of pressures chosen, with good mixing, spontaneous ignition is possible as the temperatures registered are considerably higher than the recorder 773K required for hydrogen to auto ignite as it can be seen in table 4.5.

As mentioned in the previous section about pressure, the shock strength of methane/air in comparison to hydrogen/air mixtures, is much weaker, which affects every property, one of them being temperature.

As seen from the analytical calculations we see that the shock strength produced by methane through the various driver pressures, is much lower than hydrogen (considering the scale) and as a result the maximum temperature reached in region 2, will also be much lower not being able to reach its spontaneous ignition temperature at pressure releases lower than 187.9 bar.

As shown in the following figures 4.14 to 4.16, it is possible to see the temperature profiles along the length of the tube for the final time step calculated. Once again, due to the boundary layer, the temperature is not uniform throughout the cross section of the tube as it increases the most at the wall due to viscous heating.

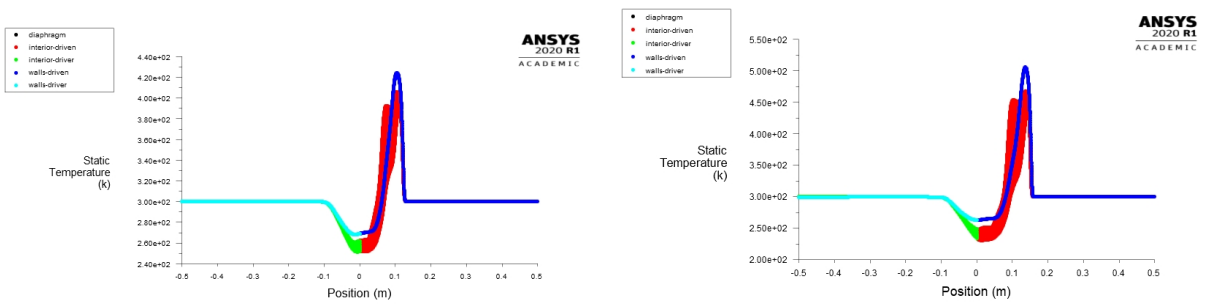

Figure 4.14: Temperature profiles computed using Fluent for initial driver pressures of 5 bar (left) and 10 bar (right) for methane/air mixture for the last time step calculated.

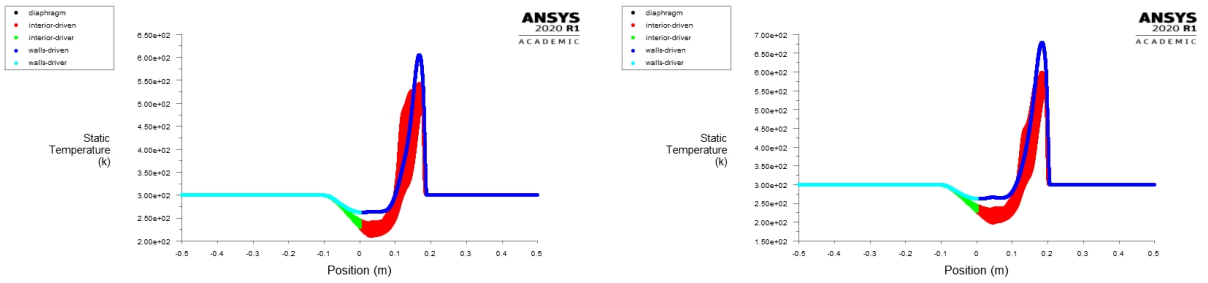

Figure 4.15: Temperature profiles computed using Fluent for initial driver pressures of 20 bar (left) and 30 bar (right) for methane/air mixture for the last time step calculated.

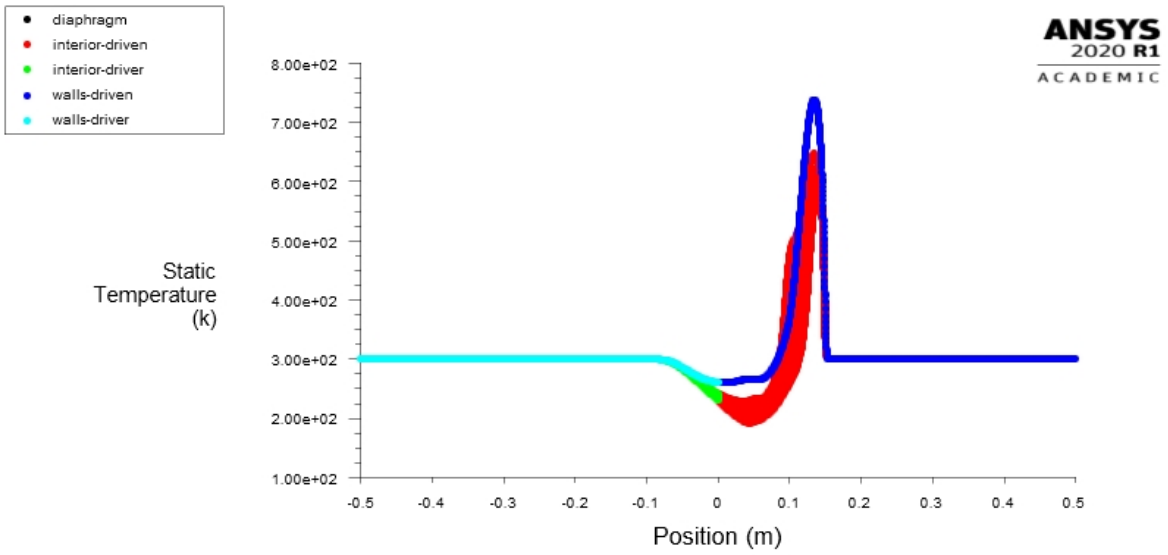

Figure 4.16: Temperature profile computed using Fluent for initial driver pressure of 40 bar for methane/air mixture for the last time step calculated.

Comparing the results extracted from Fluent and from the calculations using the governing equations, the divergence is little as both curves are very similar, however T_2 is always going to be bigger in the CFD in comparison to the analytical value due to turbulent heating. Such comparison is possible to see in the following figure 4.17. Since the temperature before the "disk burst" is known in region 1 and 4, the only values that need to be used in the comparison between the two approaches are T_2 and T_3. Just like the mixture of hydrogen/air, methane/air temperature profile acts very similarly.

With equation 4.2, the error associated in comparing results from both approaches is stated in the table 4.6. Here the methane/air mixture produced good results as the maximum error for T_2 calculations was 18.9% and for T_3 the maximum error produced was 0.93%.

Just as for hydrogen, the results printed in the figures 4.14 to 4.17 and in the table 4.6 help the conclusion that although methane will not be able to achieve the necessary temperature to auto ignite, the recorded values for temperature T_2 are much higher than the ones calculated analytically. This means that the assumption made that methane would not be able to reach its spontaneous ignition temperature until an upstream pressure of 187.9 bar was created, might be wrong as for 40 bar the temperature in region 2 peaked at 738.5K for the last time step calculated. Since methane auto ignites at 853K [26], the

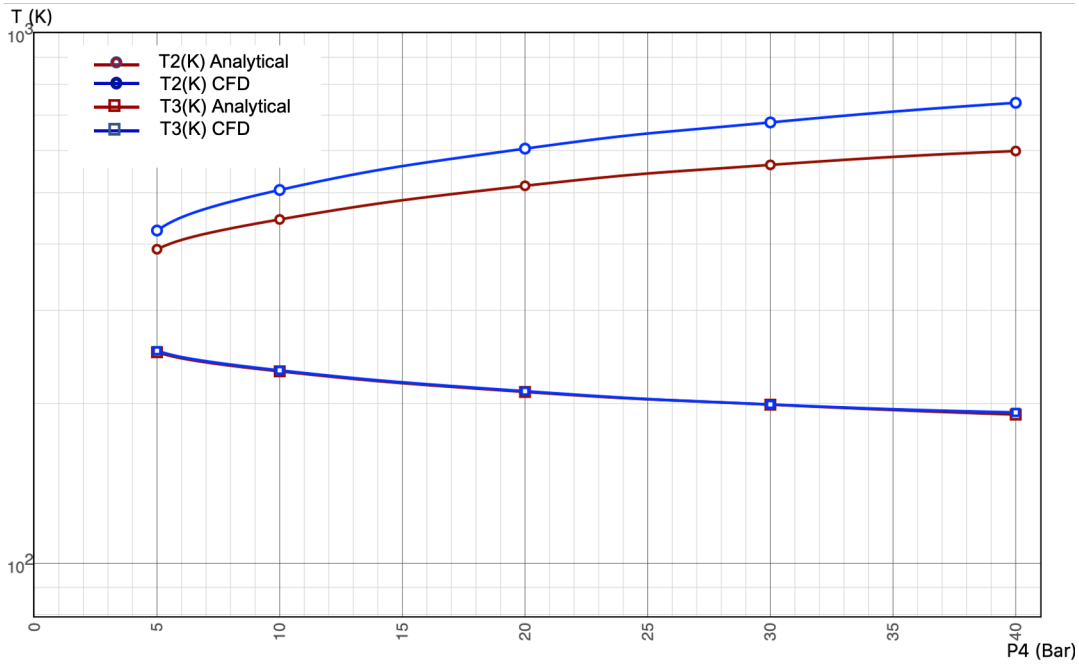

Figure 4.17: T_2 and T_3 as a function of P_4 calculated analytically and through Fluent for methane/air mixture for the last time step calculated.

Initial pressure ratio (Bar)	T2 analytical (K)	T2 Fluent (K)	Error %	T3 analytical (K)	T3 Fluent (K)	Error %
5	391	424.1	+7.8	250	251.6	+0.64
10	445	505.8	+11.9	230.1	231.1	+0.43
20	515	605.2	+14.9	210.4	211.1	+0.03
30	564	678.2	+16.8	199.1	199.3	+0.01
40	599	738.5	+18.9	190.7	192.5	+0.93

Table 4.6: Percentage error calculation from the analytical approach vs the CFD approach for temperatures across the contact surface for methane/air mixture for the last time step calculated.

necessary pressure for methane to reach such temperatures is probably going to be lower than expected.

Density

After addressing the temperature profiles extracted from Fluent, the next step should be addressing the density profiles.

From equation 2.7 we could predict that the density profiles would be very close to what the pressure profiles look like (figure 4.18, since it would work solely on temperature. Moreover, the density would be the inverse of the temperature associated and so, the density profiles should look like,
which is very close to what a pressure profile inside a shock tube looks like. However, equation 2.7 assumes that both the driver and driven section contain the same gas, and for this reason equation 2.8 should be the one used in this case.

Looking into the ideal gas law, density varies with pressure, temperature and the universal gas constant of the select gas. So, when altering the initial pressure in the driver section and leaving the temperature the same, the density of the gas will obviously increase and therefore, the density profile starts from a higher density as the driver pressure increases as can be seen in the figures 4.19 to 4.21.

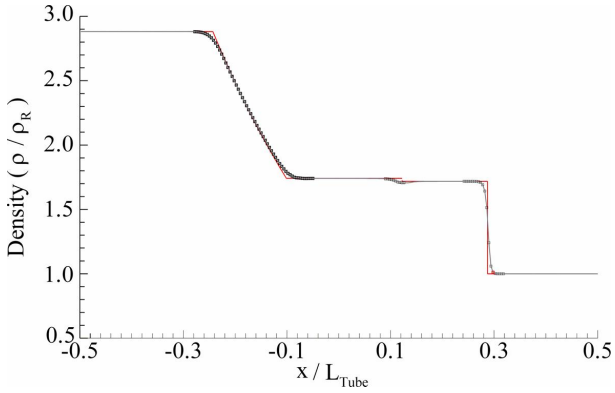

Figure 4.18: Density profile in a shock tube with the same gas in both driver and driven sections

From the density profiles for hydrogen/air mixtures, the density curve in region 2 will accompany the temperature rise and in region 3 the density will follow the cooling of the gas. However, when the driver pressure increases, the ratio of temperature across the contact surface increases as it is possible to see from figure 4.13, this means that the temperature in region 2 increases and the temperature in region 3 decreases. From the ideal gas law we know that when temperature rises the density decreases and vice versa. So, with this information, the density ratio across the contact surface, $\frac{\rho_2}{\rho_3}$, will decrease with the temperature rise as seen in figure 4.22. Once again, due to the boundary layer, the density of the fluid is not uniform throughout the cross section of the tube leading to variations of density inside of it, this is possible to see from the following figures 4.19 to 4.21 as the red represents the interior of the driven section.

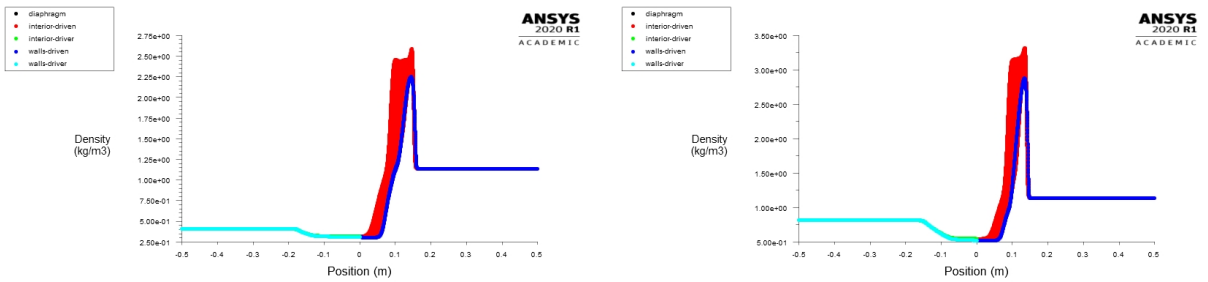

Figure 4.19: Density profiles computed using Fluent for initial driver pressures of 5 bar (left) and 10 bar (right) for hydrogen/air mixture for the last time step calculated.

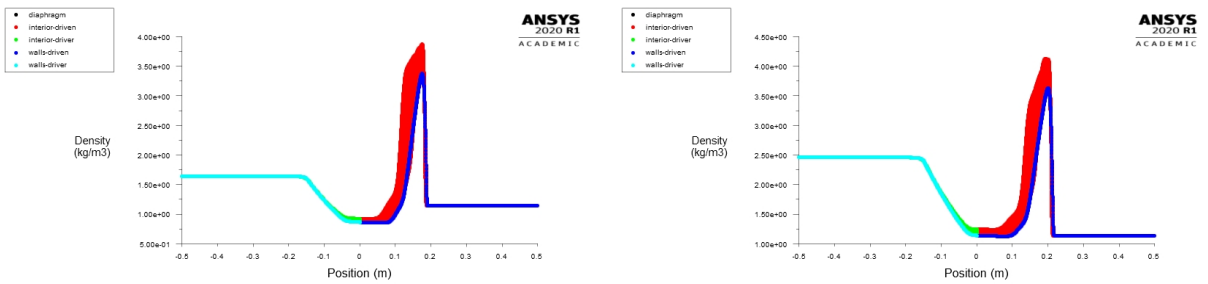

Figure 4.20: Density profiles computed using Fluent for initial driver pressures of 20 bar (left) and 30 bar (right) for hydrogen/air mixture for the last time step calculated.

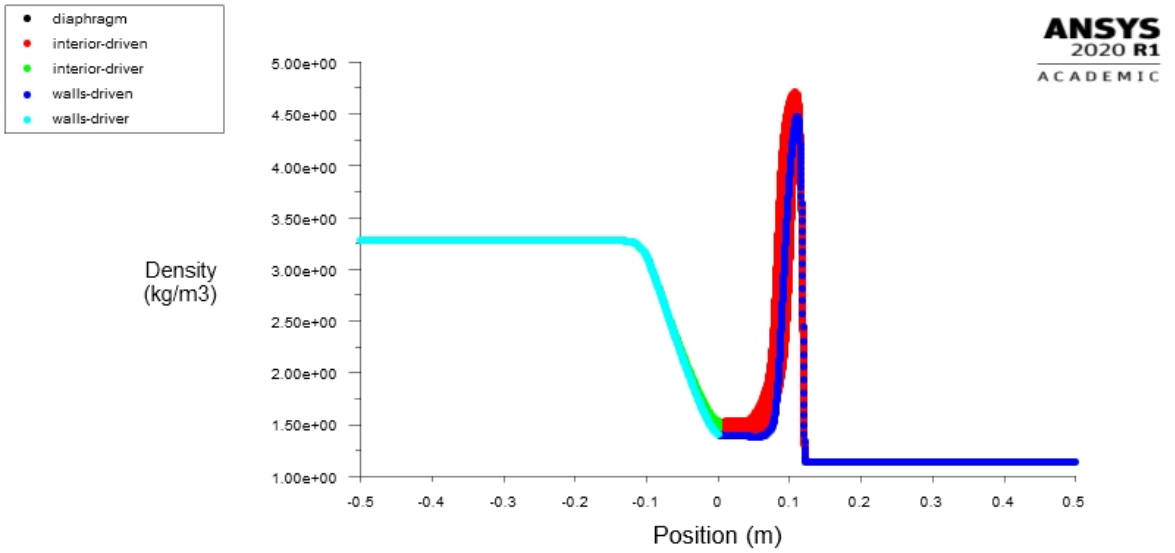

Figure 4.21: Density profile computed using Fluent for initial driver pressure of 40 bar for hydrogen/air mixture for the last time step calculated.

With the results obtained from Fluent, it is possible to compare these to the analytical values in order to verify both numerical and analytical assumptions. Comparing the density ratio across the contact surface, we get very similar results from both Fluent and analytical approaches which proves the validity of the assumptions made. Both results can be seen in figure 4.20.

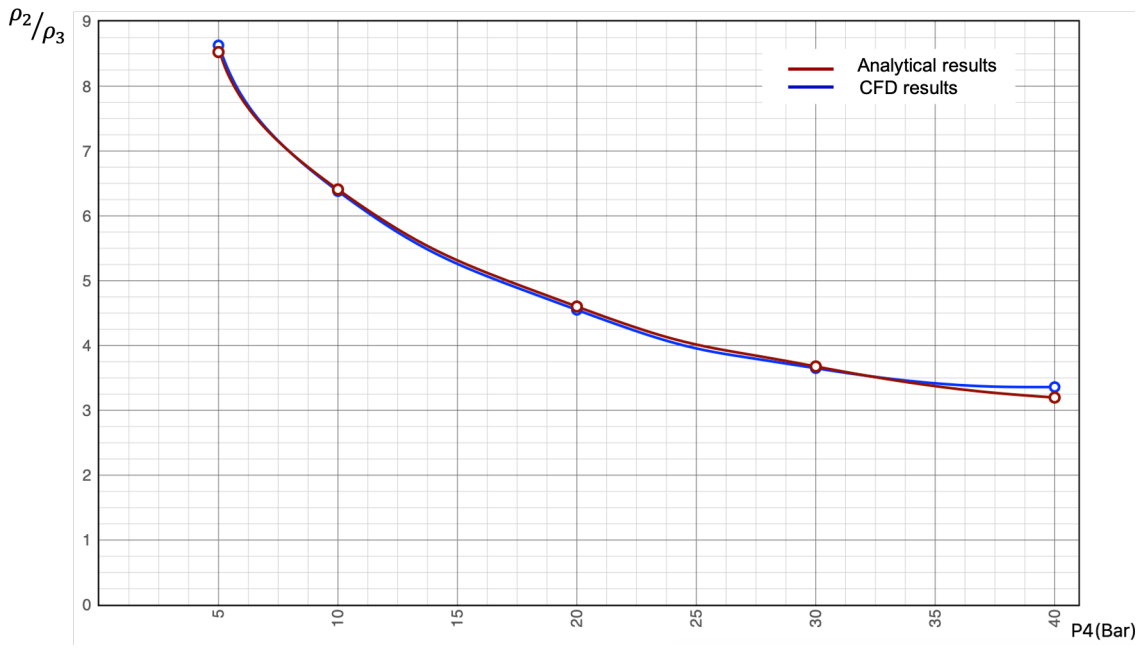

Figure 4.22: $\frac{\rho_2}{\rho_3}$ as a function of P_4 calculated analytically and through Fluent for hydrogen/air mixture for the last time step calculated.

As previously done, using equation 4.2 it is possible to obtain the error between the two calculation approaches. Once again the assumptions are verified to be correct with the maximum error occurring at

a initial driver pressure of 40 bars with a perceptual error of 5.06%.

Initial pressure ratio (Bar)	ρ_2/ρ_3 analytical	ρ_2/ρ_3 Fluent	Error %
5	8.53	8.63	+1.16
10	6.41	6.38	-0.47
20	4.60	4.55	-1.09
30	3.68	3.65	-0.82
40	3.19	3.36	+5.06

Table 4.7: Percentage error calculation from the analytical approach vs the CFD approach for density across the surface contact for hydrogen/air mixture for the last time step calculated.

Although the density profiles for Hydrogen/air mixture present a graph very similar to that of temperature profiles, in the case of methane/air mixtures, the density profiles are very different than what would be expected.

As mentioned before, density across the contact surface can be calculated using equation 2.8. For methane/air mixtures the density varies a lot with the temperature across the contact surface. This means that as the pressure input is bigger, so will the temperature behind the shock wave and the density will decrease. In relation, the density behind the contact surface will increase as the temperature cools more. Such density profiles are illustrated in the next figures 4.23 to 4.25. Once again, the density is not uniform across the diameter of the tube as it is possible to see in red, due to the boundary layer.

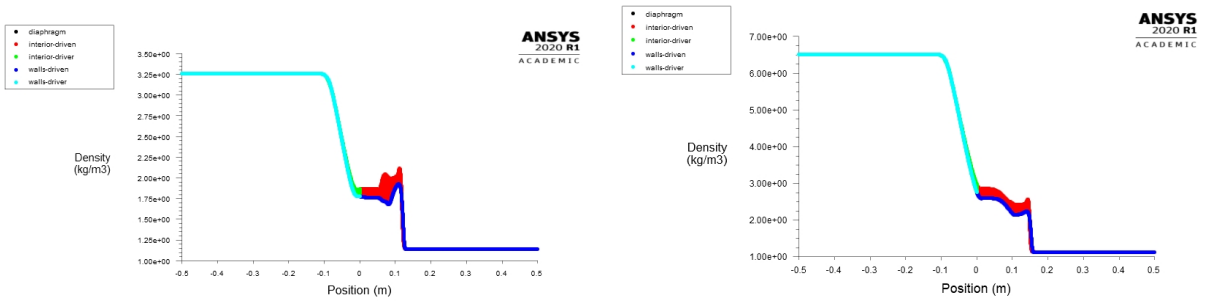

Figure 4.23: Density profiles computed using Fluent for initial driver pressures of 5 bar (left) and 10 bar (right) for methane/air mixture for the last time step calculated.

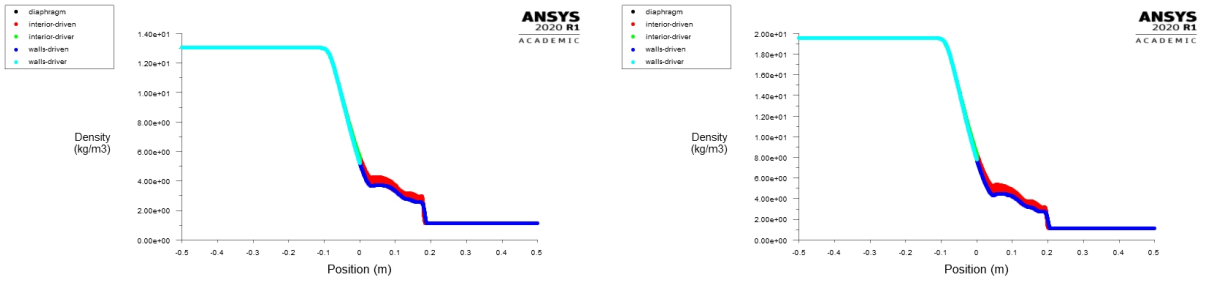

Figure 4.24: Density profiles computed using Fluent for initial driver pressures of 20 bar (left) and 30 bar (right) for methane/air mixture for the last time step calculated.

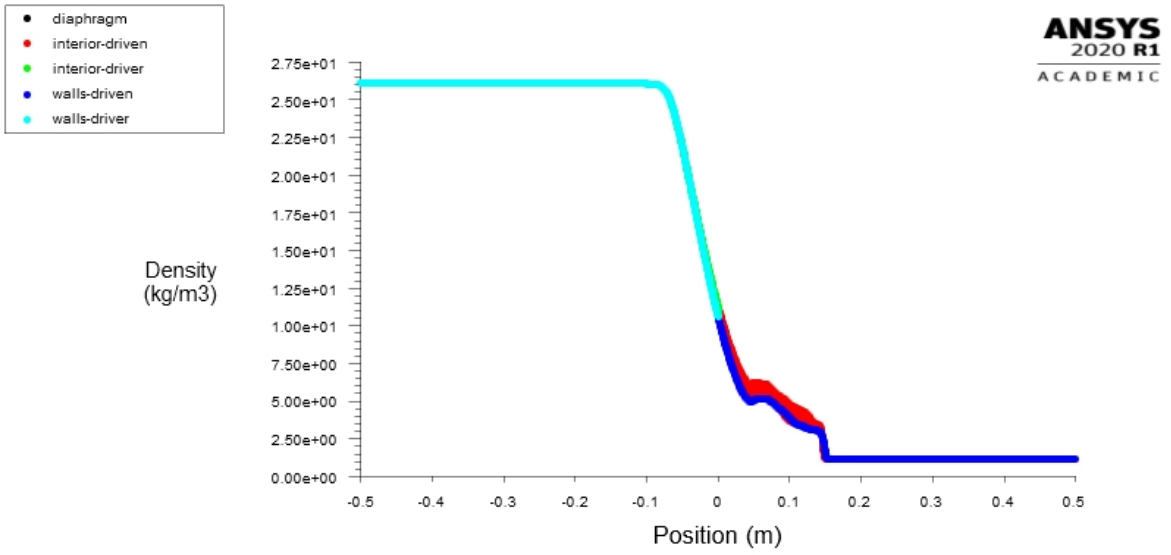

Figure 4.25: Density profile computed using Fluent for initial driver pressure of 40 bar for methane/air mixture for the last time step calculated.

Using these results and the results from the analytical calculations, it is possible to compare them and see if there is much difference in the values obtained from both approaches and from the following figure 4.26, results from Fluent do not vary that much from the results of the equations. However, like stated before, the density profiles from methane/air are very different from the hydrogen/air ones which leads to much lower values of $\frac{\rho_2}{\rho_3}$ when comparing the two mixtures.

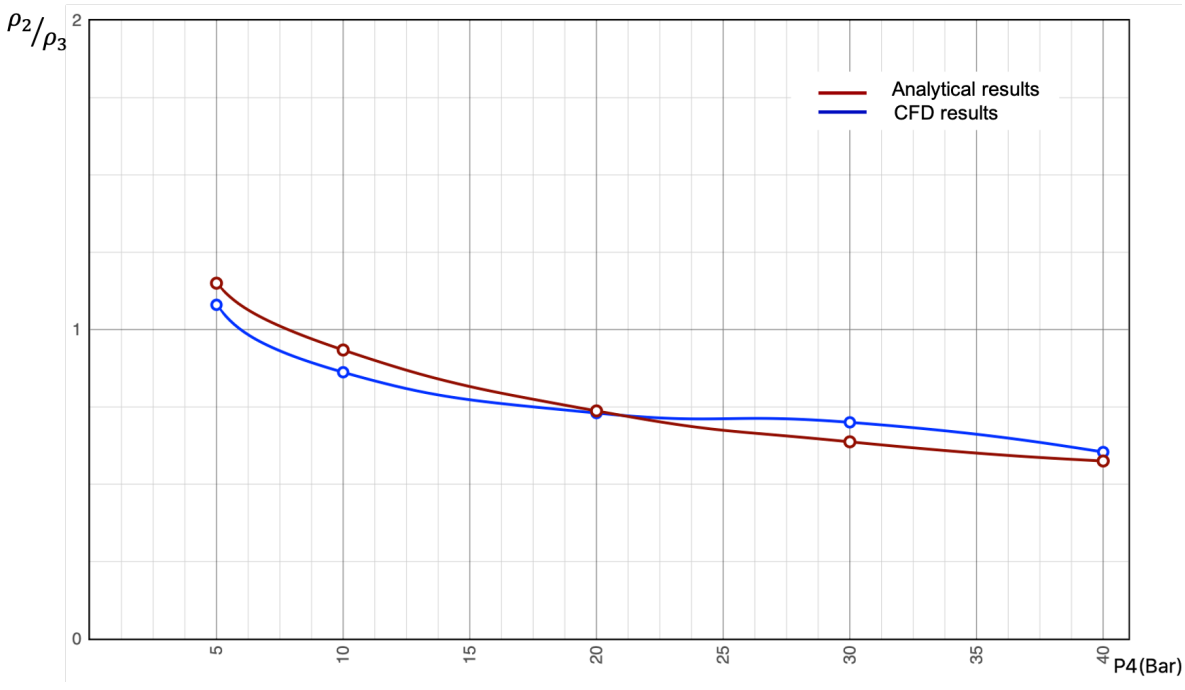

Figure 4.26: $\frac{\rho_2}{\rho_3}$ as a function of P_4 calculated analytically and through Fluent for methane/air mixture for the last time step calculated.

Once again the error associated is calculated using equation 4.2, proving once more that the results obtained from both approaches are very close. In comparison with hydrogen/air mixture results, methane/air mixture produces a maximum error of 8.57%

Initial pressure ratio (Bar)	ρ_2/ρ_3 analytical	ρ_2/ρ_3 Fluent	Error %
5	1.15	1.08	-6.48
10	0.93	0.86	-8.14
20	0.74	0.73	-1.37
30	0.64	0.70	+8.57
40	0.58	0.60	+3.33

Table 4.8: Percentage error calculation from the analytical approach vs the CFD approach for density across the surface contact for methane/air mixture for the last time step calculated.

Looking at the figures for both hydrogen and methane mixtures printed from Fluent for the last time step calculated its possible to see that the density profiles, although being affected by the local temperature, they are also influenced by the universal gas constant. As seen from figures 4.19 to 4.21, the density profiles for hydrogen are very different from the density profiles for methane as seen from the figures 4.23 to 4.25. This is due to the fact that in equation 2.8, the universal gas constant is considered. Being hydrogen's constant a lot bigger than methane, the results printed are very different as it is seen. However, $\frac{\rho_2}{\rho_3}$ behave in a very similar way for both mixtures, decreasing as the maximum temperature achieved increases.

Velocity

Lastly, one of the most important characteristics of the flow must be addressed: velocity.

From equation 2.13, we know that if the driver pressure is higher than the driven pressure, flow will move from the driver section to the driven section. Since the the pressure difference is high, the flow will achieve supersonic speeds. This is caused by the sudden release of high energy which lead to a shock wave. The bigger the energy, the stronger the shock wave and through equation 2.11, for a stronger shock wave, the faster the velocity reached.

With the results extracted from CFD for the hydrogen/air mixture for the last time step calculated, it is possible to see that there is a discrepancy between the numerical values and the analytical values. This might be explained by the viscous type assumption. When assuming laminar flow, the boundary layer is thin which might not affect the shock wave all that much, however if the viscous flow type was turbulent, the boundary layer would be thick, which through figure 2.6, the thicker the boundary layer, the more affected the shock wave. This will lead to flow speeds at the boundary layer which has been proven that the turbulent boundary layer actually increases the speed of the flow due to the formation of Eddy's. However it will not increase to the point where it is similar to that of no viscosity.

In figure 4.27 we can see how the Mach number evolves as the pressure in the driver is increased for the mixture of hydrogen and air. As mentioned above, a considerable gap in values is obtained between the analytical and numerical calculations. However, we can see that the curves are very similar to one

another which proves the validity of the calculations and the assumptions made.

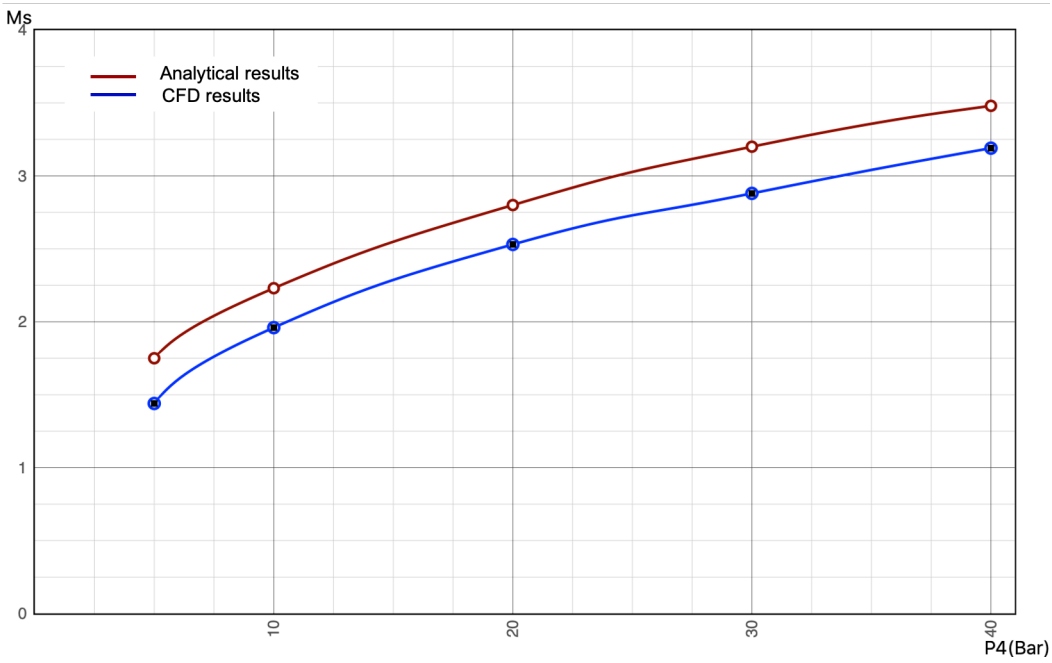

Figure 4.27: M_s as a function of P_4 calculated analytically and through Fluent for hydrogen/air mixture for the last time step calculated.

Using equation 4.2 it is possible to calculate the error from the discrepancy of values, therefore giving a more accurate result of the difference between the models studied. When looking at the figure 4.27, we can see that the values are very different between the two approaches because of the difference that the viscosity makes, which means that even though the error is not too big, the flow will never reach the same velocity unless inviscid flow is assumed.

Initial pressure ratio (Bar)	M_s analytical	M_s Fluent	Error %
5	1.75	1.44	-21.52
10	2.23	1.96	-13.78
20	2.80	2.53	-10.67
30	3.19	2.88	-10.76
40	3.48	3.19	-9.09

Table 4.9: Percentage error calculation from the analytical approach vs the CFD approach for the shock Mach number for hydrogen/air mixture for the last time step calculated.

Knowing the Mach number, it is possible to know the shock speed (equation 2.11) and since we know the length of the tube that the flow has to travel to reach the atmosphere, we can also calculate the time that the flow takes to travel the length of the tube through equation 2.12. Considering the position of the contact surface, the flow will only travel the $\frac{length}{2}$ of the tube. So, assuming that the length to travel is 0.5m and that the flow velocity is equal to the shock speed, the time required for the flow to travel the length is presented in the next table 4.10.

Initial pressure ratio (Bar)	M_s Fluent	Shock speed (m/s)	Time (s)
5	1.44	499.4	1.00^{-3}
10	1.96	680	7.35^{-4}
20	2.53	877	5.70^{-4}
30	2.65	998	5.01^{-4}
40	3.19	1102.5	4.54^{-4}

Table 4.10: Time necessary for the flow to cover half of the length of the tube into the atmosphere for hydrogen/air mixtures for the last time step calculated.

On another note, the behaviour of velocity for the methane/air mixture inside the tube is similar to the mixture of hydrogen with air, however as the shock produced is weaker, the speeds obtained are lower than those produced from the rapid release of high-pressured hydrogen into air. Therefore, the Mach number of the shock wave is also lower.

The following figure 4.28 shows the difference in values obtained through Fluent when compared with the values obtained from the governing equations.

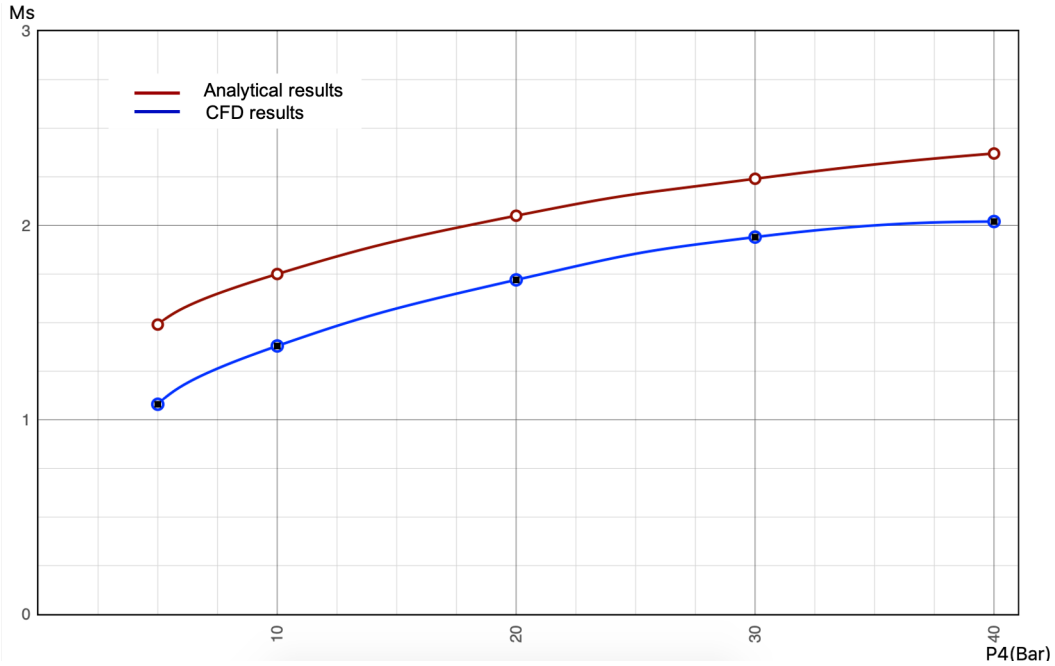

Figure 4.28: M_s as a function of P_4 calculated analytically and through Fluent for methane/air mixture for the last time step calculated.

Just as hydrogen/air mixture, there is a considerable gap in values and so the error calculated can be quite big as it is shown in the following table. However, in comparison, methane/air mixture produces an even bigger maximum error of 37.96%, although the error starts decreasing as the pressure increases and as the flow reaches higher velocities due to the increase of turbulent boundary layer.

Lastly, with the values from the the Mach number and equation 2.12, with the assumption that the flow will only travel through half of the length of the tube (size of the driven section), it is possible to calculate the time necessary for the flow to exit into the atmosphere.

As seen from the figures 4.27 and 4.28 and from the tables 4.9 to 4.12 its possible to conclude that

Initial pressure ratio (Bar)	M_s analytical	M_s Fluent	Error %
5	1.49	1.08	-37.96
10	1.75	1.38	-26.81
20	2.05	1.72	-19.19
30	2.24	1.94	-15.46
40	2.37	2.02	-17.33

Table 4.11: Percentage error calculation from the analytical approach vs the CFD approach for the shock Mach number for methane/air mixture for the last time step calculated.

Initial pressure ratio (Bar)	M_s Fluent	Shock speed (m/s)	Time (s)
5	1.08	369.7	1.35^{-3}
10	1.38	476.2	1.05^{-3}
20	1.72	597.0	8.38^{-4}
30	1.94	672.5	7.43^{-4}
40	2.02	699.5	7.15^{-4}

Table 4.12: Time necessary for the flow to cover half of the length of the tube into the atmosphere for methane/air mixtures for the last time step calculated.

although hydrogen and methane produce different results for flow speeds, as hydrogen produces flow with much higher speeds than methane, both velocity profiles act very similarly. However, the Mach produced by the initial pressure ratios are quite different than the analytically calculated values. This means that the Mach number necessary to produce such temperatures for the mixtures is lower than what was expected meaning, just like mentioned before, that auto-ignition temperature will be reachable for lower pressure ratios and lower Mach numbers.

Considering that all of these results were taken for the last time step calculated and only for comparison purposes, the originated error might be different if other tube dimensions or other time steps are chosen. On another note, since the numerical model and the analytical model are based on different set of equations, verification is not possible due to the use of viscosity. Moreover, considering that the analytical calculations are based on a stationary approach and that Fluent calculations are resolved in a transient manner, the comparison between the two serve to show that the spacial and temporal discretization of the numerical model does not lead to unrealistic values.

4.2.2 Case 2: Testing the effects of the length of the tube while maintaining the same initial pressure to study the effects on the properties development inside the tube.

Although the initial driver pressure is not changing, the size of the cells in each mesh changes. Since there is a maximum of nodes that is possible to use, the mesh was refined to complement the maximum number of nodes possible. For this, and since the length of the tube is increasing, the cell size must increase as well in order to follow the length of the tube. For this, the tube was meshed according to this calculation,

$$\frac{length/2 * diameter}{x^2} = 250000 \tag{4.2}$$

the $length/2$ allows the mesh of the driver and driven separated and x is the size of the cell to input in the mesh tab so that each section has 250000 elements making a total of 500000 elements. However, even though the mesh is made to be uniform, near the walls the cell size might be smaller which increases the number of expected cells and nodes, which is why the aim was for 500k and not the maximum 512k so that it could have some leverage.

Just like what was done in table 4.2, the time step used for each tube length was found by trial and error, however for case 1 the time step used was the same for both hydrogen/air and methane/air mixtures but in this case, only the hydrogen/air mixtures are going to be studied.

Tube length (m)	Diameter (m)	Element size (m)	H_2 Time step (s)
0.360	0.02	$1.2e^{-4}$	$9e^{-7}$
0.420		$1.29e^{-4}$	$1e^{-6}$
0.480		$1.38564e^{-4}$	$2e^{-6}$

Table 4.13: Time step used for each tube length/mixture for better results

Although case 1 is tested for both hydrogen and methane, in this case considering the pressure and the setting used, only hydrogen/air mixture is going to be tested as it was proven experimentally that hydrogen can spontaneously ignite pressures as low as 20bar. Using the setting from the the previous table 4.13, the driver section was initialized with 20 bars of pressure and with value of 1 for the mass fraction of hydrogen. The driven section was once again initialized with atmospheric conditions while both sections had an initial temperature of 300K. With these settings and the with the rest of the assumptions from table 3.3, the solution was run. Once again the properties studied were pressure, temperature, density, velocity and time along the length of the tube. However, in order to better visualize what happens inside the shock tube, besides the graphs used in case 1, the contours of each property are displayed.

Pressure

As mentioned above the pressure was the same for each case so that there would be just one variable, the length of the tube. For this the initial pressure was designated to be 20 bar, as from the case 1 it was possible to conclude that the temperature with that setting would be enough to cause spontaneous ignition of hydrogen/air mixture.

Analysing the following figures it is also possible to conclude that with the increase of the length of the tube, the pressure profile does not change maintaining every value for each region. However, for smaller tube lengths, region 2 and region 3 do not form like in case 1. This is due to the fact that viscous flow is assumed and the pressure profile fluctuates throughout the diameter of the tube due to the boundary layer. For this reason it is possible to see in red that the pressure profile, once the diaphragm bursts, fluctuates depending on the position on the tube cross section. Along with that it is very clear to see all 4 regions described in figure 4.2 in the pressure contours presented, the expansion waves moving in the opposite direction of the shock wave, the regions 2 and 3 where pressures are more or less the same with some variations due to the boundary layer, the shock wave and the region that has not been affected by the shock yet.

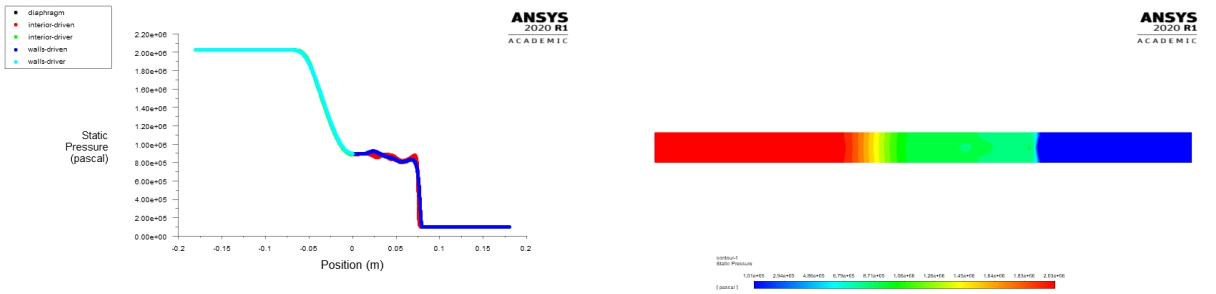

Figure 4.29: Pressure profiles computed using Fluent for the 360mm length tube with hydrogen/air mixture for the last time step calculated, at P=20 bar.

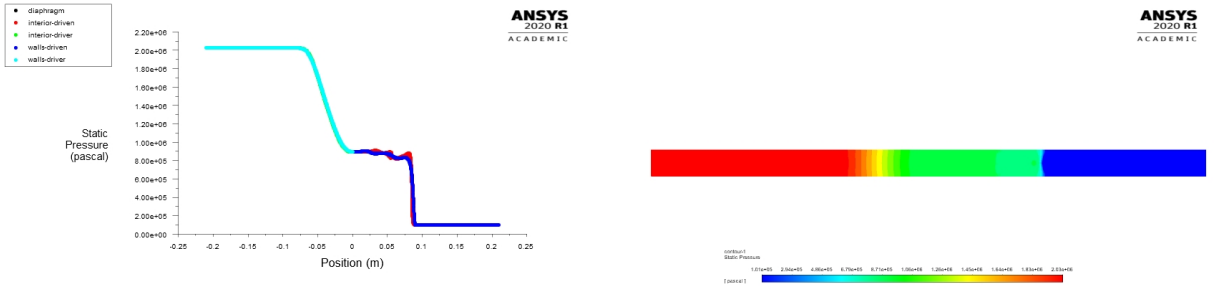

Figure 4.30: Pressure profiles computed using Fluent for the 420mm length tube with hydrogen/air mixture for the last time step calculated, at P=20 bar.

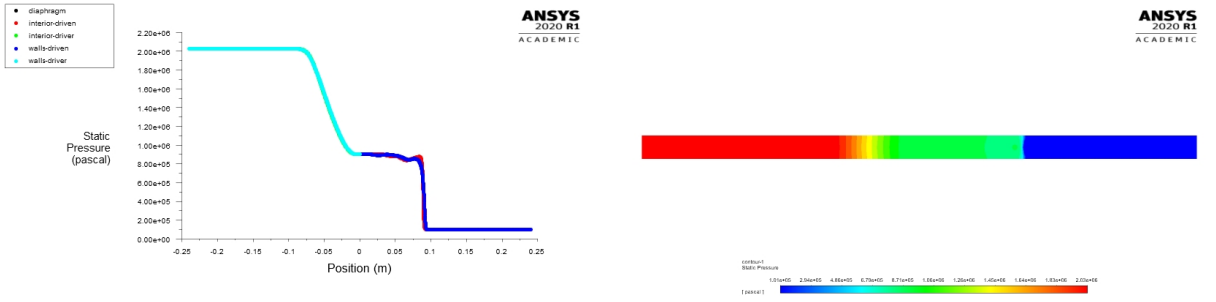

Figure 4.31: Pressure profiles computed using Fluent for the 480mm length tube with hydrogen/air mixture for the last time step calculated, at P=20 bar.

Temperature

As mentioned above, from case 1 it was possible to conclude that at just 20 bar of pressure for the hydrogen/air mixture, the shock produced from releasing the high-pressured hydrogen into the atmosphere through a tube of 0.5m, would have enough strength to cause a spike of temperature that would reach the spontaneous ignition of the mixture. So, using this same pressure, the temperature profile inside the tube was analysed throughout different lengths as shown in table 4.13.

With the following figures 4.32 to 4.34 from Fluent, for the last time step calculated, and with the temperature profile from case 1 for 20 bar of pressure it is easily concluded that with the increase of length, the maximum temperature that the mixture produces is also going to increase as the temperatures increase from 836.6K, for the 360mm long tube, to 918.2, for the 1meter long tube. This, as expected, is due to the fact that when the length of the tube is increased, the turbulent boundary layer is also able to become thicker and as the boundary layer thickens it will affect more and more the shock wave inducing

more heat through shock reflection. This phenomena is explained due to the fact that, when the contact surface breaks, turbulent mixing takes place and the initial shock, once it develops and hits the walls of the tube, is going to be reflected, creating oblique shocks. This results in reflected shock heating of the mixture, leading to higher local temperatures. From the temperature contours presented it is possible to once again identify all four regions of the shock wave. It is also possible to see that the increase of temperature is not linear presenting a high-temperature shape near the centerline of the tube however the highest temperature is achieved at the walls of the tube in the boundary layer.

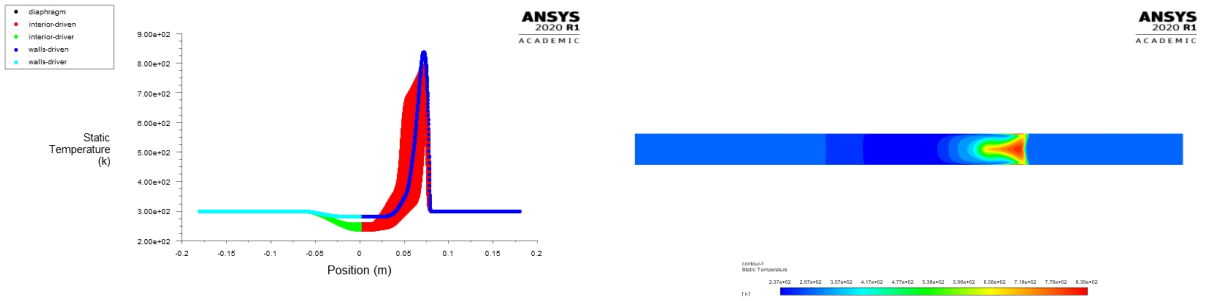

Figure 4.32: Temperature profiles computed using Fluent for the 360mm length tube with hydrogen/air mixture for the last time step calculated, at P=20 bar.

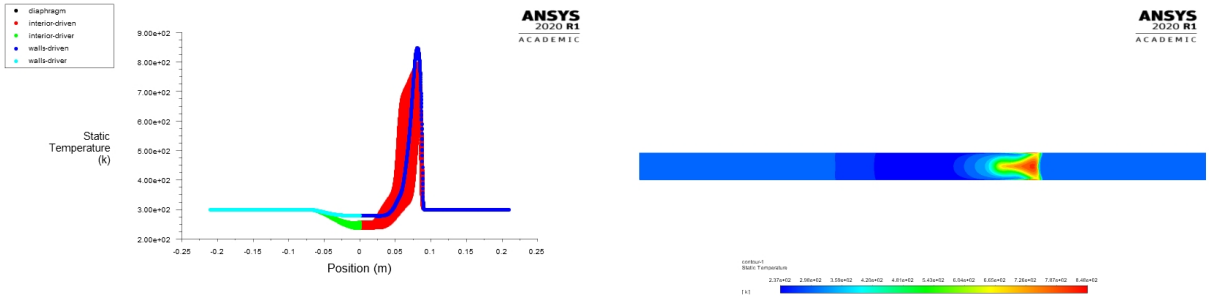

Figure 4.33: Temperature profiles computed using Fluent for the 420mm length tube with hydrogen/air mixture for the last time step calculated, at P=20 bar.

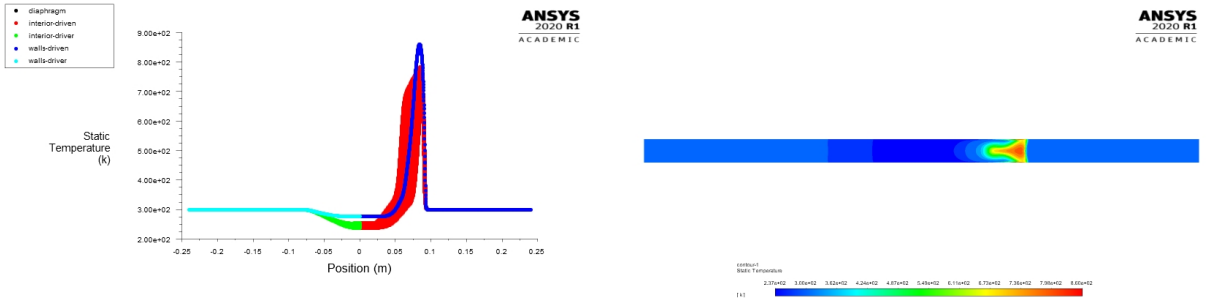

Figure 4.34: Temperature profiles computed using Fluent for the 480mm length tube with hydrogen/air mixture for the last time step calculated, at P=20 bar.

Through the contours presented its possible to see that the temperature achieved, at the last time step, in any of the cases would be enough to auto ignite hydrogen mixture with air.

Density

With the addressing of the two previous subsections, it is fairly easy to understand what is going to happen to the density profile using the ideal gas law. Since the pressure profile does not change at all, the only thing that affects the density of each region, is its temperature and as it was observed from case 1 for the hydrogen/air mixture, when the temperature increases in region 2, the density decreases.

Since the length of the tube is being increased and the temperature of region 2 increases because of it, with higher temperature we get lower densities. Since temperature in region 3 increases very slightly, $\frac{\rho_2}{\rho_3}$ becomes smaller as expected.

The difference in the density profiles is very small due to the fact the temperatures fluctuations are small as the tube is not being increased that much. However, if we compare the results with case 1 where temperature in region 2 is much higher, due to the tube length being longer, the results are more noticeable as the density in case 1 is lower because of the higher temperature.

Once again, observing the density profiles extracted in the figures 4.35 to 4.37 for the last time step calculated, the four regions of the shock tube are easily seen and as in the temperature profiles, it is seen in red that the behaviour of the properties inside the tube is not uniform due to the existence of a boundary layer.

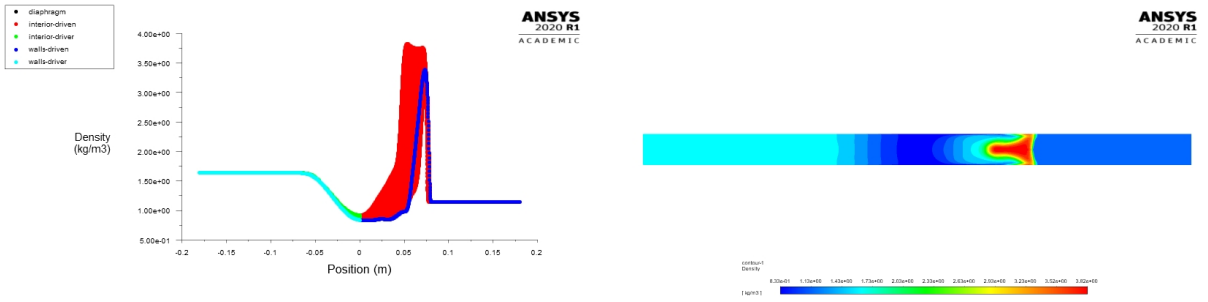

Figure 4.35: Density profiles computed using Fluent for the 360mm length tube with hydrogen/air mixture for the last time step calculated, at P=20 bar.

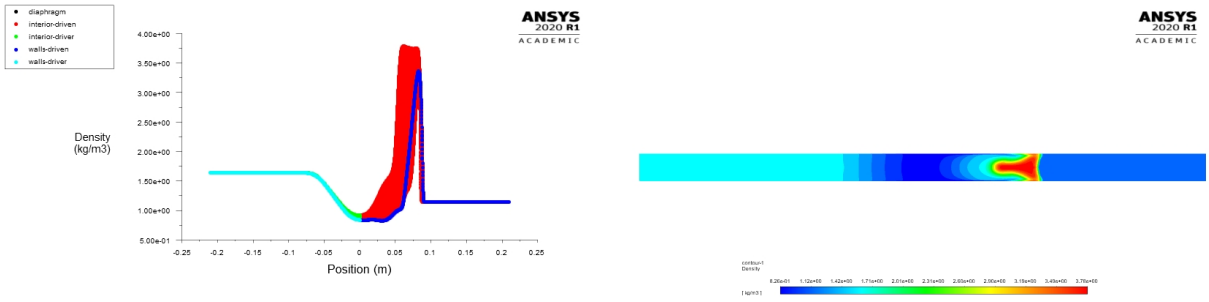

Figure 4.36: Density profiles computed using Fluent for the 420mm length tube with hydrogen/air mixture for the last time step calculated, at P=20 bar.

Just like in case 1 its possible to see that the density profile inside the tube at the last time step calculated, presents a shape that resembles a mushroom however, this only happens do the fact that the temperature profile presents this shape and the density profile follows the same route. However, as in case 1 it is possible to conclude that due to ideal as law, as the local temperature increases, the density

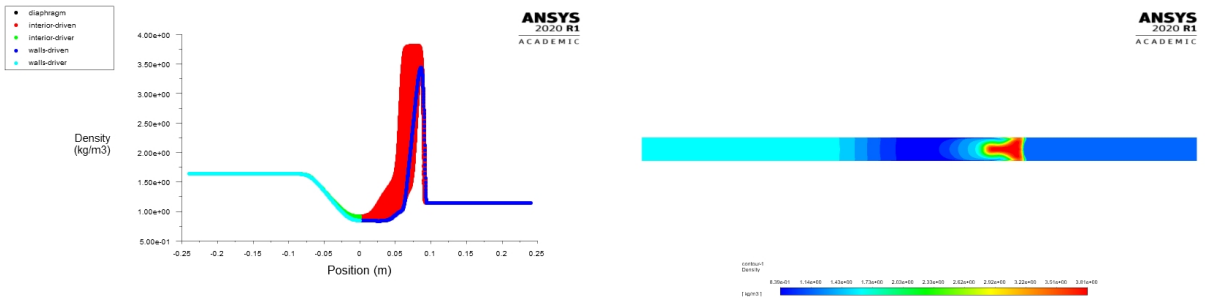

Figure 4.37: Density profiles computed using Fluent for the 480mm length tube with hydrogen/air mixture for the last time step calculated, at P=20 bar.

of the region decreases.

Velocity

In case 1, the velocity profile was quite easy to predict. As the pressure was being increased, through Bernoulli equation (2.13) it was possible to predict that the velocity of the flow would also increase. However, in case 2, the pressure is not changed which leads to a much more difficult prediction of what happens.

Looking at the following velocity profiles taken from Fluent (figures 4.38 to 4.40) at the last time step calculated, we see that for the hydrogen/air mixture, as the length of the tube increases, the maximum velocity of the flow decreases. Although the turbulent flow speeds up the flow in the boundary layer, the maximum velocity registered with turbulent flow is not going to be faster than the one registered with the equations. However, as said above, with the increase of tube length, the maximum velocity observed is lower which can be explained by the fact that the longer tube suffers more from the viscous forces caused by the viscosity of the fluid which, even though it is very small considering that it is a gas, it still has considerable effect.

Although the velocity does not change much from one length to the other, when compared to a longer tube like in case 1, the difference is noticeable, proving the assumptions made. It is easily seen from the contours, how the velocity profile acts different inside the tube, which explains why the velocity graphs are not linear.

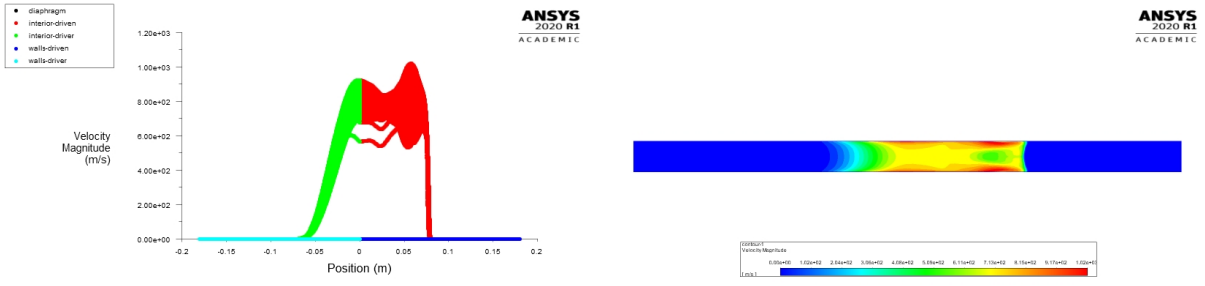

Figure 4.38: Velocity profiles computed using Fluent for the 360mm length tube with hydrogen/air mixture for the last time step calculated, at P=20 bar.

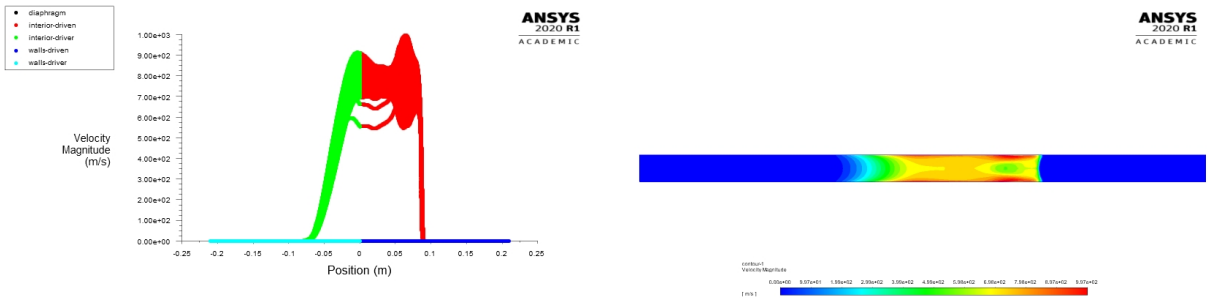

Figure 4.39: Velocity profiles computed using Fluent for the 420mm length tube with hydrogen/air mixture for the last time step calculated, at P=20 bar.

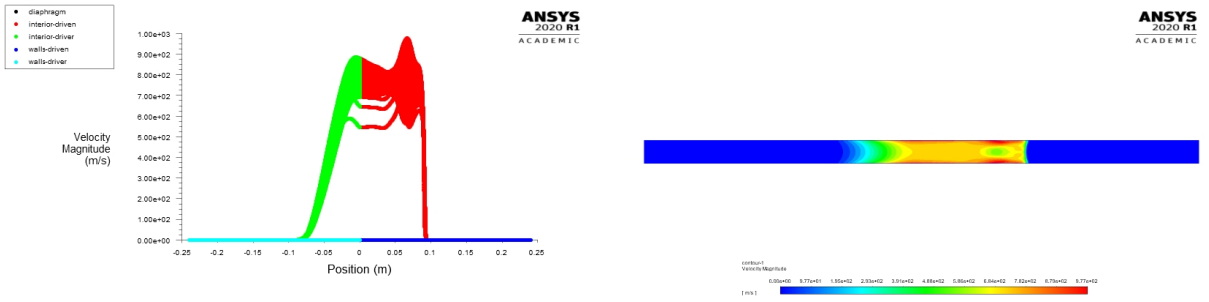

Figure 4.40: Velocity profiles computed using Fluent for the 480mm length tube with hydrogen/air mixture for the last time step calculated, at P=20 bar.

While observing the previous analysis, it is very difficult to observe a difference in the profiles for the various lengths. This is due to the number of iterations used being the same while the time step size, only varies so little. So in order to better understand the effects of the length of the tube for hydrogen/air mixture, the following table 4.14 was made with the values extracted from Fluent.

Properties	Length of the tube	360mm	420mm	480mm	1000mm
Hydrogen/air:					
Max. Flow velocity (m/s)		1018.8	997.1	976.9	877
P_2(Bar)		9	9	9	9
$T_3(k)$		236.7	236.7	237.3	238.2
$T_2(k)$		836.6	848.4	860.4	918.2
Density ratio (ρ_2/ρ_3)		4.66	4.56	4.53	4.08

Table 4.14: Case 2 results extracted from Fluent for the various properties for both hydrogen/air and methane/air mixtures

With the values of velocity decreasing with the tube length increase and using equation 2.12, it is easily understandable that the time that the shock takes to travel the length of the tube will also increase. This being said, and as previously stated, ignition only occurs in the presence of two factors: when there is enough rise in temperature to achieve spontaneous ignition values and when there is enough mixing. One of the things that influences mixing is time, and since the "reaction" time increases as the length of the tube increases it is safe to say that in the presence of a longer tube, spontaneous ignition phenomena might be easier to achieve. This is also proven since turbulent flow helps mixing meaning that with

the boundary layer increasing, turbulent mixing occurs more and so a longer tube might have a higher probability of causing spontaneous ignition if the right initial pressure is input in the driver section.

4.3 Shock evolution in the driven section for Hydrogen

In this section, it is shown an evaluation of what happens inside the shock-tube throughout the flow time.

Several studies were made in terms of ignition times and the delay it takes for the spontaneous ignition to happen. One of those studies was done by Mogi et al.[10] in 2007 where jet fire ignition was achieved with an experimental set consisting of a tube with 185mm with 5mm in diameter with a driver pressure of 145 bar with hydrogen/air mixture. With this setting, spontaneous ignition of hydrogen was achieved. With the careful observation of this paper, it was possible to conclude that ignition might start inside the tube and not outside, meaning that at the burst of the contact surface, mixing might start right away leading to the ignition. With this information, this section is dedicated to studying what happens inside the shock-tube through time.

In previous sections the properties of the mixtures are addressed and what happens to them in case of shock inside of a tube. However, one of the most important things to study when considering combustion is the quality of the mixture. When quality of a mixture is addressed the main aspect to be spoken about is the equivalence ratio (Φ). The equivalence ratio studies if a mixture is rich (>1), lean (<1) or stoichiometric (=1) by dividing the Fuel-air ratio of the mixture by the stoichiometric Fuel-air ratio.

$$\Phi = \frac{FAR}{FAR_{stoich}} \tag{4.3}$$

With information in chapter 1 it is known that, demonstrated by Alcock et al. [5], hydrogen/air stoichiometric mixture requires a minimum ignition energy of just 0.02 mJ, however the flammability limits present a very wide range of % of hydrogen in air. With this, the easiest way for hydrogen to ignite when mixed with air, is to have a concentration mixture at stoichiometric conditions, which is 29.5% of hydrogen in air. Besides this, since we are addressing auto-ignition, enough temperature is required for the mixture to combust. Since this is a numerical analysis, it is impossible to conclude if a mixture combusts or not, however it is possible to know if the conditions necessary for such phenomena are in place. This being said, in this section the equivalence ratio of the mixture along with the temperature of the mixture developments through time, inside the shock tube are going to be presented in order to conclude under which conditions is it possible to have spontaneous ignition of hydrogen/air mixture.

In order to study what happens inside the shock tube through time, four analysis are going to be pursued. Two lengths of tube are tested, 360mm where enough temperature was achieved to have spontaneous ignition and 1 metre in order to have a bigger pool of results. In these two lengths the lowest pressure input and the highest pressure input studied before are going to be used, so 5 bar and 40 bar. In order to do this, the steps were the same as before using the assumptions mentioned in table 3.3.

Since Fluent does not produce the equivalence ratio as a result property, a user defined function was developed where the mass fraction of H_2 was divided by the stoichiometric hydrogen% in air, which is

0.295.

Fluent, when analysing a transient state, prints results in a time called pseudo-transient which means that the results presented in the previous section show only the last time step calculated. In this section, the evolution of temperature along with the equivalence ratio through time inside the shock tube is going to be shown in order to verify how the temperature profile is built and if, the mixture quality is good enough to produce combustion. In order to do so, figures from the driven section were taken for several time steps as the flow moves from left to right from the diaphragm.

4.3.1 360mm Long tube

Looking at the following figures 4.41 and 4.42 for 5 and 40 bar respectively, the equivalence ratio profiles along with the temperature profiles inside the tube are shown. These are located in the above and bottom part of the figure respectively.

While carefully examining the equivalence ratio profile for 5 bar in figure 4.41, it is possible to see that through time, the mass fractions of hydrogen progress in the tube. This results in several different equivalence ratios inside the tube, meaning that there is in fact mixture inside the tube and that there is hydrogen mass moving along the boundary layer approaching the areas of higher temperatures.

Complementing the equivalence ratio we have, in the bottom the temperature profile inside the tube. With this diagram it is possible to conclude that higher temperatures are achieved near the shock wave boundary. However, it was thought that the shock wave would heat up the mixture of hydrogen/air but, when looking at both graphs and comparing them it is possible to see that the substance that is heated is the air and only part of the mixture. It is also possible to see that as the equivalence ratio increases (to the left of the graph in red), the mixture becomes richer but the temperature decreases (darker blue). This goes to prove the assumption above. However, considering the wide range of flammability of hydrogen concentration in air, hydrogen could auto ignite for smaller equivalence ratios where the temperature is higher in the bottom graph of figure 4.41. However, from Alcock et al. [5] we know that the minimum energy to lead the mixture of hydrogen/air to combust is at stoichiometric conditions, which is $\Phi = 1$, so for lean mixtures ($\Phi < 1$) the energy necessary for spontaneous ignition to occur is bigger (figure 1.2). This means that the spontaneous ignition temperature might be higher than expected for such mixtures as there is a deficiency of fuel in the mixture. Considering that for 5 bar the highest temperature recorded is 471.6K, it is impossible for the mixture to spontaneously ignite, specially because the highest temperature recorded is located near the centerline of the tube where there is practically only air and no mixture.

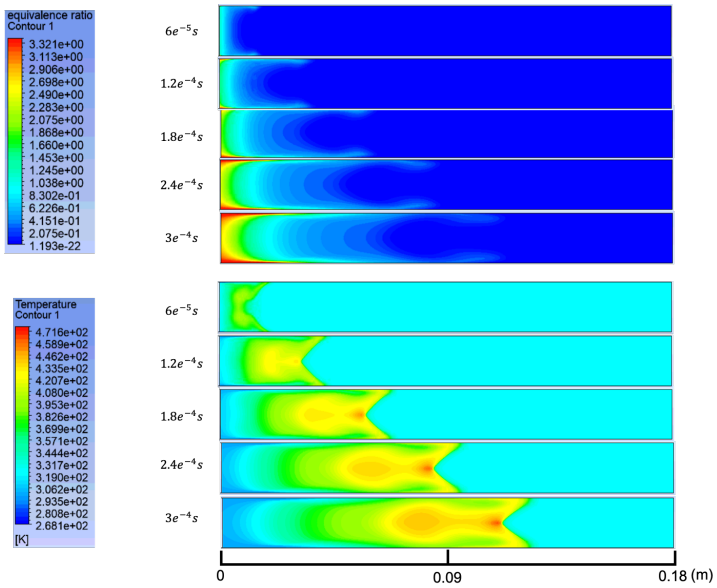

Figure 4.41: Hydrogen/air equivalence ratio profile (top), and temperature profile (bottom) for the 360mm long tube at 5 bar of initial pressure.

For the 40 bar of initial pressure case and 360mm, two things can be seen from figure 4.42. The first thing is that in the temperature profiles, right from $5e^{-5}s$, the temperature recorded behind the shock wave is already enough to cause spontaneous ignition of the mixture. The second thing to notice is that, from the equivalence ratio profiles, it is possible to conclude that the mixture at the interface separation with air, is stoichiometric. This being said, if the two profiles are overlapped, the edge of the equivalence ratio at stoichiometric conditions will be matched with a temperature above the spontaneous ignition temperature for hydrogen/air mixture. So for a driven section of 180mm and an initial pressure input of 40 bar, the conditions necessary to ignite and produce flame from a hydrogen/air mixture are gathered.

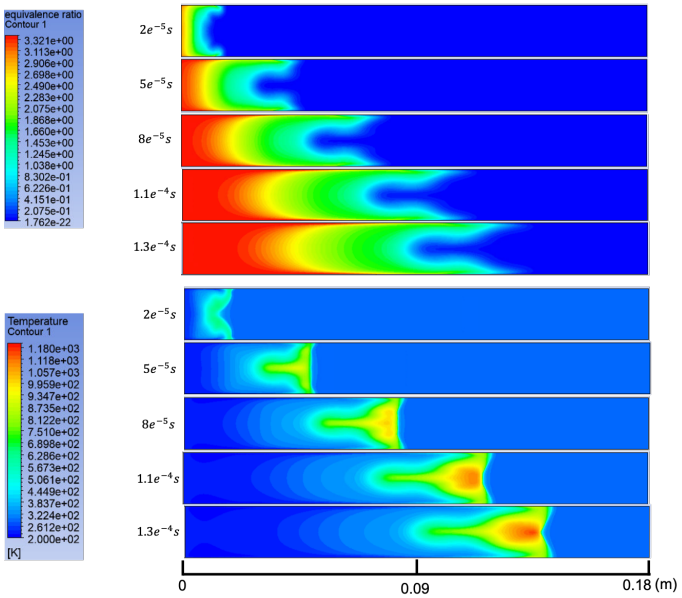

Figure 4.42: Hydrogen/air equivalence ratio profile (top), and temperature profile (bottom) for the 360mm long tube at 40 bar of initial pressure.

4.3.2 1 meter Long tube

For the 1 meter long tube, the following figures 4.43 and 4.44 represent the profiles of equivalence ratio and temperature for 5 and 40 bar respectively.

As seen for the case of 360mm long tube for 5 bar, the temperature reached would never be enough to reach the spontaneous ignition temperatures. Assuming that the spontaneous ignition temperatures recorded, taken from the engineering toolbox[26], are for stoichiometric mixture, with the observation of the figures, the temperature would have to be equal or higher than 773K, depending on the richness of the mixture. Considering that for 5 bar, even for the temperature raise from the increase of length from 471.6K to 535.5K, it would not be enough to cause combustion of the mixture. Looking at the profiles at $3.41e^{-4}s$, it is possible to see that at the end of the mixture, more or less at 0.08m, the mixture seems to be stoichiometric, however if we look at the same time steps at the same location but in the temperature profile, the maximum temperature recorded for that Φ is approximately 433K which is not enough, considering the 773K necessary to ignite a stoichiometric mixture of hydrogen/air.

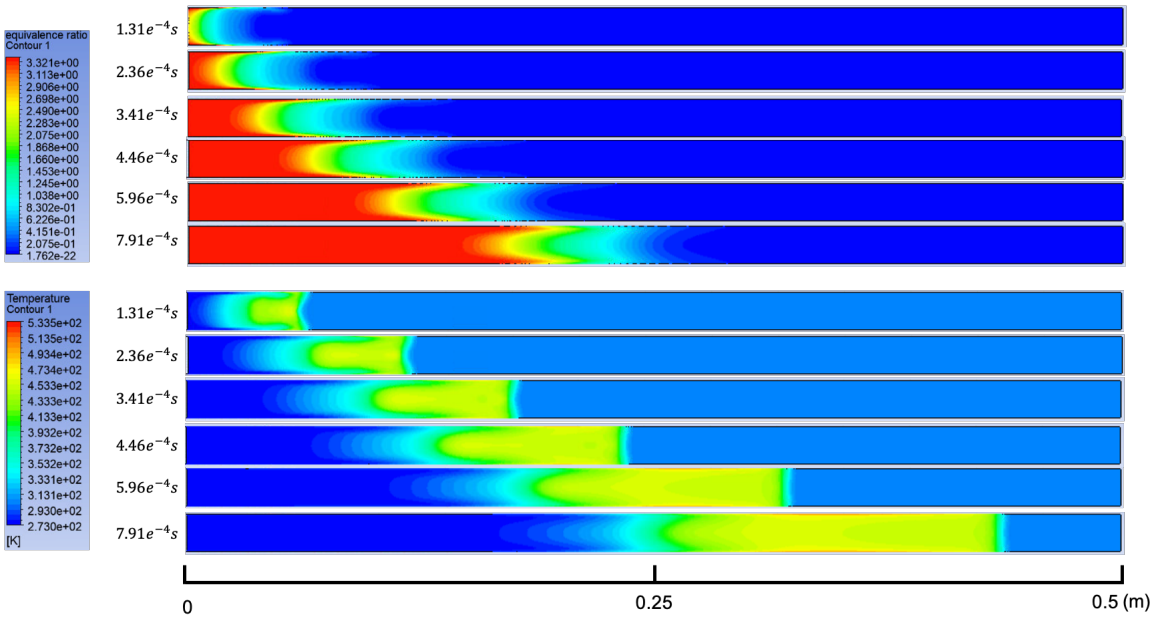

Figure 4.43: Hydrogen/air equivalence ratio profile (top), and temperature profile (bottom) for the 1 meter long tube at 5 bar of initial pressure.

When analyzing the 40 bar profiles for 1 meter long tube with figure 4.44, the profiles observed are very different than for 5 bar. In the temperature profile observed, the maximum temperature achieved by the shock wave is 1233K which is well above the spontaneous ignition temperature but is located at the boundary layer. However, most of the temperature profile exhibits temperatures in the range of 1000K (in yellow) which is still well above the temperature required.

From the equivalence ratio profile, as the flow progresses through the length of the tube, the mixture begins to spread more, creating areas where the Φ near the higher temperatures is < 1 which means that the mixture starts to fade as the length of the tube increases. By fade, what this means is that as the flow develops inside the shock tube, velocity builds up and since we are in the presence of a shock wave, air is pushed by the shock wave faster. With the expansion of fuel on the opposite direction of the shock

wave, hydrogen can not keep up with the air flow and the mixture concentration drops. For example at the time steps of $7.9e^{-5}s$, the mixture creates a shape that resembles a horse shoe where near the edges the mixture, in light blue, is stoichiometric. However, with the flow development, at $4e^{-4}s$ the mixture fades and becomes lean with $\Phi < 1$.

With the same analysis as the previous paragraph, as the flow develops the range of temperatures increase where the regions of less temperature also increase. Taking the same example, for the time steps of $7.9e^{-5}s$, temperature profile is thin and the temperatures are confined to less amount of air. With the mixture at that time step being stoichiometric near the edges, it is possible to conclude that the mixture has the necessary conditions to combust. However, in order for the mixture to exit the tube with flame, these conditions must be maintained throughout the rest of the tube length. Moving to the last time steps, at $4e^{-4}s$, the conditions to sustain the flame have faded as the mixture is lean ($\Phi < 1$) at the location with high enough temperatures. This allows the conclusion that if a tube is long enough, there might be combustion inside but once the mixture spouts to the atmosphere, there will be no visible flame as the mixture faded and the combustion was extinct.

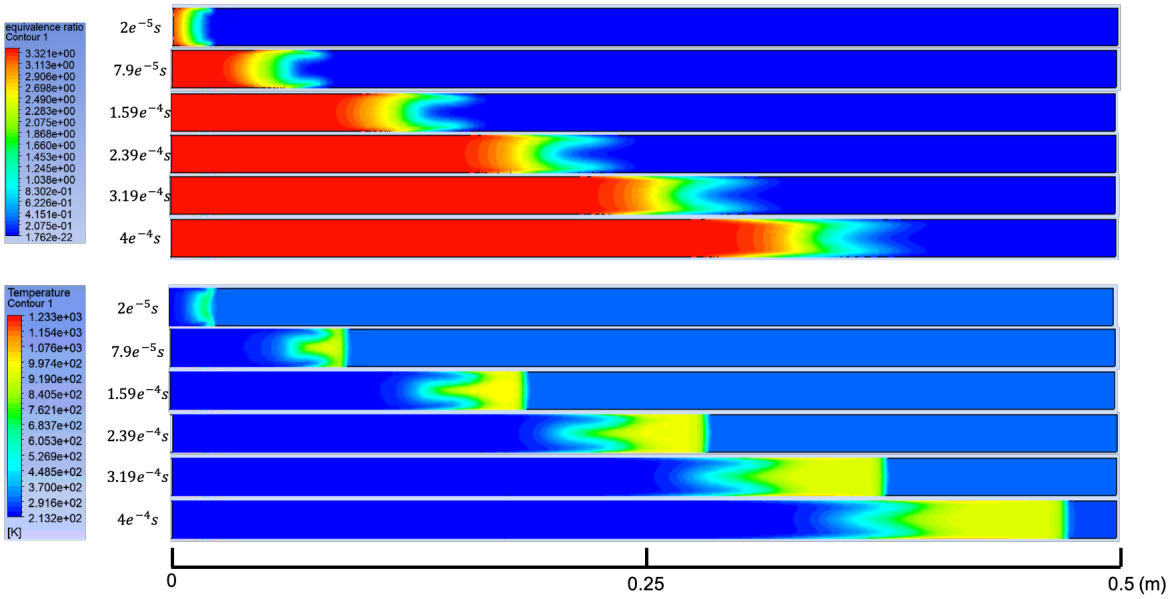

Figure 4.44: Hydrogen/air equivalence ratio profile (top), and temperature profile (bottom) for the 1 meter long tube at 40 bar of initial pressure.

With this analysis of the shock temperature profiles and equivalence ratios, the increase of length of the tube, although it helps to build higher temperatures (over the auto-ignition temperatures for hydrogen), it might also lead the mixture to fade and become lean. As seen from the case of 1 meter long tube with 40 bar of pressure, the conditions for spontaneous ignition were gathered at around 80mm from the contact surface, however as the flow developed the mixture started to fade. This means that ignition might occur but later down the length of the tube it might extinct and not show flame at the outside of the tube. However, for a shorter tube like the case of 360mm, the input of 40 bar of pressure was sufficient to gather the right conditions to ignite the mixture of hydrogen/air.

With all the analysis made with fluent, it is possible to conclude at what lengths and pressure there

might be an ignition considering that the conditions are gathered for such phenomena to take place. With the studied analysis, it is concluded that for 5 bar of initial pressure, much like for 10 bar, the shock wave produced is not strong enough to cause enough increase of temperature to lead the mixture to spontaneous ignition. However, for 20 bar and up, it is possible to see that for some tube lengths the conditions are gathered for spontaneous ignition to take place. With the results from case 1 and 2 and with the results from 4.41 to 4.44, it is possible to conclude that the higher the pressure input, the longer the mixture quality is sustained. This means that for 20 bar and up, of initial pressure it is possible to say that spontaneous ignition conditions are gathered for at least up to 240mm of tube length from the burst disk (driven section). However, from figure 4.44 it is concluded for 40 bar of pressure ignition might occur until further down the length of the tube. With the analysis of the figure, we can see that the conditions that allow ignition are gathered at least until 300mm of tube length, meaning that the bigger the input pressure, the longer the conditions for spontaneous ignition are sustained, just as mentioned before. With these conclusions it is possible to plot the following graph in figure 4.45.

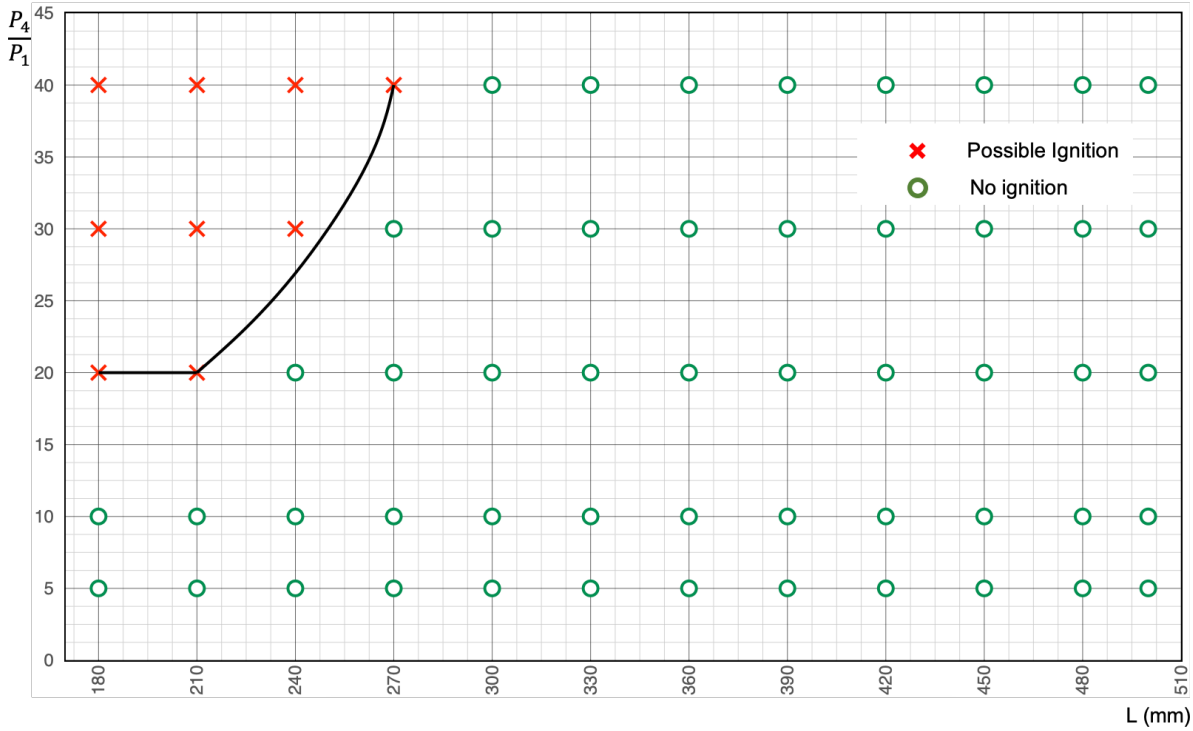

Figure 4.45: Initial pressure as a function of the length of the tube where the conditions are or not gathered for spontaneous ignition to occur.

As previously mentioned, since this is a numerical study, it is impossible to say with certainty if there is or not spontaneous ignition. Such conclusion is only possible in an experimental study. However, with all the analysis made it is possible to conclude whether it is possible or not to have ignition. In the graph above we see just that, where above the black line it is concluded that the conditions to have spontaneous ignition are gathered and such phenomena is possible to occur. For this two analysis were used, the analysis of temperature and the analysis of mixture quality. The graph was then plotted where the red crosses indicate where both of these conditions are gathered, high enough temperature to cause

spontaneous ignition and stoichiometric mixture to facilitate the combustion of hydrogen/air mixture. For the green circles it was seen that, above 20 bar, the temperature was high enough, however the mixture was lean at the interface from hydrogen and air, disallowing the combustion of the mixture.

Chapter 5

Conclusions

In this chapter the conclusions of the work studied are presented.

The present dissertation has two primary objectives. The first objective is the analysis of the existing analytical equations to define the flow properties inside the shock tube with the comparison of a numerical analysis done with the program Fluent. The second objective is to study, through the analysis of CFD, the effects of the tube length in the event of a shock wave formation once a high-pressured gas is released into a low-pressured atmosphere. The reason for this dissertation is the need to improve and aid, even if in a very small scale, the implementation of hydrogen as a fuel in the modern society by studying the physical phenomena behind the spontaneous ignition of a leak of high-pressured gas into the atmosphere. It serves the purpose of complementing the information that already exists in order to be able to provide further knowledge to aid the engineering construction of high-pressured hydrogen systems.

In order to study the above objectives the first step to be made was the review of literature where the governing equations were found. With the testing of these equations for the various gaseous fuels, it was possible to conclude that different gases have different reactions for the release of high-pressured gas into low-pressured atmosphere. With this we were able to conclude how hydrogen behaves different from other common gaseous fuels and how dangerous it can be even at low pressures. Another thing that was possible to understand from the equations used is how different pressures can produce very different shock waves considering different fuels where a shock wave can be stronger just considering a different gas.

After concluding the analytical study, verification was necessary. For this CFD was used, creating a shock tube like geometry in order to simulate what happens inside a hole when high-pressured gas is released into the atmosphere with a sudden burst. In order to verify the calculations from the previous step the same setting of boundary and initial conditions was used with some assumptions necessary. Turbulent flow was tested with the conclusion that it was the most appropriate flow to use, as Reynolds numbers over 4000 were produced inside the tube due to high-velocity flow with very little viscosity due to the fluid being considered an ideal gas. With the assumption of turbulent, the verification of the equations was possible as the curves of each property studied were very similar. However, there was considerable error as the equations studied did not complement the viscous effects and the equations from

both approaches were very different. The CFD study allowed the conclusion that, due to turbulent flow, the temperatures achieved by the gases when spouting at supersonic speeds, even if there was no ignition present, could be very dangerous in case of a leak. However verification of the assumptions made was possible to an extent that a hydrogen leak at 20 bar can be enough to auto-ignite if the tube is long enough for the flow to develop. Through Fluent it was possible to understand visually what happens inside a shock tube and understand that as soon as the contact surface breaks, both the driver gas and driven gas start mixing, through turbulent mixing, allowing the mixture to reach high enough temperatures and ignite from the inside of the tube. This was all concluded for the last time step calculated meaning that the solution may vary if other dimensions and other time steps are used, as well as if other assumptions are made..

The third and final step was to study the effect that the length of the tube has on the shock properties. The objective of this last step was to see if, by increasing the length of the tube, it would be easier or not to ignite the mixture. As it was previously proven experimentally that the longer the tube leading the mixture into the atmosphere, the lower the pressure needed for the mixture to spontaneously ignite. From the study made it was conclude that, due to turbulent flow, as the length of the tube increases, so will the boundary layer and with this the shock wave properties will be more affected. It was observed that as the length of the tube increased, the maximum temperature reached also increases as the maximum velocity of the flow would decrease. This leads to higher temperatures and longer flow time which can all contribute to an easier combustion of the mixture. It was possible to conclude that a tube of 360mm length with a driven section of 180mm, would be enough to produce high enough temperatures that might ignite a mixture of hydrogen/air at 20 bar. Therefore, it is possible to conclude that with the increase of the tube length, the temperature of the mixture reaches higher values, possibly leading to easier ignition.

It was proven that for longer tubes the temperature achieved is higher than for smaller tubes at the same pressure. However, with the analysis of the equivalence ratio done in section 4.3 with the temperature profiles in the shock tube, it was possible to conclude that longer tubes might promote leaner mixtures leading to no ignition. Although smaller tube lengths might lead to lower maximum temperatures, the mixtures observed have better quality. With this, a smaller tube with a pressure ratio capable of producing a shock wave that provokes high enough temperatures to ignite a fuel/air mixture, gathers better conditions to produce spontaneous ignition than a longer tube, as the mixture maintains its stoichiometric conditions for longer. With the results achieved it is safe to say that the length of the tube affects spontaneous ignition but not in a linear way, meaning that it can not be said that the longer, or smaller, the tube the better probability of spontaneous ignition. What can be said is that, for certain tube lengths, there is a minimum critical pressure that might lead the mixture to ignite, which will vary for different lengths, as seen in figure 4.45.

5.1 Future Work

Although in this thesis a lot of what happens inside the shock tube was addressed, what happens when the mixture spouts to the atmosphere and creates a flame is not addressed. Therefore, in order to complement

the work done in this dissertation, further work on what happens when the mixture spouts into the atmosphere is needed. Although some work has been done in this area, it could be further developed, through numerical analysis and experimental analysis such as what conditions lead to stabilized jet fire of hydrogen spontaneous leaks.

Considering that the study preformed used a spatial discretization method that might cause numerical diffusion, it is proposed to do the same study but using a different method, like MUSCL third-order method.

Another thing to be studied, would be the use of friction and curvature of the real pipelines in order to analyse cases closer to reality.

Last but not least, to verify and validate the present study experimentally in order to prove the validation of the conclusions made.

Bibliography

[1] Wikipedia contributors. Hydrogen — Wikipedia, the free encyclopedia, 2020. URL `https://en.wikipedia.org/w/index.php?title=Hydrogen&oldid=976585349`. Last accessed on 2020/08/10.

[2] W. contributors. Hindenburg disaster, 2020. URL `https://en.wikipedia.org/w/index.php?title=Hindenburg_disaster&oldid=977175034`. Last accessed on 2020/08/10.

[3] Hydrogen europe, 2017. URL `https://hydrogeneurope.eu/`. Last accessed on 2020/08/15.

[4] T. Okino, S. Yamahira, S. Yamada, Y. Hirose, A. Odagawa, Y. Kato, and T. Tanaka. A real-time ultraviolet radiation imaging system using an organic photoconductive image sensor. *Sensors*, 18(1): 314, 2018.

[5] J. Alcock, L. Shirvill, and R. Cracknell. Compilation of existing safety data on hydrogen and comparative fuels. *Deliverable Report, EIHP2, May*, 2001.

[6] G. Astbury and S. Hawksworth. Spontaneous ignition of hydrogen leaks: a review of postulated mechanisms. *International Journal of Hydrogen Energy*, 32(13):2178–2185, 2007.

[7] P. Wolanski. Investigation into the mechanism of the diffusion ignition of a combustible gas flowing into an oxidizing atmosphere. In *Fourteenth Symposium (International) on Combustion, 1973*, 1973.

[8] Hiad, 2020. URL `https://odin.jrc.ec.europa.eu/giada/`. Last accessed on 2020/08/22.

[9] J. Chaineaux, G. Mavrothalassitis, and J. Pineau. Modelization and validation tests of the discharge in air of a vessel pressurized by a flammable gas. *Progress in Astronautics and Aeronautics*, 134: 104–137, 1991.

[10] T. Mogi, D. Kim, H. Shiina, and S. Horiguchi. Self-ignition and explosion during discharge of high-pressure hydrogen. *Journal of Loss Prevention in the process industries*, 21(2):199–204, 2008.

[11] V. Golub, D. Baklanov, T. Bazhenova, M. Bragin, S. Golovastov, M. Ivanov, and V. Volodin. Shock-induced ignition of hydrogen gas during accidental or technical opening of high-pressure tanks. *Journal of Loss Prevention in the process industries*, 20(4-6):439–446, 2007.

[12] F. L. Dryer, M. Chaos, Z. Zhao, J. N. Stein, J. Y. Alpert, and C. J. Homer. Spontaneous ignition of pressurized releases of hydrogen and natural gas into air. *Combustion science and technology*, 179 (4):663–694, 2007.

[13] M. V. Bragin and V. V. Molkov. Physics of spontaneous ignition of high-pressure hydrogen release and transition to jet fire. *International Journal of Hydrogen Energy*, 36(3):2589–2596, 2011.

[14] S. Xiaobo and S. Jinhua. Numerical simulation on the spontaneous ignition of leaking high pressure hydrogen from terminal unit. *Physics Procedia*, 33:1833–1841, 2012.

[15] A. Al-Falahi, M. Yusoff, and T. Yusaf. Numerical simulation of inviscid transient flows in shock tube and its validations. *International Journal of Mechanical, Aerospace, Industrial and Mechatronics Engineering*, 2(7):1–11, 2008.

[16] A. Bandyopadhyay and A. Majumdar. Modeling of compressible flow with friction and heat transfer using the generalized fluid system simulation program. 2007.

[17] S. Downes, A. Knott, and I. Robinson. Towards a shock tube method for the dynamic calibration of pressure sensors. *Philosophical Transactions of the Royal Society A: Mathematical, Physical and Engineering Sciences*, 372(2023):20130299, 2014.

[18] Q. Duan, H. Xiao, W. Gao, X. Shen, Q. Wang, and J. Sun. Experimental investigation on shock waves generated by pressurized gas release through a tube. *Journal of Loss Prevention in the Process Industries*, 36:39–44, 2015.

[19] Q. Duan, H. Xiao, W. Gao, L. Gong, Q. Wang, and J. Sun. Experimental study on spontaneous ignition and flame propagation of high-pressure hydrogen release via a tube into air. *Fuel*, 181: 811–819, 2016.

[20] P. Huang, S. Yonkers, D. Hokey, and D. Olenick. Screw pulsation generation and control: a shock tube mechanism. In *Proceedings of the 8th International Conference on Compressors and Their Systems*, pages 113–128, 2013.

[21] T. Mogi, Y. Wada, Y. Ogata, and A. K. Hayashi. Self-ignition and flame propagation of high-pressure hydrogen jet during sudden discharge from a pipe. *International Journal of Hydrogen Energy*, 34 (14):5810–5816, 2009.

[22] F. M. Young and T. Simon. A one-dimensional combined-change model for compressible flow. *The International journal of engineering education*, 9(5):391–405, 1993.

[23] E. Yamada, N. Kitabayashi, A. K. Hayashi, and N. Tsuboi. Mechanism of high-pressure hydrogen auto-ignition when spouting into air. *International Journal of Hydrogen Energy*, 36(3):2560–2566, 2011.

[24] H. S. Rupal, J. D. Sharma, and R. Arora. Validation of cfd modeling and simulation of a shock tube. 2018.

[25] A. H. Shapiro. *The dynamics and thermodynamics of compressible fluid flow*. Number BOOK. John Wiley & Sons, 1953.

[26] Engineering toolbox, 2001. URL https://www.engineeringtoolbox.com/. Last accessed on 2020/08/30.

[27] H. W. Liepmann and A. Roshko. *Elements of gasdynamics*. Courier Corporation, 2001.

[28] A. G. Gaydon and I. R. Hurle. *The shock tube in high-temperature chemical physics*. Chapman and Hall, 1963.

[29] Fluent user manual. URL https://www.afs.enea.it/project/neptunius/docs/fluent/. Last accessed on 2020/09/13.

[30] ANSYS. Ansys fluent - cfd software | ansys, 2020. URL http://www.ansys.com/products/fluids/ansys-fluent. Last accessed on 2020/09/10.

Appendix A

Shock evolution in the driven section of L=500mm for 20 bar and 30 bar

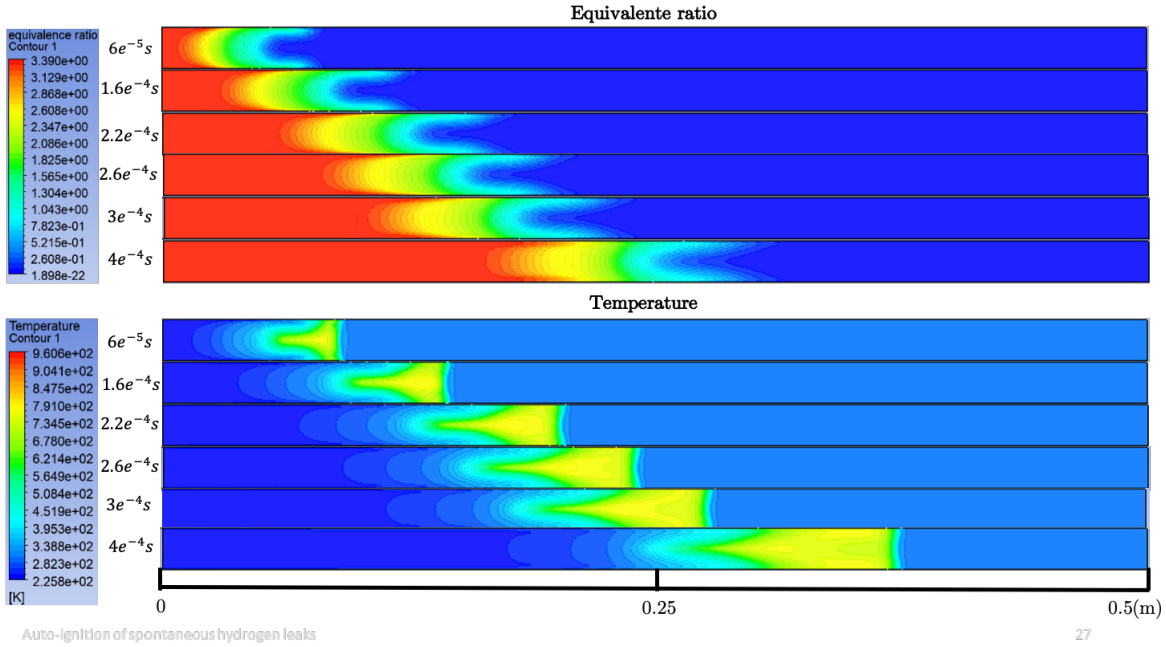

Figure A.1: Shock evolution in the driven section of L=500mm for 20 bar

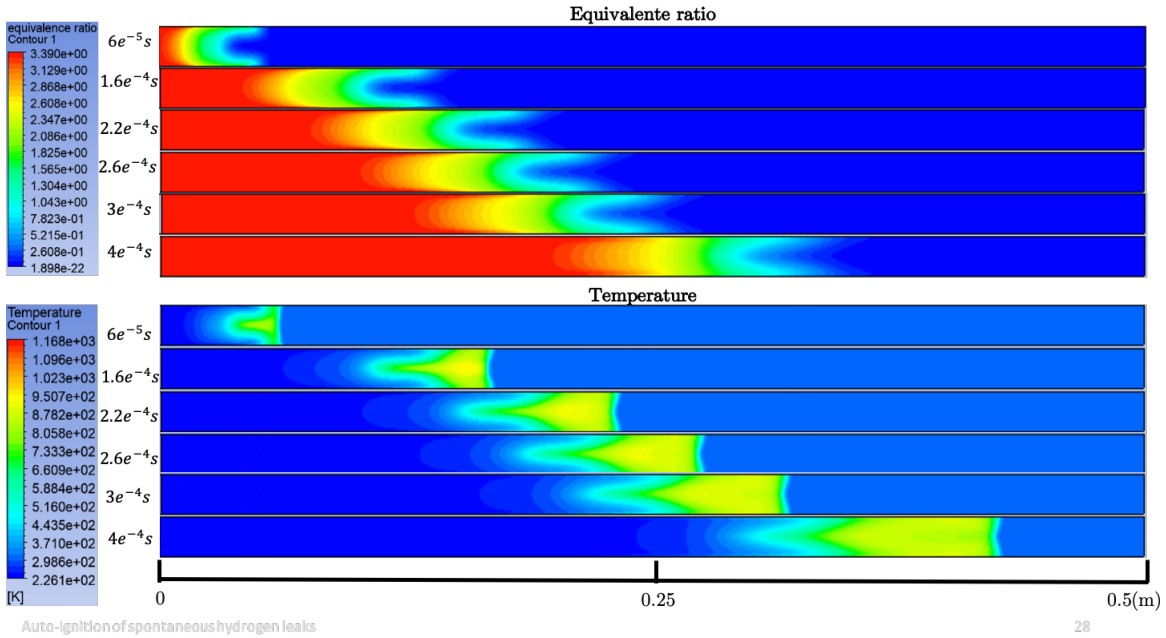

Figure A.2: Shock evolution in the driven section of L=500mm for 30 bar